EXTRACTION AND CHARACTERISATION OF CELLULOSE NANOCRYSTALS (CNCS) FROM SUGARCANE BAGASSE USING IONIC LIQUIDS

Thesis Submitted in fulfilment of the academic requirements for the Master in Applied Sciences (Chemistry) in the Faculty of Applied Sciences at Durban University of Technology, Chemistry Department, Durban, South Africa

GCINILE PRETTY MDLETSHE

2019

PREFACE

The work reported in this thesis was performed under the supervision of Professor N. Deenadayalu at the Durban University of Technology, Durban, South Africa. To the best of the authors' knowledge, the thesis does not contain any materials previously published or written by any other person and references to the source were fully acknowledged where applicable. I further declare that the work contained in this thesis has not been previously submitted in any form to another institution.

Signed: [redacted] Date: 11/04/19

Gcinile Mdletshe

Signed: [redacted] Date: 11/4/19

Prof. N. Deenadayalu

Signed: [redacted] Date: 11 April 2019

Prof. S. Suprakas

ACKNOWLEDGEMENTS

Ngiqala ngokubonga uNkulunkulu, uMvelinqangi ngokungipha ukuphila, uthando lwakhe olungapheli, amandla angipha wona kanye nobumnene bakhe. Ngimbonga ngehubo 103;

Ihubo 103

Ihubo lokudumisa uNkulunkulu ngomusa wakhe

Mbonge uJehova, mphefumulo wami; konke okuphakathi kwami makubonge igama lakhe elingcwele.

Ngibonge nabakwa Mdletshe, oMsindazwe, Ngomane, mfuyi wamatshe for blessing me with an amazing woman, Thembisile, whom I call my mother. She's been my great support system throughout this study. I love her to bits.

- I am grateful to the following people for their support throughout my MSc study:
- Supervisors, Prof. N. Deenadayalu and Prof. S. S. Ray.
- National Research Foundation of South Africa and DUT research office for their financial support.
- National Centre for Nano-Structured Materials at The Council for Scientific and Industrial Research, Pretoria staff and colleagues for their warm welcome and assistance with analysis of this work. It was great meeting all of them.
- DUT chemistry staff particularly Mrs Devrani Naicker, she gave me so much academic and emotional support. I will forever be grateful.
- Bryan Barker from SMRI for providing us with sugarcane bagasse.

ABSTRACT

Lignocellulosic materials have the potential to partly replace fossil-based resources as a source of bio-fuels, bio-chemicals, bio-composites and other bio-products. In this study, ionic liquids (ILs) were used in the pre-treatment of ground sugarcane bagasse (SCB). The ILs used were 1-butyl-3-methylimidazolium hydrogen sulphate or 1-butyl-3-methylimidazolium methyl sulphate at varied times. The ILs were able to remove lignin and hemicellulose from biomass. The IL [bmim][HSO_4] had the highest amount of lignin removed after 12 h than all samples. Moreover, it resulted in the greatest cellulose amount.

Milled SCB was pre-treated with IL/dimethyl sulphoxide (DMSO) mixtures. The IL [bmim][HSO_4] was able to produce cellulose nanocrystals (CNCs) at 90 % IL and 100 % IL. The other IL failed to produce CNCs.

Freeze drying the CNC suspension showed morphologies of long fibrous structures and rods which were evident in the scanning electron microscopy (SEM) and transmission electron microscopy (TEM) images. The crystallinity index of cellulose in the form of CNCs was calculated from powder X-ray diffraction (P-XRD). Thermal analysis of the CNCs was obtained from thermogravimetric analysis (TGA). Attenuated total reflection-Fourier transform infrared (ATR-FTIR) was used to confirm the absence of lignin and hemicellulose in CNCs. The size distribution of CNCs was obtained by using a dynamic light scattering (DLS) which showed that all the CNCs for the 100 % IL [bmim][HSO_4] pre-treatment had a length < 500 nm. It was found that [bmim][HSO_4], with no DMSO, was the most effective in terms of cellulose dissolution and the crystal sizes of CNCs. The conversion of cellulose to CNCs was successful with a 80 % and 100 % conversion for 90 % [bmim][HSO_4]/DMSO and 100 % [bmim][HSO_4], respectively.

CONTENTS

List of Tables

List of Figures

List of Abbreviations

AIL : acid insoluble lignin

ASL : acid soluble lignin

ATR : attenuated total reflection

CNCs : cellulose nanocrystals

DLS : dynamic light scattering

DMSO : dimethyl sulfoxide

FTIR : Fourier transform infrared

H_2O_2 : hydrogen peroxide

HPLC : high performance liquid chromatography

I_{SCB} : initial mass of SCB weighed

F_{pulp} : final pulp mass

IL : ionic liquid

ILs : ionic liquids

ILIL : ionic liquid insoluble lignin

ILSL : ionic liquid soluble lignin

MCC : microcrystalline cellulose

NaOH : sodium hydroxide

SCB	: sugarcane bagasse
SEM	: scanning electron microscopy
TEM	: transmission electron microscopy
TGA	: thermogravimetric analysis
Uv-Vis	: ultraviolet-visible
XRD	: X-ray diffraction
[bmim][HSO_4]	: 1-butyl-3-methylimidazolium hydrogen sulphate
[bmim][$MeSO_4$]	: 1-butyl-3-methylimidazolium methyl sulphate
[bmim][HSO_4]-4	: 4 h pre-treatment time with [bmim][HSO_4]
[bmim][HSO_4]-8	: 8 h pre-treatment time with [bmim][HSO_4]
[bmim][HSO_4]-12	: 12 h pre-treatment time with [bmim][HSO_4]
[bmim][HSO_4]-50	: [bmim][HSO_4]/DMSO (ratio of IL/DMSO - 50:50)
[bmim][HSO_4]-75	: [bmim][HSO_4]/DMSO (ratio of IL/DMSO - 75:25)
[bmim][HSO_4]-90	: [bmim][HSO_4]/DMSO (ratio of IL/DMSO - 90:10)
[bmim][HSO_4]-100	: [bmim][HSO_4]/DMSO (ratio of IL/DMSO - 100:0)

[bmim][HSO_4]-50 (30) : 30 min pre-treatment with [bmim][HSO_4]/DMSO (ratio of IL/DMSO - 50:50)

[bmim][HSO_4]-75 (30) : 30 min pre-treatment time with [bmim][HSO_4]/DMSO (ratio of IL/DMSO - 75:25)

[bmim][HSO_4]-90 (30) : 30 min pre-treatment with [bmim][HSO_4]/DMSO (ratio of IL/DMSO – 90:10)

[bmim][HSO_4]-100 (30) : 30 min pre-treatment with [bmim][HSO_4]/DMSO (ratio of IL/DMSO - 100:0)

[bmim][HSO_4]-50 (45) : 30 min pre-treatment with [bmim][HSO_4]/DMSO (ratio of IL/DMSO - 50:50)

[bmim][HSO_4]-75 (45) : 30 min pre-treatment time with [bmim][HSO_4]/DMSO (ratio of IL/DMSO - 75:25)

[bmim][HSO_4]-90 (45) : 30 min pre-treatment with [bmim][HSO_4]/DMSO (ratio of IL/DMSO – 90:10)

[bmim][HSO_4]-100 (45) : 30 min pre-treatment with [bmim][HSO_4]/DMSO (ratio of IL/DMSO - 100:0)

[bmim][HSO_4]-50 (60) : 30 min pre-treatment with [bmim][HSO_4]/DMSO (ratio of IL/DMSO - 50:50)

[bmim][HSO_4]-75 (60) : 30 min pre-treatment time with [bmim][HSO_4]/DMSO (ratio

of IL/DMSO - 75:25)

[bmim][HSO_4]-90 (60) : 30 min pre-treatment with [bmim][HSO_4]/DMSO (ratio of IL/DMSO – 90:10)

[bmim][HSO_4]-100 (60) : 30 min pre-treatment with [bmim][HSO_4]/DMSO (ratio of IL/DMSO - 100:0)

[bmim][HSO_4]-50 (30-B) : 30 min pre-treatment with [bmim][HSO_4]/DMSO (ratio of IL/DMSO - 50:50) followed by bleaching

[bmim][HSO_4]-75 (30-B) : 30 min pre-treatment time with [bmim][HSO_4]/DMSO (ratio of IL/DMSO - 75:25) followed by bleaching

[bmim][HSO_4]-90 (30-B) : 30 min pre-treatment with [bmim][HSO_4]/DMSO (ratio of IL/DMSO – 90:10) followed by bleaching

[bmim][HSO_4]-100 (30-B) : 30 min pre-treatment with [bmim][HSO_4]/DMSO (ratio of IL/DMSO - 100:0) followed by bleaching

[bmim][HSO_4]-50 (45-B) : 45 min pre-treatment with [bmim][HSO_4]/DMSO (ratio of IL/DMSO - 50:50) followed by bleaching

[bmim][HSO_4]-75 (45-B) : 45 min pre-treatment time with [bmim][HSO_4]/DMSO (ratio of IL/DMSO - 75:25) followed by bleaching

[bmim][HSO_4]-90 (45-B) : 45 min pre-treatment with [bmim][HSO_4]/DMSO (ratio of IL/DMSO – 90:10) followed by bleaching

[bmim][HSO_4]-100 (45-B) : 45 min pre-treatment with [bmim][HSO_4]/DMSO (ratio of IL/DMSO - 100:0) followed by bleaching

[bmim][HSO_4]-50 (60-B) : 60 min pre-treatment with [bmim][HSO_4]/DMSO (ratio of IL/DMSO - 50:50) followed by bleaching

[bmim][HSO_4]-75 (60-B) : 60 min pre-treatment time with [bmim][HSO_4]/DMSO (ratio of IL/DMSO - 75:25) followed by bleaching

[bmim][HSO_4]-90 (60-B) : 60 min pre-treatment with [bmim][HSO_4]/DMSO (ratio of IL/DMSO – 90:10) followed by bleaching

[bmim][HSO_4]-100 (60-B) : 60 min pre-treatment with [bmim][HSO_4]/DMSO (ratio of IL/DMSO - 100:0) followed by bleaching

[bmim][$MeSO_4$]-4 : 4 h pre-treatment time with [bmim][$MeSO_4$]

[bmim][$MeSO_4$]-8 : 8 h pre-treatment time with [bmim][$MeSO_4$]

[bmim][$MeSO_4$]-12 : 12 h pre-treatment time with [bmim][$MeSO_4$]

[bmim][$MeSO_4$]-50 : [bmim][$MeSO_4$]/DMSO (ratio of IL/DMSO - 50:50)

[bmim][$MeSO_4$]-75 : [bmim][$MeSO_4$]/DMSO (ratio of IL/DMSO - 75:25)

[bmim][$MeSO_4$]-90 : [bmim][$MeSO_4$]/DMSO (ratio of IL/DMSO - 90:10)

[bmim][$MeSO_4$]-100 : [bmim][$MeSO_4$]/DMSO (ratio of IL/DMSO - 100:0)

[bmim][$MeSO_4$]-50 (30) : 30 min pre-treatment with [bmim][$MeSO_4$]/DMSO (ratio of

IL/DMSO - 50:50)

[bmim][$MeSO_4$]-75 (30) : 30 min pre-treatment time with [bmim][$MeSO_4$]/DMSO (ratio of IL/DMSO - 75:25)

[bmim][$MeSO_4$]-90 (30) : 30 min pre-treatment with [bmim][$MeSO_4$]/DMSO (ratio of IL/DMSO – 90:10)

[bmim][$MeSO_4$]-100 (30) : 30 min pre-treatment with [bmim][$MeSO_4$]/DMSO (ratio of IL/DMSO - 100:0)

[bmim][$MeSO_4$]-50 (45) : 45 min pre-treatment with [bmim][$MeSO_4$]/DMSO (ratio of IL/DMSO - 50:50)

[bmim][$MeSO_4$]-75 (45) : 45 min pre-treatment time with [bmim][$MeSO_4$]/DMSO (ratio of IL/DMSO - 75:25)

[bmim][$MeSO_4$]-90 (45) : 45 min pre-treatment with [bmim][$MeSO_4$]/DMSO (ratio of IL/DMSO – 90:10)

[bmim][$MeSO_4$]-100 (45) : 45 min pre-treatment with [bmim][$MeSO_4$]/DMSO (ratio of IL/DMSO - 100:0)

[bmim][$MeSO_4$]-50 (60) : 60 min pre-treatment with [bmim][$MeSO_4$]/DMSO (ratio of IL/DMSO - 50:50)

[bmim][$MeSO_4$]-75 (60) : 60 min pre-treatment time with [bmim][$MeSO_4$]/DMSO (ratio

of IL/DMSO - 75:25)

[bmim][$MeSO_4$]-90 (60) : 60 min pre-treatment with [bmim][$MeSO_4$]/DMSO (ratio of IL/DMSO – 90:10)

[bmim][$MeSO_4$]-100 (60) : 60 min pre-treatment with [bmim][$MeSO_4$]/DMSO (ratio of IL/DMSO - 100:0)

[bmim][$MeSO_4$]-50 (30-B) : 30 min pre-treatment with [bmim][$MeSO_4$]/DMSO (ratio of IL/DMSO - 50:50) followed by bleaching

[bmim][$MeSO_4$]-75 (30-B) : 30 min pre-treatment time with [bmim][$MeSO_4$]/DMSO (ratio of IL/DMSO - 75:25) followed by bleaching

[bmim][$MeSO_4$]-90 (30-B) : 30 min pre-treatment with [bmim][$MeSO_4$]/DMSO (ratio of IL/DMSO – 90:10) followed by bleaching

[bmim][$MeSO_4$]-100 (30-B) : 30 min pre-treatment with [bmim][$MeSO_4$]/DMSO (ratio of IL/DMSO - 100:0) followed by bleaching

[bmim][$MeSO_4$]-50 (45-B) : 45 min pre-treatment with [bmim][$MeSO_4$]/DMSO (ratio of IL/DMSO - 50:50) followed by bleaching

[bmim][$MeSO_4$]-75 (45-B) : 45 min pre-treatment time with [bmim][$MeSO_4$]/DMSO (ratio of IL/DMSO - 75:25) followed by bleaching

[bmim][$MeSO_4$]-90 (45-B) : 45 min pre-treatment with [bmim][$MeSO_4$]/DMSO (ratio of

IL/DMSO – 90:10) followed by bleaching

[bmim][$MeSO_4$]-100 (45-B) : 45 min pre-treatment with [bmim][$MeSO_4$]/DMSO (ratio of IL/DMSO - 100:0) followed by bleaching

[bmim][$MeSO_4$]-50 (60-B) : 60 min pre-treatment with [bmim][$MeSO_4$]/DMSO (ratio of IL/DMSO - 50:50) followed by bleaching

[bmim][$MeSO_4$]-75 (60-B) : 60 min pre-treatment time with [bmim][$MeSO_4$]/DMSO (ratio of IL/DMSO - 75:25) followed by bleaching

[bmim][$MeSO_4$]-90 (60-B) : 60 min pre-treatment with [bmim][$MeSO_4$]/DMSO (ratio of IL/DMSO – 90:10) followed by bleaching

[bmim][$MeSO_4$]-100 (60-B) : 60 min pre-treatment with [bmim][$MeSO_4$]/DMSO (ratio of IL/DMSO - 100:0) followed by bleaching

CHAPTER 1

INTRODUCTION

1.1 Background

Large quantities of biomass residues are generated from agricultural processing in South Africa annually and poor utilisation of these invariably leads to land pollution. Sugarcane bagasse (SCB) is an abundant agricultural lignocellulosic by-product of sugarcane after the cane stalks are crushed and the juice is extracted. Utilising lignocellulosic materials to replace fossil-based fuels and chemicals without competing for land is a major concern not only in South Africa but globally as well (Liu *et al.* 2007; Walford 2008). SCB contains lignin, hemicellulose and cellulose and should be pre-treated in an economically sound and green manner to obtain the different component fractions to meet the requirements put forward in the principles of Green Chemistry (Anastas and Beach 2007). One of the principles of Green Chemistry is the reduction and recyclability of a solvent.

A group of molten salts with glass transition or melting temperatures below 100 °C known as ionic liquids (ILs) have been used to replace volatile organic compounds used in the pre-treatment of biomass (Wang *et al.* 2011; Zhang *et al.* 2015). Ever increasing interest in ionic liquids is a result of their unique properties such as non-flammability, recyclability, extremely low vapour pressure, high chemical and thermal stability, and excellent structure and property designability.

ILs can also extract cellulose under mild conditions (Jiang *et al.* 2011; Lu, Xu and Wang 2014). Production of cellulose nanocrystals (CNCs) from biomass extracted cellulose using an ionic liquid is a new approach which replaces the use of strong acids during hydrolysis.

The use of 1-butyl-3-methyimidazolium hydrogen sulphate has similar properties to hydrogen sulphate in terms of removing the amorphous regions of cellulose and increasing the yield of crystalline cellulose (Man *et al.* 2011; Mao *et al.* 2015; Tan, Hamid and Lai 2015). Many of the currently used technologies employ the use of non-green organic solvents for the extraction of cellulose from biomass. The limitations of these solvents are their volatility, toxicity, and difficulty for solvent recovery, use of high temperatures and pressures, and instability in applications (Ding *et al.* 2012; Akhtar *et al.* 2016).

ILs consists of an organic cation (e.g. imidazolium) and an organic (e.g. acetate) or inorganic (e.g. chloride) anion (Karimi and Taherzadeh 2016). Recently, lignocellulosic biomass was pre-treated with ILs to dissolve it and the latter is published widely as a green solvent that can effectively extract cellulose from biomass. The dissolution of cellulose using ionic liquids was discovered in 2002 by Swatloski *et al.* (2002) and co-workers. The process of dissolution of cellulose is considered a success when the solvent effectively breaks down the intermolecular hydrogen bonds in cellulose. Moreover, the dissolution of cellulose is dependent on the acidic nature of the ILs and is highly successful during protonation at low pH and deprotonation at high pH (Abe, Fukaya and Ohno 2012).

Crystalline regions of cellulose can be extracted as cellulose nanocrystals (CNCs) traditionally obtained from the hydrolysis of cellulose by concentrated acids (Kargarzadeh *et al.* 2012; Lu and Hsieh 2012; Börjesson and Westman 2015; Mao *et al.* 2015). The length of rigid and rod-shaped CNCs varies from tens to hundreds of nanometres and the diameter between 1-100 nm (Fortunati *et al.* 2013). CNCs have low density, biocompatibility and biodegradability, high flexibility, good thermal properties, modifiable properties (Šturcová, Davies and Eichhorn 2005; Fortunati *et al.* 2013). The inherent stiffness and high degree of crystallinity makes it suitable for a range of applications (Sheltami *et al.* 2012).

1.2 Problem statement

The large amounts of sugarcane waste fills up landfills and causes land pollution. Utilising SCB to extract the cellulose and convert it to useful bio-based products will reduce the current environment issues.

1.3 Aim

The aim of this study was to extract cellulose nanocrystals from sugarcane bagasse using polar ionic liquids followed by cellulose nanocrystal structural characterisation. The first step is the fractionation of sugarcane bagasse with different ionic liquids 1-butyl-3-methylimidazolium methyl sulphate ([bmim][$MeSO_4$]) or 1-butyl-3-methylimidazolium hydrogen sulphate ([bmim][HSO_4]) to obtain cellulose. The amounts of lignin and hemicellulose removed and the regenerated cellulose yield was determined. The extracted cellulose was then treated with 1-butyl-3-methylimidazolium hydrogen sulphate ([bmim][HSO_4]), the latter was both a catalyst and a solvent to obtain cellulose nanocrystals.

1.4 Objectives

- To determine which IL: 1-butyl-3-methylimidazolium hydrogen sulphate or than 1-butyl-3-methylimidazolium methyl sulphate will effectively remove lignin.
- To determine whether ILs/DMSO mixtures be more effective in removing lignin and hemicellulose effectively?
- Can ILs extract cellulose nanocrystals directly from biomass at a short reaction time?

1.5 Thesis outline

Chapter 1: Introduction

Background to the study is outlined.

Chapter 2: Literature review

Introduction of the biomass types, composition of SCB and pre-treatment of biomass using different techniques including ILs, nanocellulose and its applications.

Chapter 3: Experimental

Theory of instruments used to characterise SCN and CNCs.

Experimental section of the pre-treatment of SCB with ILs and IL/DMSO mixtures and conversion of extracted cellulose with [bmim][HSO_4] to CNCs.

Chapter 4: Results and Discussion

The results from the pre-treatment of SCB with ILs and the discussion of the results based on literature.

Chapter 5: Conclusion

Bibliography

Appendices

CHAPTER 2

LITERATURE REVIEW

2.1 Lignocellulosic biomass

"Biomass is considered as renewable source of energy because it releases heat energy for work when combusted in air (oxygen) or allowed to undergo natural decomposition and can be replenished unlike fossil fuels" (Mohlala *et al.* 2016). Therefore, there is an equal distribution of CO_2 released during combustion and the amount absorbed during photosynthesis- the process being known as "carbon neutral". As much as biomass is usually referred to as plant-based materials, biomass is also inclusive of animal-based materials since "biomass is a biological material derived from living, or recently living organisms or dead organic material" (Mohlala *et al.* 2016). Lignocellulosic biomass includes forest residues (hardwood and softwood); agricultural residues (SCB, palm trunk, corn stover, wheat straw, corn cob, coconut husks, wheat rice, and empty fruit brunches); industrial residues and municipal solid waste (pulp and paper processing waste); energy crops (switch grass) and food wastes (Lee, Hamid and Zain 2014; Akhtar *et al.* 2016). Lignocellulosic biomass is a renewable, sustainable resource that can replace or supplement fossil fuels used for liquid fuel and chemical production.

SCB is a fibrous agricultural lignocellulosic by-product of sugarcane after a process of crushing and extraction of the juice from sugarcane (*Saccharum officinarum*) stalk. It is an abundant, renewable, inexpensive, and readily available cellulose rich material (Sun *et al.* 2004; Kaur and Uppal 2015). Sugarcane is a very tall grass with big stems, is largely grown in countries like Brazil, India, South Africa, Cuba, Australia, Mexico, and Peru according to

Rípoli, Molina Jr and Rípoli (2000). SCB can be considered either as waste that contributes to land pollution or can be converted to useful products (Contreras *et al.* 2009).

Hulett (2013) reported that in South Africa 2.2 million tons of sugar is generated per season from six milling companies with 14 sugar mills operating in the sugarcane-growing regions with an average annual production of 19.9 million tons of sugarcane. In a recent presentation by Cele (2017) the tonnage of sugarcane crushed per year to extract the cane juice is shown on Table 2-1 below with a decrease over the past 3 years.

Table 2-1. Amounts of crushed sugarcane in tons per year.

Crushed sugarcane per year (tons)			
Year/s	**2013/14**	**2014/15**	**2015/16**
Crushed cane in tons	20 032 696	17 755 504	14 561 401

SCB and molasses are sugar industrial waste used to generate electricity in sugar mills, produce ethanol, manufacture paper and animal feed (Mohlala *et al.* 2016). SCB is eco-friendly, cheap and also gives low pollutant indexes (Loh *et al.* 2013). Utilization of SCB have been reported by several authors; it is an effective adsorbent for industrial effluent wastewater treatment, textile treatments, is a raw material in: animal feeds, drug manufactures, enzymes and fertilizers, production of biofuels, production of cellulose and nanocellulose (Pandey *et al.* 2000; Sasaki, Adschiri and Arai 2003; Liu *et al.* 2007; Raymundo *et al.* 2010; Mandal and Chakrabarty 2011; Karatzos, Edye and Doherty 2012; Chen *et al.* 2013; Loh *et al.* 2013; Maryana *et al.* 2014; Gardare *et al.* 2015; de Oliveira *et al.* 2016; Mohlala *et al.* 2016; Tahir *et al.* 2016).

2.1.1 Composition of sugarcane bagasse

Lignocellulosic biomass example SCB, is a major source of cellulose, an abundant natural renewable resource (Zhang *et al.* 2010). (Zhang *et al.*, 2010). Lignocellulose consists mainly of three groups of organic polymers: cellulose and hemicellulose which form part of carbohydrates and lignin (Figure 2-1) held together by the non-covalent forces and covalent cross-linkages in lignocellulosic biomass (Zhong *et al.* 2016). Lignocellulose also contains various other organic compounds including protein, small quantities of waxes, sugars, salts and insoluble ash (Sun *et al.* 2004; Mandal and Chakrabarty 2011; Ghaffar and Fan 2013). The composition of the SCB reported by several authors was cellulose is ± 40-55 %, hemicellulose ± 25-35 % and lignin ± 15-25 % (Pandey *et al.* 2000; Sun *et al.* 2004; Mandal and Chakrabarty 2011; Espinoza-Acosta *et al.* 2014; Templeton *et al.* 2016). The structure of the plant cell wall is shown in Figure 2-1.

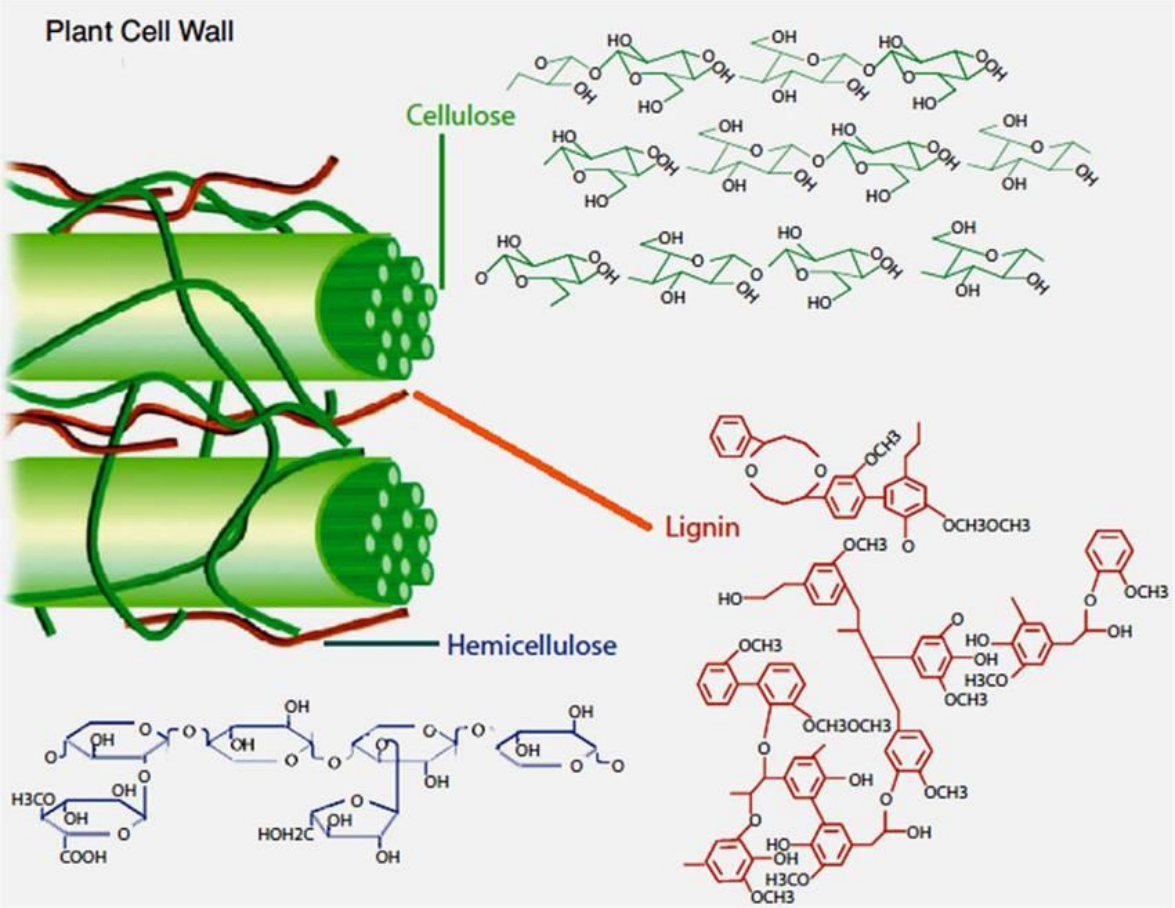

Figure 2-1. Structure of the plant cell wall depicting cellulose, lignin and hemicellulose (Bamdad, Hawboldt and MacQuarrie 2017).

2.1.2 Hemicellulose

Hemicellulose is an amorphous polymer composed of hetero-polysaccharides which are xylose, arabinose, galactose, glucose, and mannose (Figure 2-2). Xylans are the most abundant which can constitute to more than 30 % (mass/mass) dry mass in hemicelluloses (Sun *et al.* 2004; Lan, Liu and Sun 2011). Hemicellulose is crosslinked with multiple polysaccharide polymers which are formed through biosynthetic route different from that of cellulose. Hemicellulose has a degree of polymerisation in the order of 200-300 units and it is less ordered than cellulose, although some may form crystalline units. They are a supporting material in the cell wall as filler between cellulose and lignin. Hemicellulose is

very hydrophilic, soluble in alkali and easily hydrolysed into sugars (Berg *et al.* 2005; Hill 2007). The structure of hemicellulose is shown in Figure 2-2.

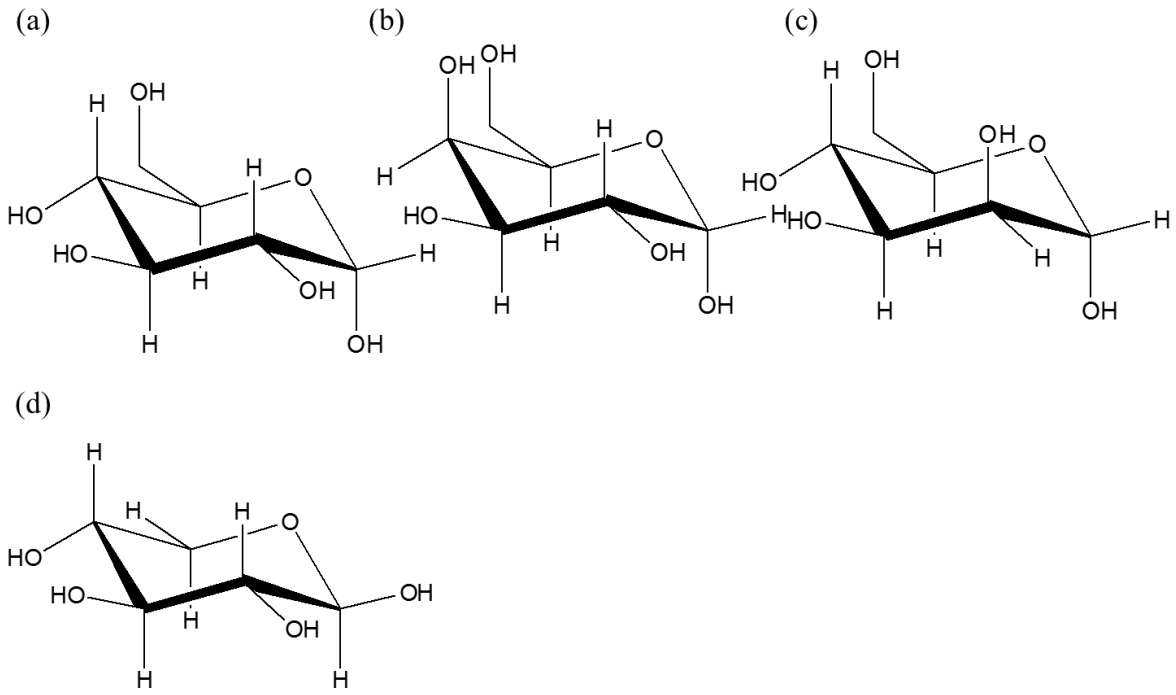

Figure 2-2. Structure of hemicellulose; (a) glucose, (b) galactose, (c) mannose and (d) xylose (Sun *et al.* 2004).

2.1.3 Lignin

Lignin is a hydrophobic polymer that adds strength and rigidity to cell walls and constitutes between 15 to 40 % mass fraction of dry matter of plants (Ghaffar and Fan 2013). Lignin is an extremely complex three-dimensional polymer formed by radical coupling polymerization of p-hydroxycinnamyl, coniferyl and sinapyl alcohols (Figure 2-3). The structure of lignin is shown in Figure 2-3.

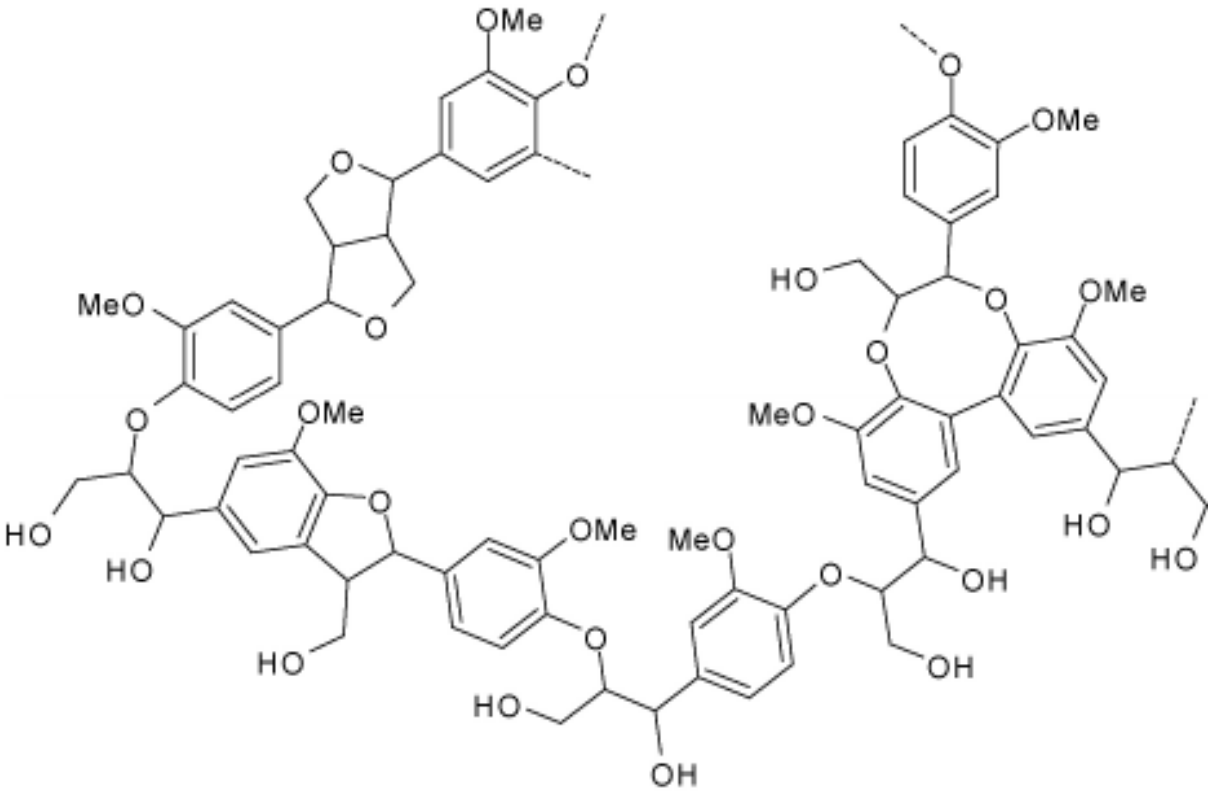

Figure 2-3. Structure of lignin (Custodis *et al.* 2015).

These three lignin compounds: p-coumaryl, coniferyl and sinapyl alcohols are precursors of the monolignols: p-hydroxyphenyl (H), guaiacyl (G) and syringyl (S) phenylpropanoid units (Figure 2-4), which show different abundances in lignin from different plant tissues and cell wall layers (Ghaffar and Fan 2013). About 40-60 % of all inter-unit linkages in lignin are a result of an ether bond. A linkage called β-O-4 linkage which is a variety of ether and carbon-

carbon bonds interlink these monolignols. Phenyl propane units form three-dimensional net structures from different types of linkages which makes a complete degradation of non-regular lignin macromolecules difficult. Lignin does not have a model chemical and physical structure due to its structural complexity as seen on Figure 2-3 (Kirk 1971; Akin and Benner 1988; Baurhoo, Ruiz-Feria and Zhao 2008). The structure of lignin precursors is shown in Figure 2-4.

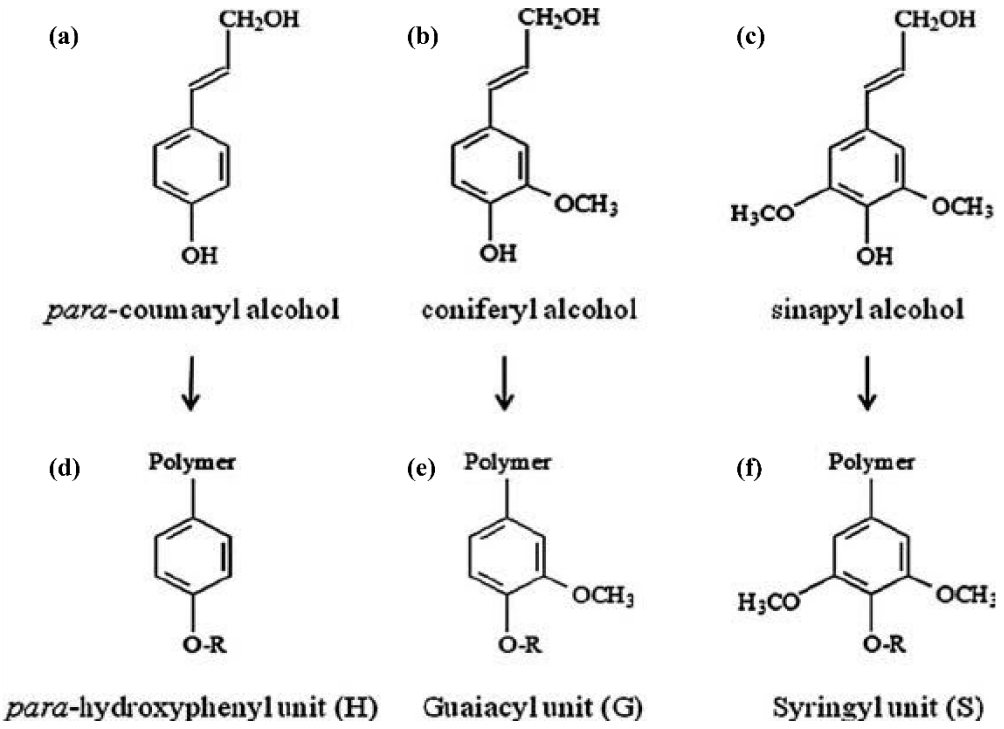

Figure 2-4. Structure of three lignin precursors; (a) *para*-coumaryl alcohol, (b) coniferyl alcohol and (c) sinapyl alcohol; and their monolignols units (d) *para*-hydroxyphenyl (H), (e) guaiacyl (G) and (f) syringyl (S) (Moon *et al.* 2011).

2.1.4 Cellulose

Cellulose is a major constituent of all plant materials including wood, cotton, cereal straws, sugarcane bagasse, rice straws etc. It forms about one-third of plant tissues and it is constantly replenished by photosynthesis. Thus, it is the most abundant and renewable natural resource on earth. Cellulose is the main structural component that provides strength and stability to the plant cell walls and the fibres (Rowell 2005; John and Thomas 2008). Cellulose is formed from repetitive D-glucose units, which are linked through β-1,4-D-glycosidic linkages at C_1 and C_4 position (Figure 2-5). Cellulose is the most used biomaterial due to its structural and physical properties, high tensile strength and biocompatibility. Its high tensile strength arises from multiple hydrogen bonding interactions resulting in a semicrystalline polymer containing highly structured crystalline regions. Thus cellulose consists of crystalline and amorphous regions (Isik, Sardon and Mecerreyes 2014). The structure of inter- and intramolecular hydrogen bonds of cellulose is shown in Figure 2-5.

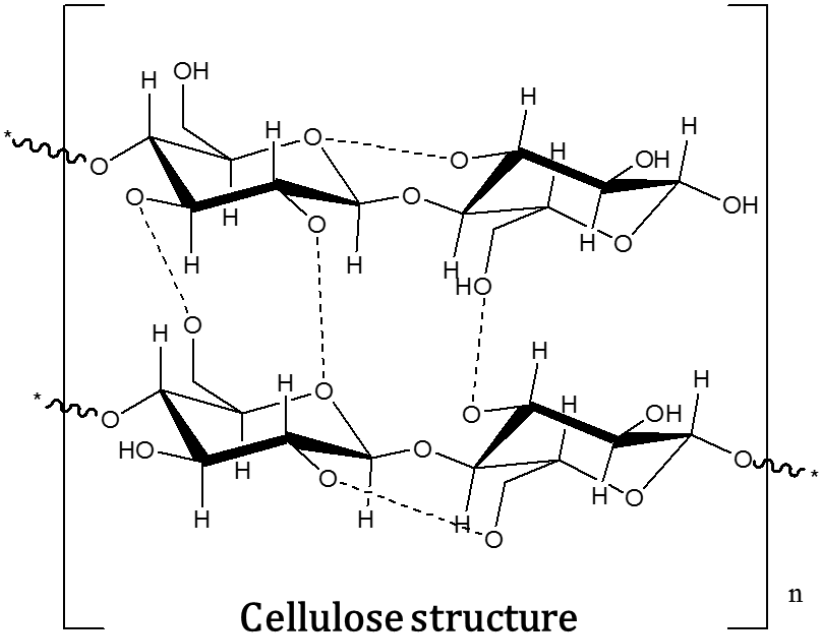

Figure 2-5. Structure of cellulose depicting inter- and intramolecular hydrogen bonds (Isik, Sardon and Mecerreyes 2014).

There are different molecular orientations of cellulose known as polymorphs which results from inter- and intramolecular bonds in cellulose. There are six polymorphs of cellulose, namely cellulose I, cellulose II, cellulose III_I, cellulose III_{II}, cellulose IV_I and cellulose IV_{II} (Wada *et al.* 2001; Nishiyama *et al.* 2003). Cellulose I is the native form of cellulose which can exist in the α or β form that are different with respect to hydrogen bond patterns and the β-1,4-anhydroglucose linkages (Atalla and Vanderhart 1984; Atalla and VanderHart 1999; Nishiyama *et al.* 2003). The pre-treatment of cellulose I by mercerisation produces cellulose II (Wada *et al.* 2001; Nishiyama, Langan and Chanzy 2002; Nishiyama *et al.* 2003; Wada *et al.* 2004). (Wada *et al.*, 2001, 2004; Nishiyama, Langan and Chanzy, 2002; Nishiyama *et al.*, 2003). Cellulose III is obtained by treatment of either cellulose I or cellulose II with liquid ammonia. Samples of cellulose III prepared from cellulose I are often referred to as cellulose III_I in order to distinguish them from the allomorph cellulose III_{II} prepared from cellulose II. The detailed structural differences between cellulose III_I and cellulose III_{II} have not been

established. Cellulose IV_I and cellulose IV_{II} is obtained by heating both cellulose III_I and cellulose III_{II}.

A summarised diagram of the six cellulose allomorphs is shown in Figure 2-6 below.

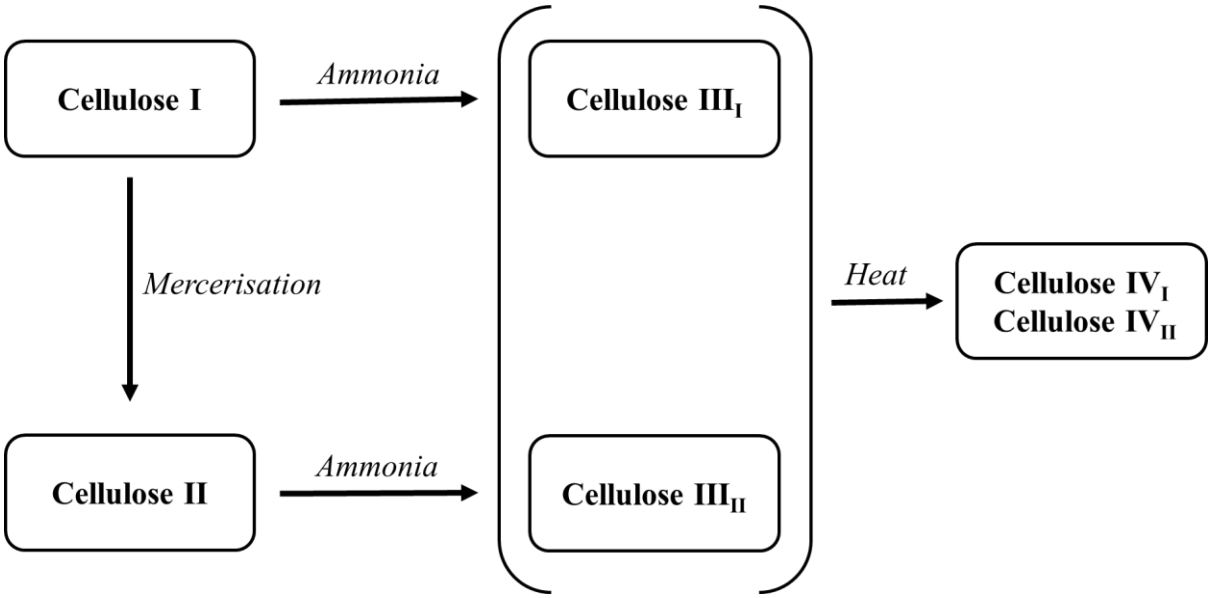

Figure 2-6. Illustration of interconversion of cellulose six allomorphs.

2.2 Pre-treatment methods of lignocellulosic biomass

Lignocellulosic biomass is the primary building block of plant cell walls. The complexity in the hierarchy of the structure of biomass is the main obstacle for key components fractionation, where cellulose, hemicellulose, and lignin are hindered by many physicochemical, structural and compositional factors (Lee, Hamid and Zain 2014). The pre-treatment process is a way of disrupting the complex structure of lignocellulose (Agbor *et al.* 2011) which is bonded by cross linkages of covalent bonds and non-covalent forces by removing hemicelluloses and lignin (Sindhu, Binod and Pandey 2016). There are several types of pre-treatment methods that are used for biomass deconstruction. These methods are categorized into physical (also known as mechanical), chemical, physicochemical and

biological pre-treatment methods as shown in Figure 2-7 (Lee, Hamid and Zain 2014; Akhtar *et al.* 2016).

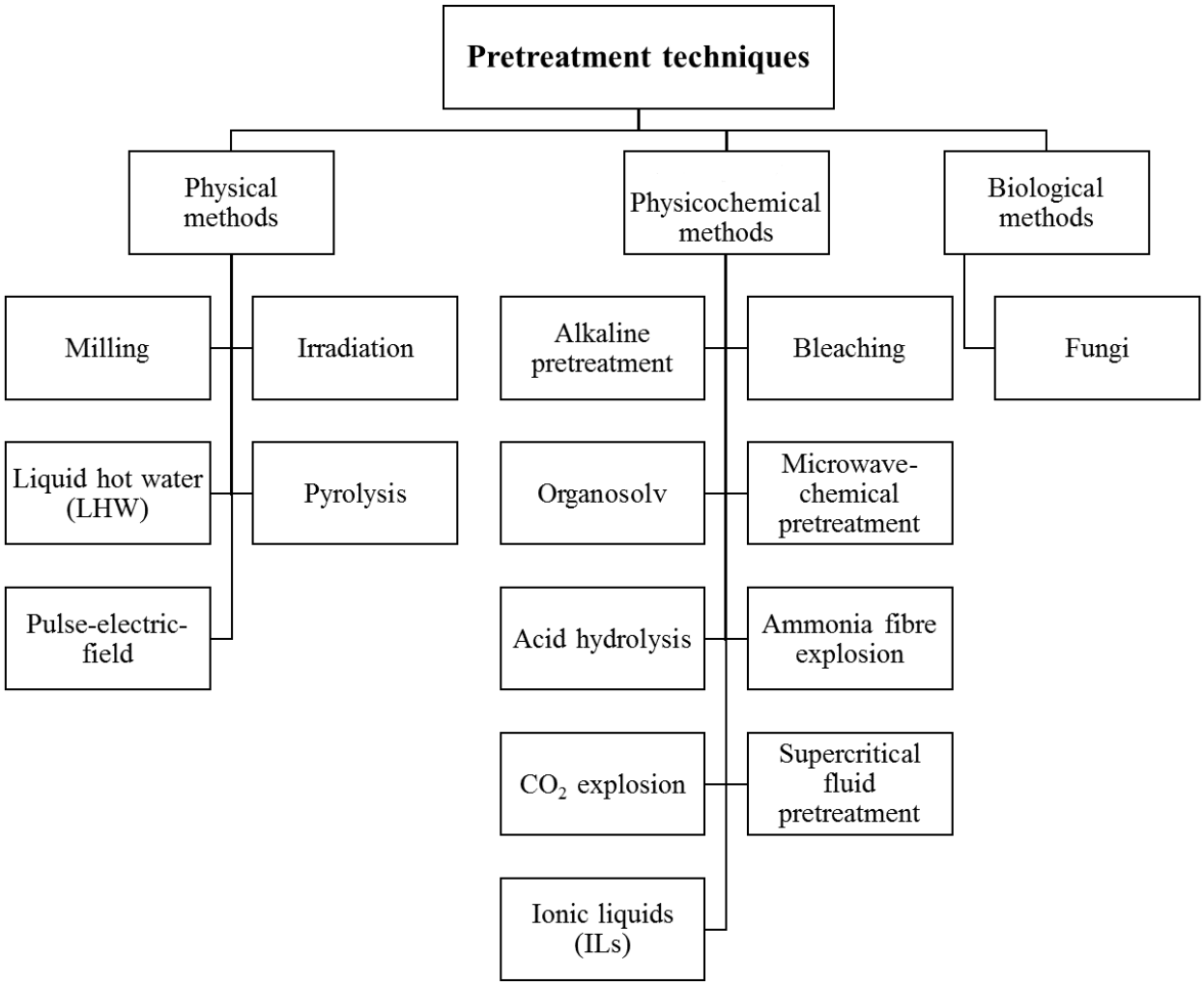

Figure 2-7. Summary of biomass pre-treatment techniques (Lee, Hamid and Zain 2014).

2.2.1 Physical methods

Physical methods include milling, irradiation, and liquid hot water, pyrolysis and pulse-electric-field also known as ultrasound (Akhtar *et al.* 2016). In ball milling, the particle size of biomass is reduced with the degree of crystallinity of cellulose. However, this method consumes energy and requires high power (Fan, Lee and Beardmore 1980; Taherzadeh and Karimi 2008; Alvira *et al.* 2010). Irradiation is a technique that reduces the molecular mass of cellulose. Moreover, it yields high amounts of reducing sugars and enzymatic hydrolysis improvement. However, it is very expensive and not applicable in industry (Taherzadeh and Karimi 2008). The removal of hemicellulose and lignin while hydrating cellulose under high pressure is known as liquid hot water (LHW). This technique is corrosion resistant and is not selective to biomass size. The toxicity is also non-existent due to no chemicals being used. It is also selective to biomass with an exception of softwood (Mosier *et al.* 2005; Dien *et al.* 2006; Martin *et al.* 2011). The rapid decomposition of cellulose to gaseous molecules (H_2 and CO) to produce less volatile products above 300 °C is known as pyrolysis. The disadvantage of using this technique is the low decomposition rate of cellulose (Sarkar *et al.* 2012). The use of an electric field to increase the mass permeability and the mechanical breakdown of plant tissue from biomass is known as pulse-electric field. This technique can be operated at ambient conditions where low energy is required (Kumar *et al.* 2009).

2.2.2 Biological methods

Biological method is a pre-treatment technique that employs the usage of a metabolic microorganism to degrade both lignin and hemicellulose during the pre-treatment. The metabolism of these microorganisms which are white, brown or soft-rot fungi which enhances the enzymatic saccharification rate during the pre-treatment of biomass (Akhtar *et al.* 2016; Sindhu, Binod and Pandey 2016). This technique can effectively remove lignin and

hemicellulose from biomass leaving cellulose. The advantage of this technique is that it consumes low energy, no toxic compounds are released to the environment, thus eco-friendly, no recycling of chemicals needed. However, it is very time consuming (Akhtar *et al.* 2016; Sindhu, Binod and Pandey 2016).

2.2.3 Physicochemical methods

A pre-treatment technique that requires low temperatures and high alkali concentration is known as alkaline pre-treatment. The alkali medium breaks the ester bonds between lignin, hemicellulose and cellulose while cellulose remains intact. A disadvantage of this method is that it results in an altered structure of lignin and the alkaline catalyst is costly (Samayam and Schall 2010; Brodeur *et al.* 2011). An oxidizing agent (bleaching) is used to oxidatively remove lignin and hemicellulose from biomass by using oxygen as a catalyst. The reaction takes place at low temperatures and short reaction time. Bleaching degrades lignin and hemicelluloses matrix, releasing cellulose fibres (Pereira *et al.* 2010). The organosolv process heats up an organic liquid with water to partially remove hemicellulose and dissolve lignin. Moreover, cellulose remain intact with the recovery of pure lignin (Sun and Cheng 2002; Pan *et al.* 2006). However, toxic inhibitors are formed and the solvent must be recycled. The process that utilizes a microwave and aqueous solution's thermal and non-thermal effects as a way of removing lignin and hemicellulose is known as microwave-chemical pre-treatment. The resulting cellulose is from an accelerated reaction which improves the carbohydrate content. It is expensive and impossible to perform in a large scale (Zhu *et al.* 2006; Narayanaswamy *et al.* 2013). Acid hydrolysis is a simple technique that is "operated under very high temperatures with dilute acid or under low temperatures with concentrated acids" (Akhtar *et al.* 2016). Hemicellulose is completely hydrolysed to a high yield and no operational energy is required. However, the recyclability of acids is costly and it produces

toxic compounds (Taherzadeh and Karimi 2007). In addition to these methods, there are other pre-treatment techniques i.e. ammonia fibre explosion (AFEX), CO_2 explosion and supercritical fluid pre-treatment which are less effective on lignin and hemicellulose and requires high pressure (Zheng *et al.* 1995; Brodeur *et al.* 2011).

2.3 Ionic liquids (ILs)

2.3.1 Properties of ILs

Many of the currently used technologies employ the use of non-green organic solvents for the extraction of cellulose from biomass. The limitations of these solvents are volatility, toxicity, and difficulty for solvent recovery, use of high temperature and pressure, and instability in applications (Ding *et al.* 2012; Akhtar *et al.* 2016). ILs have been used for many aspects, ranging from media for organic synthesis and catalysis to lubricants, and more recently have generated much interest as replacements for environmentally damaging volatile organic solvents (Berg *et al.* 2005).

ILs consists of an organic cation (e.g. imidazolium) and an organic (e.g. acetate) or inorganic (e.g. chloride) anion (Karimi and Taherzadeh 2016). Common cations and anions that forms ILs are shown in Figure 2-8.

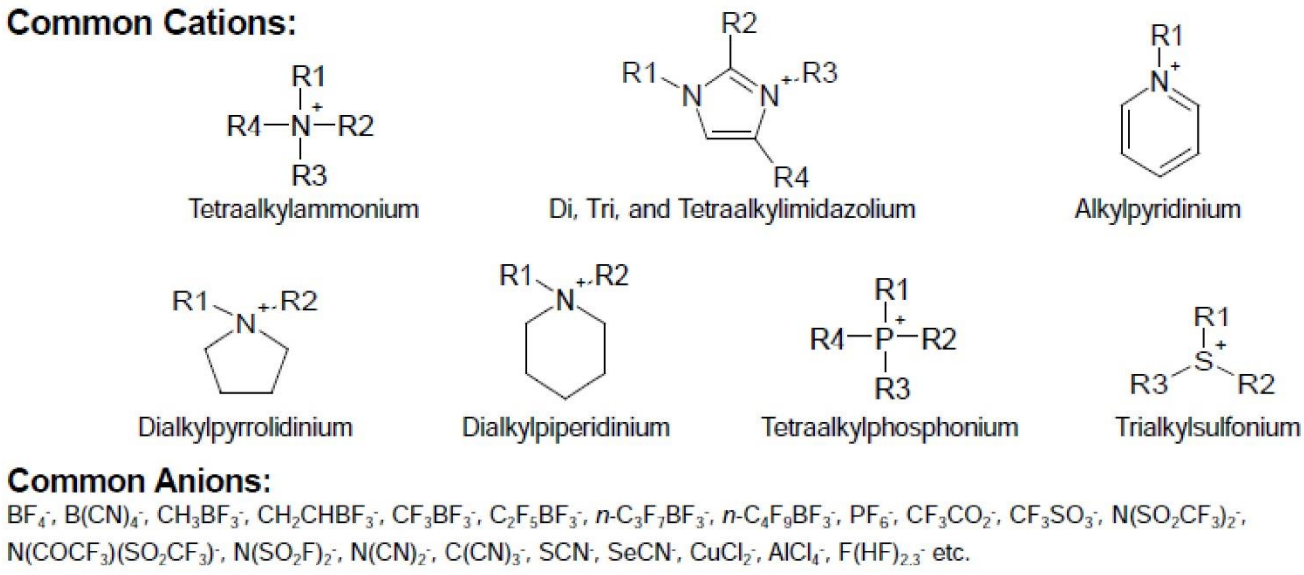

Figure 2-8. Illustration of common cations and anions that form ILs (Moosavi 2013).

Many ILs are non-volatile, non-explosive, stable at a wide range of temperatures and reaction condition severities and compatible with a wide array of organic and inorganic functional chemicals and solvents (Swatloski *et al.* 2002; Romero *et al.* 2008; Lan, Liu and Sun 2011; Karatzos, Edye and Doherty 2012; Isik, Sardon and Mecerreyes 2014; Abushammala, Krossing and Laborie 2015; Zhang *et al.* 2015). ILs are also non-toxic (Romero *et al.* 2008), which makes them suitable solvents to replace the common solvents used in biomass pre-treatment.

2.3.2 Dissolution of cellulose in ILs

The nature of IL enables them to be labelled “green solvents” have widened their application from cellulose to lignocellulosic biomass due to their ability to extract biomass components (Mäki-Arvela *et al.* 2010; Brandt *et al.* 2011; Isik, Sardon and Mecerreyes 2014). ILs can selectively fractionate biomass which serves as another advantage over other pre-treatment methods (Silveira *et al.* 2015). Over the years a lot of research has been done in the ability of ionic liquids to dissolve cellulose from biomass.

As Li *et al.* (2016) wrote, “it has been reported that ILs have the ability of dissolving biopolymers, especially cellulose, and reducing the crystallinity of cellulose, thus enhancing the enzymatic hydrolysis of cellulose”. Dissolution of carbohydrates with ILs is dependent on the physical and chemical properties of ILs which can be tuned by adjusting their anions and cations (Zakrzewska, Bogel-Łukasik and Bogel-Łukasik, 2010; da Costa Lopes *et al.*, 2013). The dissolution of cellulose is the disruption of inter and intra-chain hydrogen bonds on the cellulose structure (Swatloski *et al.*, 2002). Cellulose contains numerous intermolecular or intramolecular hydrogen bonds which plays a role in inhabitation of cellulose extraction efficiency (Zhong *et al.*, 2016). The hydrogen bonding between the anion and cellulose is much stronger than the cation and cellulose. Ionic liquids with strong hydrogen bond accepting ability are designed to incorporate into the side chains of anions (Zhang *et al.*, 2015). The solubility of cellulose have been linked mostly with ILs containing anions with high hydrogen-bond basicity such as chloride, phosphates, phosphonates and carboxylates (Pinkert *et al.*, 2009). However, it is not only the hydrogen-bond basicity that plays a role but the hydrogen-bond acidity. ILs with high hydrogen-bond acidity has a low cellulose solubilisation (Zhao *et al.*, 2008; Pinkert, Marsh and Pang, 2010) compared to the ones with high hydrogen-bond basicity. Moreover, the high hydrogen-bond acidity favours a very high solubility of lignin (Pu, Jiang and Ragauskas, 2007; Lee *et al.*, 2009) as shown when biomass was pre-treated with ILs 1,3-dimethylimidazolium methyl sulfate, $[C_1C_1im][MeSO_4]$, and 1-butyl-3-methylimidazolium methyl sulfate, $[C_4C_1im][MeSO_4]$ (Pu, Jiang and Ragauskas, 2007).

2.4 Bleaching

Silveira *et al.* (2015) reported that in order to reach desirable effects when extracting cellulose from biomass, two or more pretreatment techniques can be used. In this study, the

additional technique used in the removal of residual lignin and hemicellulose after IL pre-treatment was bleaching. The main objective of bleaching is to increase the brightness of the SCB fibers after IL pretreatment to make it suitable for the preparation of CNCs by removal of lignin and hemicelluloses completely. Bleaching degrades lignin and hemicelluloses matrix, releasing cellulose fibers (Pereira *et al.* 2010). This is accomplished by a series of treatments involving chlorine, caustic and oxidizing agents, such as hypochlorites, chlorine dioxide, and peroxides, which solubilise and selectively oxidize to the colourless state any trace of coloured material remaining. Bleaching of SCB plant fibers is purification of colloidal cellulose. It is a continuation of the alkali solution process (Pulp and Industry 1993).

There are four basic conditions that affect the chemical reactions in bleaching, namely temperature, time, concentration and pH of the solution (Hise and Hintz 1990; Pulp and Industry 1993). The practical temperature ranges varies with different bleaching agents. An increase in temperature speeds up the bleaching reaction. The longer the time that the pulp is exposed to a chemical, the greater the extent of bleaching, provided the other factors remain constant (Pulp and Industry 1993). There are two very important factors in choosing the bleaching agent; reactvity and selectivity. Reactivity is the rate and extent of which the lignin reacts with the bleaching agent. Selectivity is the rate of reaction of the bleaching agent with lignin in relation to the rate of reaction of the bleaching agent with carbohydrates (van Heiningen *et al.* 2003).

The following are bleaching methods that are used, namely; oxygen delignification, chlorine bleaching, ozone and peroxide bleaching.

2.4.1 Oxygen

Oxygen delignification which is also known as oxygen bleaching is a bleaching method that uses oxygen coupled with alkali to effectively remove lignin from the pulp (van Heiningen *et al.* 2003). This process reduces the emission of toxic compounds to the environment which are chlorinated lignin's (resultant of chlorine bleaching). It is also a lower cost compared to other bleaching methods due to oxygen being less pricy. However, it has a low reactivity and low selectivity when it comes to the removal of lignin and requires high temperature and pressure (van Heiningen *et al.* 2003).

2.4.2 Ozone

Ozone is an oxidising agent that is capable of bleaching the pulp by extensive delignification. However, ozone is not selective to lignin only but even cellulose is degraded and the pulp strength is compromised. It is also an expensive technique to operate (McDonough 1992).

2.4.3 Chlorine

Chlorine is a bleaching technique that removes residual lignin that is soluble in alkali medium. The solubilisation takes place in a solution of $pH < 2$ so that chlorine is not hydrolysed to hypochlorous acid which affects cellulose negatively (McDonough 1992). Chlorine removes small amounts of lignin and is therefore not a preferable method. Moreover, chlorine is a major environmental hazard due to the bleaching process resulting in chlorinated organic compounds as by-products (McDonough 1992).

2.4.4 Hypochlorite

Calcium and sodium hypochlorite are cheap and have the ability of bleaching the pulp. As much as hypochlorite is capable of removing lignin, it produces chloroform as a by-product. Moreover, it degrades cellulose since it is not selective (McDonough 1992).

2.4.5 Peroxide bleaching

Hydrogen peroxide is a weak acid and a strong oxidizing agent. It improves pulp quality, decrease environmental emissions and has lower bleaching cost. Under alkaline conditions, it forms perhydroxyl anion (HOO^-) which is very effective in reacting with various coloured carbonyl structures in lignin. Hydrogen peroxide increases the brightness of the pulp. Hydrogen peroxide decomposition is very vital for the delignification but the rate of decomposition should be kept low to avoid excessive cellulose degradation. The delignification reactions are conducted under alkaline conditions (McDonough 1992; Pulp and Industry 1993).

2.5 Nanocellulose

Nanocellulose (NC) is a product or extract of native cellulose. There are three types of nanocellulose (Lin and Dufresne 2014): Bacterial cellulose (BC), cellulose nanofibrils (CNFs) and cellulose nanocrystals (CNCs) (Abitbol *et al.* 2016). CNF morphology is soft and long chained due to both individual and aggregated nanofibrils made of alternating crystalline and amorphous cellulose domains as shown on Figure 2-9. Long cellulosic chains make it difficult to determine the length of CNF, the width varies from 10 to 100 nm depending on the source of cellulose, defibrillation process and pre-treatment (Lin and Dufresne 2014). CNCs are rigid rod-like crystals with diameter in the range of 10–20 nm, can also be in the

range of 5-70 nm and lengths of a few hundred nanometres (Liu *et al.* 2014; de Carvalho Mendes *et al.* 2015).

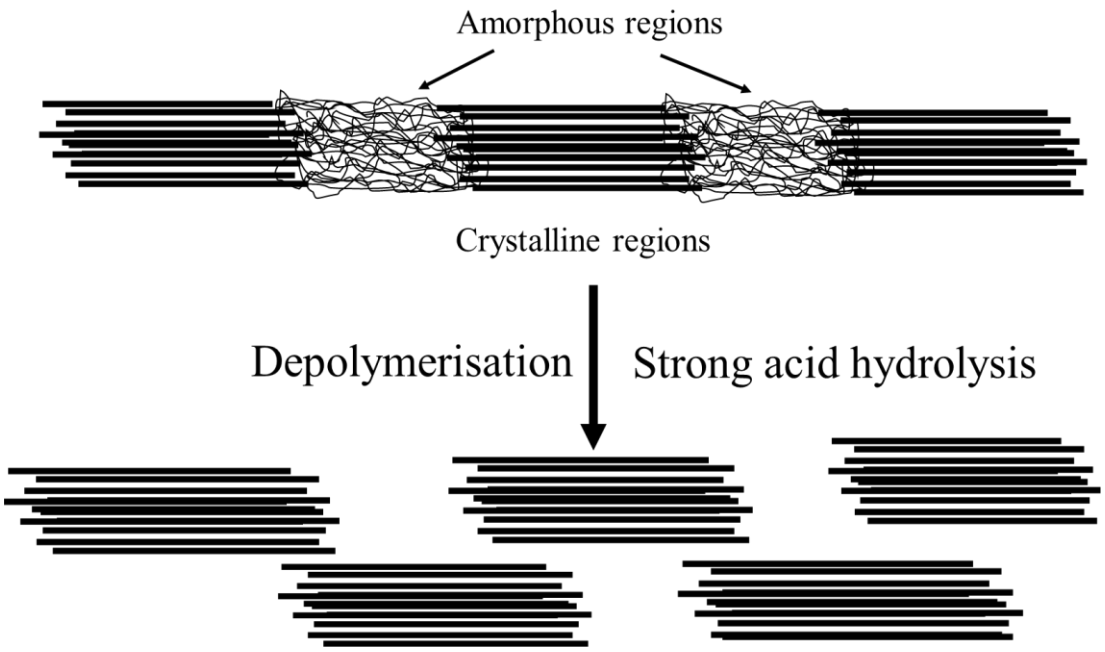

Figure 2-9. Structure of cellulose crystalline and amorphous regions.

There are different ways in which to convert the cellulose to CNCs: ultrasonic treatment, oxidation, and enzymatic hydrolysis, strong acid hydrolysis of cellulose and IL hydrolysis of cellulose.

2.5.1 Ultrasonic treatment

Ultrasonic treatment is a sono-chemical technique used to obtain nanocellulose. Ultrasonication is coupled with acid hydrolysis to obtain CNCs in either water or maleic acid medium. The method results is extremely poor yields of nanocellulose; water as a medium with 2-5 % yield and maleic acid as a medium with 10 % yield (Filson and Dawson-Andoh 2009).

2.5.2 Oxidation

Oxidation is done in a system containing 2,2,6,6-tetramethylpiperidine-1-oxy (TEMPO)-NaBr-NaOCl coupled with ultrasonication to produce surface carboxylated CNCs. The hydrolysis of amorphous region of cellulose occurs with stable CNC aqueous suspension. However, this method is highly toxic and costly (Qin *et al.* 2011).

2.5.3 Enzymatic hydrolysis

Enzymatic hydrolysis uses combined pre-treatment methods such as mechanical shearing, acid hydrolysis and enzymatic hydrolysis. However, this method has only been reported to result in microfibrils cellulose (MFC) than CNCs (Pääkkö *et al.* 2007; Duran *et al.* 2011).

2.5.4 Acid hydrolysis of cellulose

CNC can be extracted from cellulosic biomass using strong acid hydrolysis. The hydrolysis conditions and cellulose source affect the surface chemistry and particle size of isolated CNC particles (Shafiei-Sabet, Hamad and Hatzikiriakos 2012). As natural nano-scaled material, CNCs possess diverse characteristics different from traditional materials, including special morphology and geometrical dimensions, crystallinity, high specific surface area, rheological properties, liquid crystalline behaviour, alignment and orientation, mechanical reinforcement, barrier properties, surface chemical reactivity, biocompatibility, biodegradability and lack of toxicity (Ng *et al.* 2015). Colloidal aqueous suspensions of CNCs are known to form chiral nematic ordered structure above a critical concentration and birefringent gel-like material at even higher concentrations (Peng *et al.* 2011). The formation and characteristics of chiral nematic ordered domains in suspension depend on size, polydispersity, physical dimension, surface charge, and the ionic strength of the CNC particles.

An important characteristic of CNCs, when prepared in sulphuric acid, is that they possess negative charges on their surface due to the formation of sulphate ester groups during acid treatment, which enhances their stability in aqueous solutions (Peng *et al.* 2011). "The presence of surface hydroxyl groups on the CNCs may permit further modification to alter its hydrophilicity, provide a stabilization matrix for anchoring metallic nanoparticles, or prepare the biomaterial for targeted applications" (Lam *et al.* 2012). The acid hydrolysis of cellulose with sulfuric acid degrades cellulose and the thermal stability of CNCs is greatly affected (Yu *et al.* 2013; Tang *et al.* 2015). Hydrochloric acid has also been used as an alternative for sulfuric acid hydrolysis of cellulose to CNCs. However, as much as it results in much more thermally stable CNCs, the yield is also poor (Yu *et al.* 2013).

The disadvantages of using concentrated acids are:

- Toxicity and hazardous (Mäki-Arvela *et al.* 2010; Man *et al.* 2011).
- Difficulty in separating nanocellulose from acidic solution (Man *et al.* 2011).
- It is time consuming and tedious (Man *et al.* 2011; Tan, Hamid and Lai 2015).
- Requires corrosion resistance reactors (Man *et al.* 2011).
- Common acids result in poor CNCs yield and poor thermal stability (Yu *et al.* 2013).

2.5.5 IL hydrolysis of cellulose to nanocellulose

In an attempt to produce more thermally stable CNCs and to improve the yield, ILs have been used to hydrolyse cellulose to nanocellulose (Abushammala, Krossing and Laborie 2015). The IL: [bmim][HSO_4] has similar properties to hydrogen sulphate in terms of removing the amorphous regions of cellulose and increasing the yield of the crystalline portion of cellulose (Man *et al.* 2011; Mao *et al.* 2015; Tan, Hamid and Lai 2015). (Man *et al.*, 2011; Mao *et al.*, 2015; Tan *et al.*, 2015). Moreover, [bmim][HSO_4] The ionic liquid acted as both a catalyst

and solvent due to its acidic properties in the hydrolysis microcrystalline cellulose (MCC) into nanocellulose (Tan, Hamid and Lai 2015). The [bmim][HSO_4] consists of sulphate groups which does not require dialysis or desulfonation which are both time consuming and complicated and mostly results in particle aggregation (Yu *et al.* 2013; Liu *et al.* 2014).

CNCs are usually produced from pulp or microcrystalline cellulose when ionic liquids are the solvent used in the hydrolysis process. Abushammala, Krossing and Laborie (2015) extracted CNCs using IL 1-ethyl-3-methylimidazolium acetate ([EMIM][OAc]) from wood which was then followed by bleaching. The IL of choice was capable of dissolving lignin and swelling cellulose fibres. Moreover, acted as a catalyst for cellulose hydrolysis. The outcome of their study resulted in a simultaneous defibrillation of wood and a production of CNCs directly from wood. The cellulose pulp had a crystallinity index of 70 % and the yield was 20 % of the original wood.

2.5.6 Application of CNCs

CNC is an emerging renewable nanomaterial that holds promise in many different applications (Orts *et al.* 2005; John and Thomas 2008; Eichhorn *et al.* 2010; Habibi, Lucia and Rojas 2010; Ibrahim *et al.* 2010; Khan *et al.* 2012; Zaman *et al.* 2012) such as:

- Pharmaceuticals,
- Electronic devices,
- Biosensors,
- Biocomposites,
- Paper industry,
- Paints and vanish,
- Modification of structural properties of other materials.

The advantages of nanocellulose are that it is renewable and biodegradable, cheap, recyclable and non-toxic. It has great mechanical properties and its nano-scaled dimensions open a wide range of possible properties to be discovered, interesting for the development of new materials (Peng *et al.* 2011; Brinchi *et al.* 2013). By appropriate modification of CNCs, various functional nanomaterials with outstanding properties can be developed.

CHAPTER 3

EXPERIMENTAL

3.1 Instrumentation

The quantification of carbohydrates and lignin before and after pre-treatment was analysed using high performance liquid chromatography (HPLC) and ultraviolet-visible spectroscopy (UV-Vis). The characterisation techniques of CNCs extracted from SCB are structural characterisation was done using attenuated total reflection-Fourier transform infrared (ATR-FTIR), scanning electron microscopy (SEM), transmission electron microscopy (TEM) and X-ray diffraction (XRD). Thermal properties of the material was done through thermogravimetric analysis (TGA) while dynamic light scattering (DLS) was used for particle size analysis.

3.1.1 High performance liquid chromatography (HPLC)

High performance liquid chromatography (HPLC) is a chromatographic separation analytical technique that has a liquid mobile phase and a stationary phase of inert solids (Levinson, 2001). The inert solid is usually porous silica particles with a high surface area, alumina or cellulose in a glass column. The solids are packed in a stationary phase inside a short column. The components present in the mixture are adsorbed onto the surface of the stationary phase or are dissolved in the mobile phase. HPLC consists of a mobile phase, pump, injection port, a column, a detector (Lee *et al.*, 1999) and a screen where the chromatograms are displayed after each run (Figure 3-1). The pump produces a uniform pressure. The injection volume of samples are also small (5 - 20 mm^3) with a slow flow rate of 0.5 – 5 cm^3 min^{-1} (Levinson, 2001). HPLC diagram is shown in Figure 3-1.

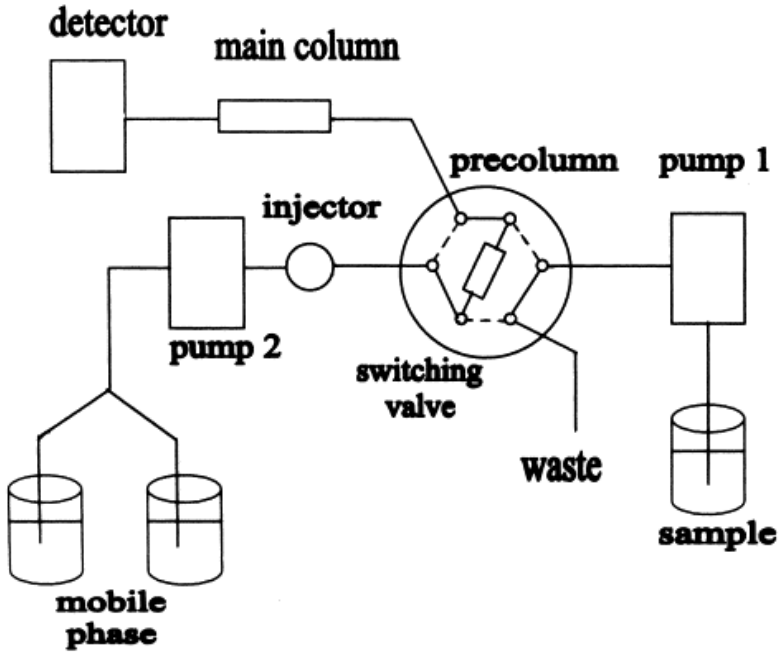

Figure 3-1. HPLC diagram reproduced from Lee *et al.* (1999).

3.1.2 Ultraviolet-visible spectroscopy (UV-Vis Spectroscopy)

Ultraviolet-visible spectrometry (Uv-Vis) is an analytical technique that absorbs visible and Ultraviolet radiation by the excitation of electrons from lower levels to higher levels (Skoog *et al.,* 2013). The analysis of a component is a mixture is obtained by the absorption of light at a specific wavelength thus the molecule is identified due to a unique ground state energy each electron in a molecule has (Skoog *et al.,* 2013). The absorption of light is used to obtain the concentration of samples. The UV-Vis instrument consists of a light source, diffraction grating, aperture, sample cuvette and a detector (Skoog *et al.,* 2013). The UV and/or visible light source as a single beam passes into a monochromator by an entrance slit where it is separated into desired wavelength through a dispersion device (Skoog *et al.*, 2013; Mäntele and Deniz, 2017). The sample beam passes through the exit slit to the electronic detector. The detector analyses the sample by quantifying the intensity of radiation absorbed or emitted by the material (Fifield and Kealey, 1995). Beer- Lambert's law is used to quantify the light transmitted and the intensity absorbed or emitted of the sample (Mäntele and Deniz, 2017).

Beer-Lambert's law states that the absorbance of a material sample is directly proportional to the concentration of the attenuated species in the material sample (Mäntele and Deniz, 2017)

Uv-Vis schematic diagram is shown in Figure 3-2.

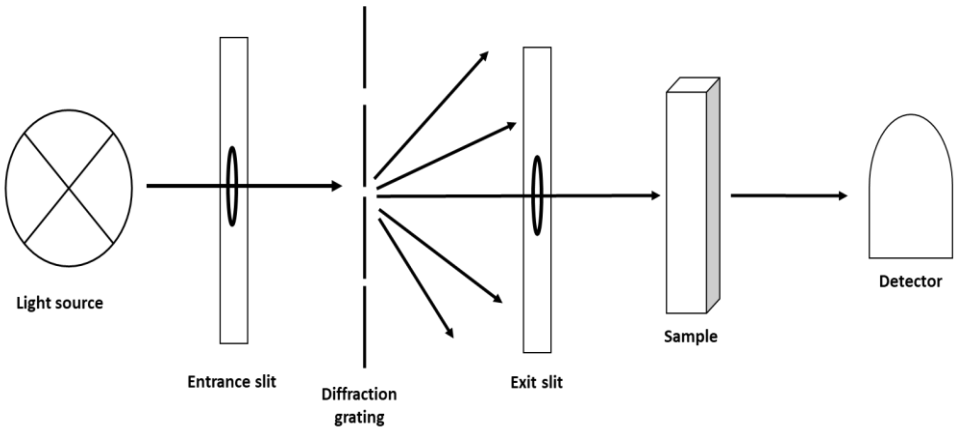

Figure 3-2 Schematic diagram of UV-Vis spectrophotometer.

3.1.3 Attenuated total reflectance-Fourier-transform infrared (ATR-FTIR)

Infrared (IR) is a class of an electromagnetic spectrum where absorption occurs as a result of molecular vibrations (Faix 1992; Stuart 2005). Fourier-transform infrared (FTIR) is a type of IR spectrometer that is used to obtain IR spectrum of molecules. It "is based on the idea of interference of radiation between two beams to yield an interferogram" (Stuart 2005). An interferogram is dependent on a signal that emits vibrations at a different pathlength. The Fourier-transform in FTIR is a concept of distance and frequency in the molecular analysis in IR spectroscopy (Faix 1992; Stuart 2005). FTIR diagram is shown in Figure 3-3.

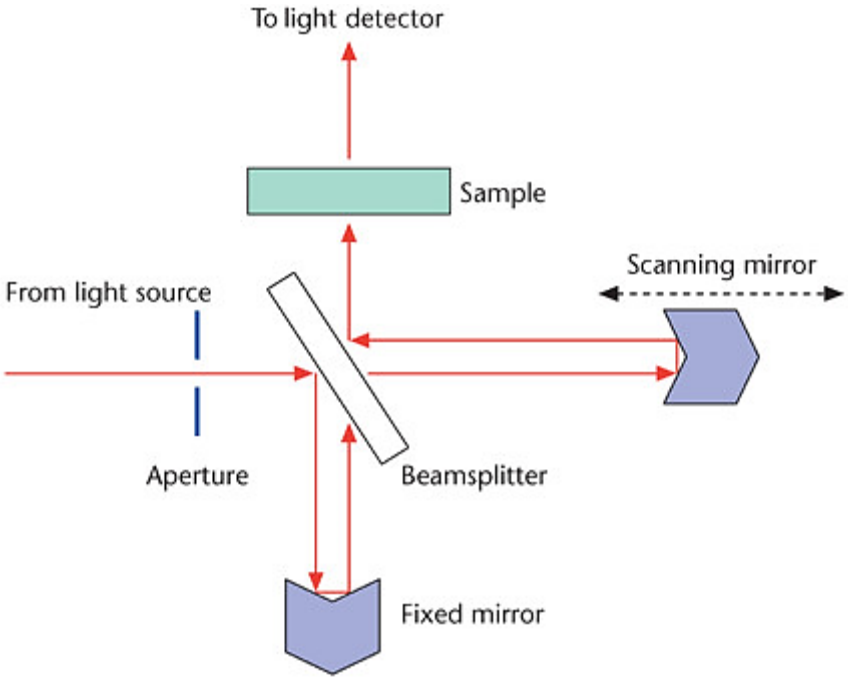

Figure 3-3. FTIR diagram (Gerwert and Kötting 2010).

Attenuated total reflectance (ATR) spectroscopy is a technique that can be coupled to an IR spectroscopy a total internal reflection phenomenon to help analyse samples that are hard to analyse on IR alone (Urban 1996; Stuart 2005). ATR relies the crystal allowing a beam of radiation to be totally internally reflected between the sample and the crystal, resulting in an angle of incidence. The angle of incidence must be greater than the critical angle. The critical angle is a "function of the refractive indices of two surfaces" (Stuart 2005). The molecule will selectively absorb the radiation further from the reflected crystal radiation, thus the beam losing energy due to distance. ATR is measured when the beam loses the materials radiation energy which results in absorption spectra of the materials (Urban 1996; Stuart 2005). An ATR diagram is shown in Figure 3-4.

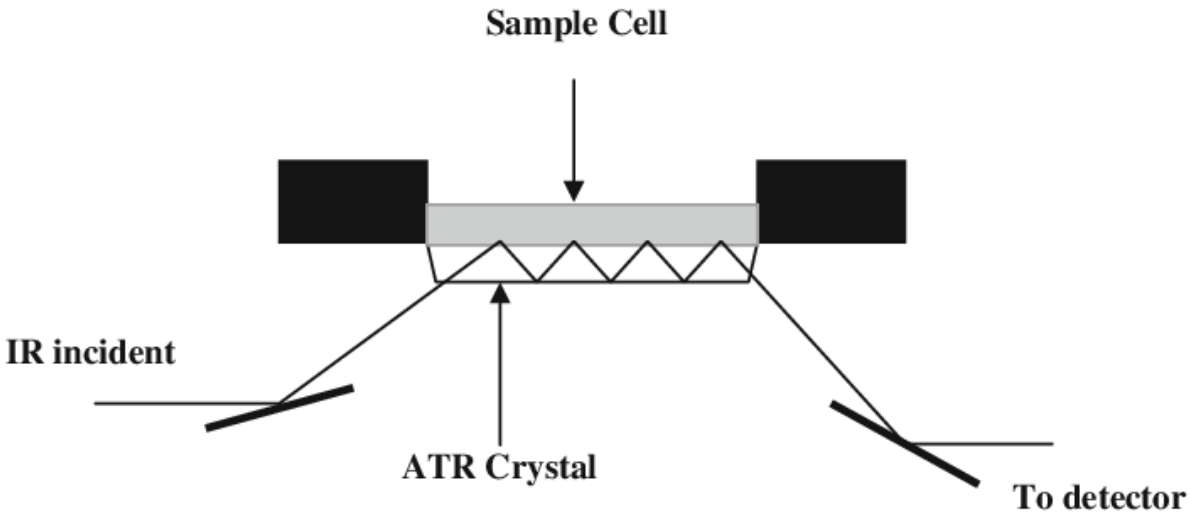

Figure 3-4. ATR diagram (Du and Zhou 2009).

3.1.4 Scanning electron microscopy (SEM)

A microscope that generates a variety of signals at the surface of solid specimens using a focused beam of high-energy electrons is known as scanning electron microscopy (SEM). The sample information obtainable from SEM varies from external morphology, crystalline structure and orientation of materials and the chemical composition of the material over scanning selected area of the surface (Reichelt, 2007). Image obtained from SEM should have the right resolution which is dependent on the electron probe and interaction of the electron probe with the material. Scanning an incident electron beam across the samples surface and producing energy from the collision of the primary electrons anode with the sample results in secondary electrons. The secondary electrons are collected by an electron detector (secondary) and image is produced (Shingange, 2016).

SEM diagram is shown in Figure 3-5.

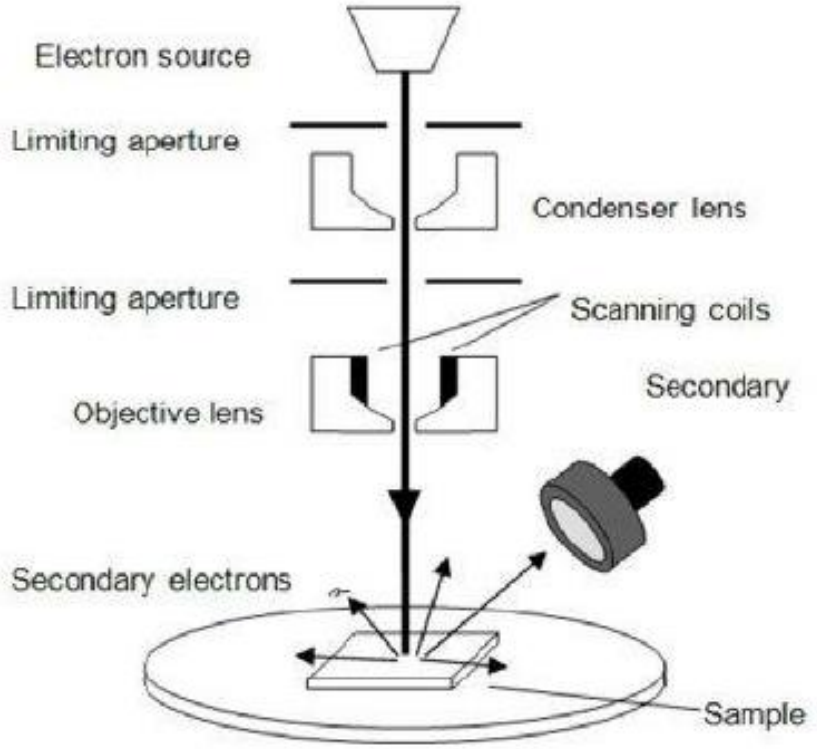

Figure 3-5. SEM diagram (Mukhopadhyay, 2015).

3.1.5 Transmission electron microscopy (TEM)

A high spatial resolution microscopic technique whereby a beam of electrons is transmitted through a specimen and results in an image is known as transmission electron microscopy (TEM) (Shingange, 2016). TEM is an electron microscope that is equipped with an electron gun, image producing system and image recording system. The electron gun is where the electron beams are produced with a condenser system responsible for focusing the beam on the object. The image producing system focuses the electrons that pass through to form real and highly magnified image through objective and projector lenses. The image recording system converts an electronic image into an image visible to the human eye through a digital camera (Ford, Joy and Bradbury, 2011). TEM diagram is shown in Figure 3-6.

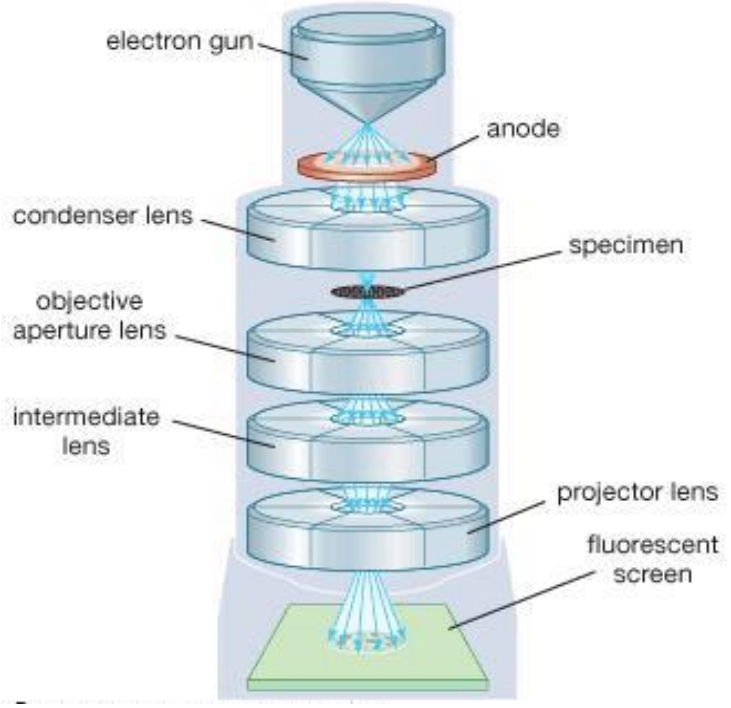

Figure 3-6. TEM diagram (Ford, Joy and Bradbury, 2011).

3.1.6 X-ray diffraction (XRD)

The non-destructive technique that is used to study crystal structures and atomic spacing of materials is known as X-ray diffraction (XRD) (Cao, 2004). The discovery of three dimensional diffraction gratings of crystalline substances for X-ray wavelengths was by Max von Laue in 1912 when he found similarities to the crystal lattice spacing of planes (Eckert, 2012). X-rays are generated by a heated filament in a cathode ray tube to produce fast moving electrons that are accelerating towards a target. Electrons gain sufficient energy to freely move in the inner shell of the target material and result in characteristic X-ray spectra. Constructive interference and diffracted rays result from the sample interaction with incident rays when conditions satisfy Bragg's Law ($n\lambda=2d \sin \theta$) (Cullity, 1978). An XRD diagram is shown in Figure 3-7.

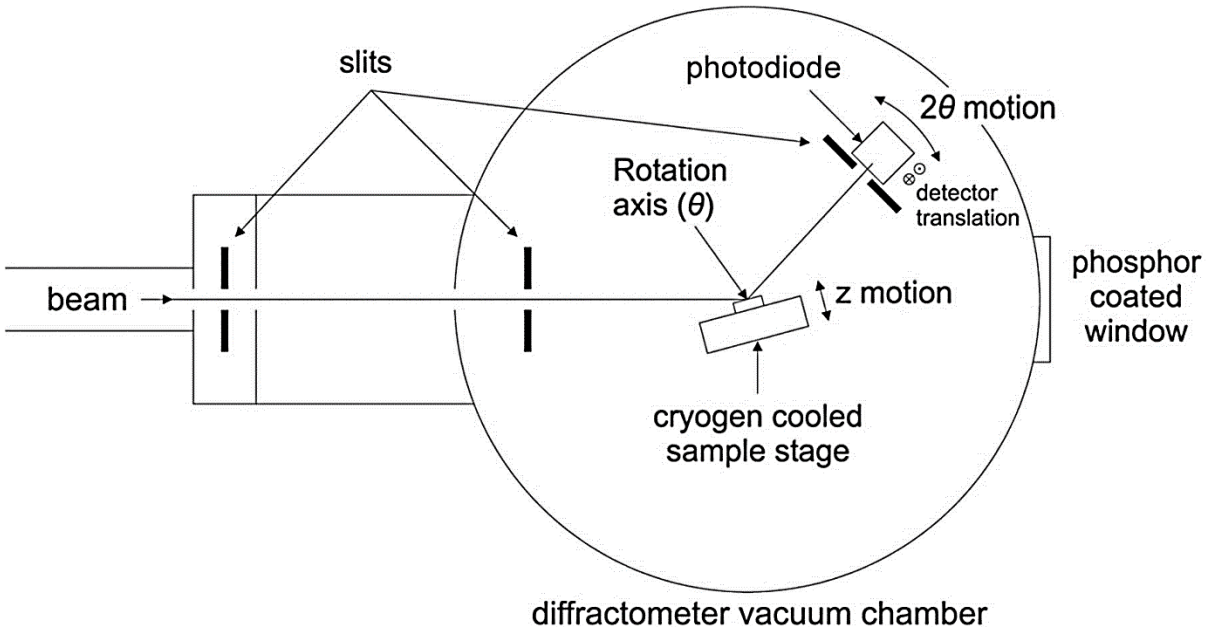

Figure 3-7. XRD diagram (Hatton *et al.* 2005).

3.1.7 Thermogravimetric analysis (TGA)

A thermal technique that can quantifies the mass of a sample with respect to temperature under inert or reactive gas is known as thermogravimetric analysis (TGA). This technique can give information on the weight loses due to: water loss, solvent loss, decarboxylation, oxidation, decomposition, pyrolysis and inorganic compounds, as well as the ash content of materials. These parameters are examples of TGA thermal analysis which are based on the type of materials. Samples are placed on a pan incorporated with a precision balance inside either a heated or cooled furnace whereby the required properties of the material are studied (Laye *et al.*, 2007). TGA diagram is shown in Figure 3-8.

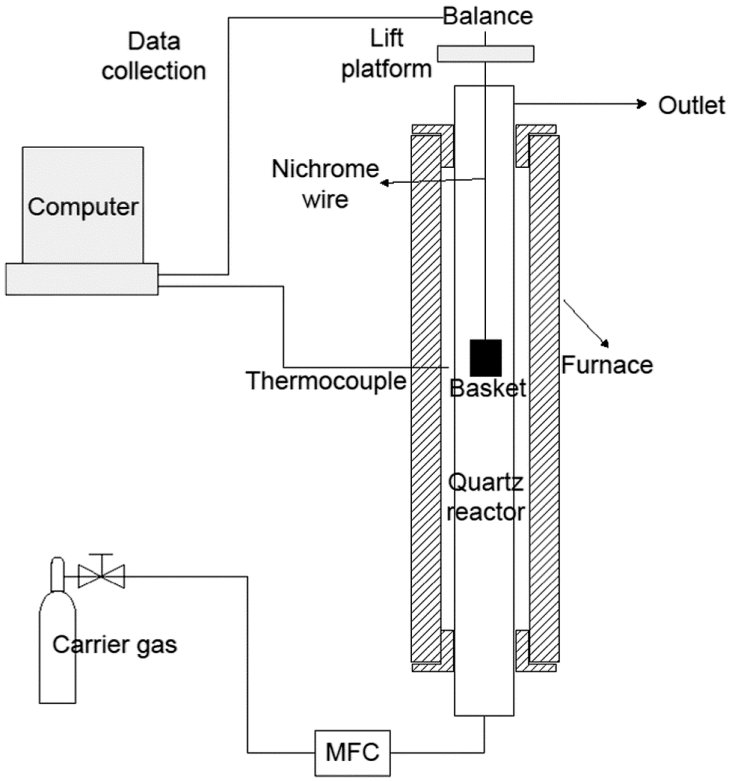

Figure 3-8. TGA diagram (Zhou *et al.*, 2015).

3.1.8 Dynamic light scattering (DLS)

A common technique for the random changes measured from a scattered suspension or solution of nanoparticles intensity is known as dynamic light scattering (DLS). The DLS applications are micelles, polymers, proteins, colloids, emulsions and nanoparticles. The illumination of a sample by a laser beam which results in a detection of scattered light (a scattering angle) through a fast photon detector. A review by Powers *et al.* (2006) found DLS a vital technique in the evaluation of size of particles, the distribution of particles and the zeta potential of a suspended nanomaterial. DLS diagram is shown in Figure 3-9.

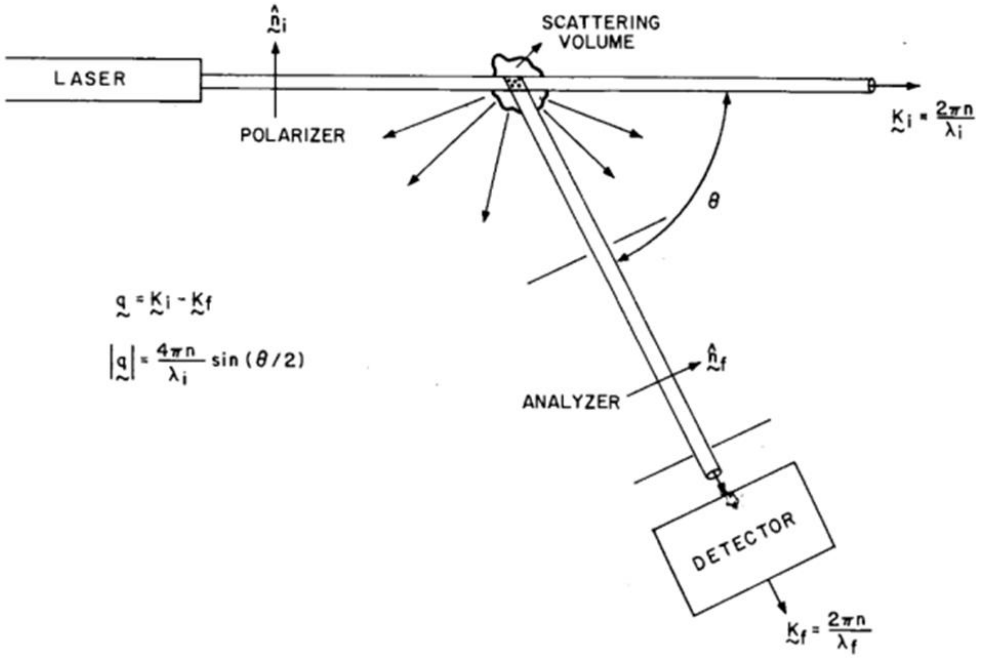

Figure 3-9. DLS diagram (Burchard, 1983).

3.2 Methodology

Two ILs: 1-butyl-3-methylimidazolium hydrogen sulphate ([bmim][HSO_4]) or 1-butyl-3-methylimidazolium methyl sulphate ([bmim][$MeSO_4$]) were used to pre-treat SCB to remove lignin and hemicellulose at varied times and at a fixed temperature. The results are discussed in section 4.2.

The pre-treatment of SCB with ILs/DMSO mixtures was to extract cellulose from biomass and to further extract CNCs from the extracted cellulose. Two ILs: [bmim][HSO_4] or [bmim][$MeSO_4$] were used to pre-treat SCB at different DMSO concentrations for both ILs. DMSO was used as a co-solvent to reduce the viscosity of the neat IL. Following the pre-treatment, the recovered solids, which contained the cellulose were pre-treated with IL [bmim][HSO_4] to obtain cellulose nanocrystals. After pre-treatment with [bmim][HSO_4], the

resulting pulp was bleached to remove the residual hemicellulose and lignin and recover the cellulose nanocrystals. The results are discussed in section 4.2.

3.2.1 Materials

3.2.1.1 Sugarcane bagasse

SCB manually depithed fibre was donated by the Sugar Milling Research Institute (SMRI, Durban, South Africa). SCB was ground at the Council for Scientific and Industrial Research (CSIR, Pretoria) in a KIKA WERKE M20 coffee grinder (IKA Mills, Wilmington, USA).

3.2.1.2 Reagents

Reagents used in this study were all purchased from Sigma Aldrich and used without further purification. All water used was purified by the Purite Select HP 40 water purifier (Purite Ltd, United Kingdom). The reagents used were 1-butyl-3-methylimidazolium hydrogen sulfate ([bmim][HSO_4]; 98 % (v/v)), 1-butyl-3-methylimidazolium methyl sulfate ([bmim][$MeSO_4$]; 98 % (v/v)), microcrystalline cellulose (MCC; > 99 % (m/m)), hydrogen sulfate (H_2SO_4; 72 % (v/v)), calcium carbonate ($CaCO_3$; > 99 % (m/m)), sodium hydroxide (NaOH; 98 % (m/m)), hydrogen peroxide solution (H_2O_2; 30 % (v/v)), ethanol (98 % (v/v)), alkali lignin (> 98 % (m/m)), dimethyl sulfoxide (DMSO; > 98 % (v/v)). The sugar standards were glucose, xylose, galactose, mannose and arabinose all had a purity of 99 % (m/m).

3.2.2 Experimental Methods

3.2.2.1 Sample preparation

The SCB sample was ground until the particle sizes were reduced as shown in Figure 3-10. The ground SCB sample was sieved using a mechanical sieve with different mesh sizes in the range of < 4 mm.

Figure 3-10. Photograph of milled SCB.

The sieved SCB was milled using a Retsch PM 100 (Retsch GmbH, Germany) laboratory ball miller. A 125 ml stainless steel grinding jar (volume of material inside the jar: 15-50 ml) with a mass of 1454 g was used (Figure 3-11). The maximum feed grain size was 4 mm which means that particles with sizes greater than 4 mm cannot be ground. Thirty (10 mm diameter) stainless steel balls with total mass of 121.70 g were used.

Figure 3-11. Photograph of the stainless steel grinding jar with stainless steel balls.

The power was 34 % which is directly proportional to the energy needed to grind sieved SCB sample. The operation time was 15 min and the speed of milling was 500 rpm. The conditions were optimised for best results resulting in SCB with particle size less than 150 μm (Figure 3-12 a-b). The ground SCB was stored in plastic bags at room temperature prior to pre-treatment with ILs.

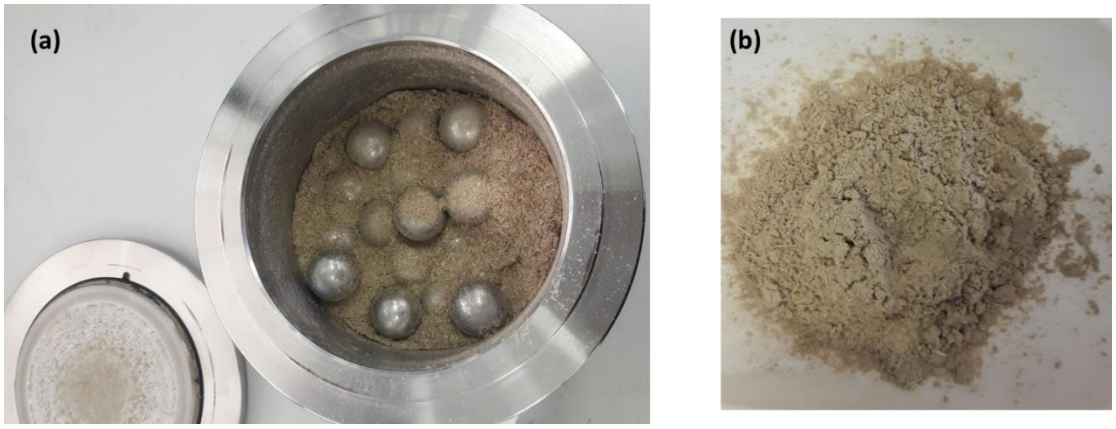

Figure 3-12. Photographs of (a) SCB during the milling process; and (b) milled SCB.

3.2.2.2 Composition analysis of untreated SCB

The compositional analysis for SCB was undertaken by the method prescribed by the National Renewable Energy Laboratory (NREL).

3.2.2.2.1 Moisture and ash content

Moisture and ash content were determined by Moisture & Ash analyser with a Computrac software (Computrac Max 5000) following NREL procedure for the determination of ash content in biomass (Sluiter *et al.* 2010) with optimisation of holding time. About 3.5-4.0 g of SCB was weighed on an aluminium dish and put on the instrument. The temperature for quantifying moisture content was 105 ˚C and for the ash content was at 575 ˚C. The samples were heated up to 105 °C for a period of 12 min. The samples were then ramped to 250 °C at 10 °C/min and held at this temperature for 30 min. The samples were then ramped to 575 °C at 20 °C/min and held at this temperature for 90 min. The instrument software called Computrac software, was used to calculate the moisture and ash content and reported it to 4 decimal places for all runs. The samples were run in quintuplicates. The mass for moisture and ash content was converted to % (m/m).

3.2.2.2.2 Carbohydrate and lignin quantification

Compositional analysis of cellulose, hemicellulose and lignin were carried out using the standard NREL procedure for determination of structural carbohydrates in biomass (Sluiter *et al.* 2008; Sluiter *et al.* 2010). Mixed sugar standards of known concentrations (0.05, 0.1, 0.2 and 0.4 %) were used to generate standard curves to calculate the concentration of released sugars. Each sample (300 mg, in duplicates) was treated with 3 ml of 72 % H_2SO_4 (v/v) at 30 °C for 1 h in a water bath. After the required time, the 72 % H_2SO_4 was diluted to 4 % H_2SO_4 by the addition of 84 ml of deionised water in 100 ml Schott bottles. Following this

step, the samples were then autoclaved at 121 °C for 1 h using an autoclave (Vertical Type Steam Steriliser, WM-340 Model, Taiwan). The hydrolase was neutralised with $CaCO_3$ until the pH was 7. The clear liquid was decanted and kept in labelled 60 ml sample vials for analysis of sugars by high performance liquid chromatography (Perkin Elmer Binary LC Pump 250 with 20 μL injection loop, Utah USA) and analysis of acid soluble lignin (ASL) by Uv-Visible Spectroscopy (Varian Cary 50, Uv-Visible Spectrophotometer, USA) at 280 nm. The solids remaining after the desired amount of liquid was decanted from the solution was used for the determination of acid insoluble lignin (AIL). The untreated SCB samples and NIST (National Institute of Standards and Technology, USA) standard SCB sample were analysed using HPLC with a refractive index detector (RI detector, Perkin Elmer LC-235, Diode Array Detector, Utah USA). Specifically, monosaccharides were determined using a Bio-Rad HPX-87P column (Bio-Rad Laboratories, Life Science Research, Hercules, CA) equipped with a Carbo-P guard column at 80 °C column temperature. The mobile phase was degassed deionised water with a flow rate of 0.6 ml min^{-1}.

The cellulose and hemicellulose content were determined as glucan and xylan content based on a calculation method adopted from Gao, Kumar and Wyman (2014). The following equations (Equation 3.1 and 3.2) represent the calculations and conversions of hydrolysed sugars to their polymers without any conversion since they represent the hydrolysed polymers. The amount of glucan and xylan are equal to the cellulose and xylose amounts, respectively.

Equation (3.1) was used for the calculation of glucan content:

$$\%\,\mathbf{Glucan} = \frac{(\mathbf{Glucose\ (mg)} + \mathbf{Cellobiose\ (mg)}) \times \mathbf{1.053/1.111}}{\mathbf{sample\ mass\ (mg)}} \times \mathbf{DF} \times \mathbf{100} \qquad \mathbf{(3.1)}$$

Whereby 1.053 was the mass conversion factor of cellubiose to glucose (mannose or galactose); 1.111 was the mass conversion factor of glucose to cellulose; and sample mass was amount of sample weighed for acid hydrolysis (~300 mg). DF was the dilution factor. The percentage glucan should give the cellulose content.

A sugar recovery standard (SRS) of glucose was used to obtain the corrected amount of glucan loss after acid hydrolysis. SRS sugar concentration was chosen by considering the sample concentrations. Glucose with mass 100 mg was dissolved in 10 ml deionised water. A pipetted 348 µL of 72% sulfuric acid was added to the solution. The SRS was autoclaved at 121 °C for 1 h using an autoclave. The hydrolase was neutralised with $CaCO_3$ until the pH was 7. The clear liquid was decanted and kept in labelled 60 ml sample vial for HPLC SRS analysis.

The amount of xylan content was calculated using Equation (3.2):

$$\%\,\mathbf{Xylan} = \frac{\mathbf{Xylose\ (mg)/1.136}}{\mathbf{sample\ mass\ (mg)}} \times \mathbf{DF} \times \mathbf{100} \qquad \textbf{(3.2)}$$

Whereby 1.136 was mass conversion of xylose to xylan and DF is the dilution factor. The percentage xylan should give the hemicellulose content.

The linear regression calibration curves of cellubiose, xylose and arabinose were used to calculate carbohydrates in the untreated SCB and pre-treated SCB using Equation (3.3):

$$y = mx + c \qquad \textbf{(3.3)}$$

Whereby the y value was the peak height of the standards; and the x value was the concentration of the standards.

The acid hydrolysis process fractionates lignin into acid soluble lignin (ASL) and acid insoluble lignin (AIL). The ASL was analysed using Uv-Vis spectroscopy, whereas AIL was obtained using crucibles.

ASL was calculated using Equation (3.4):

$$\% \mathbf{ASL} = \frac{\mathrm{UVab} \times \mathbf{DF} \times \mathbf{V_F}}{E \times \mathbf{ODW} \times \boldsymbol{l}} \times \mathbf{100}\% \qquad \textbf{(3.4)}$$

% ASL = percentage acid soluble lignin

UV_{ab} = measured absorbance

DF = dilution factor was 10

V_F = filtrate volume which was the total volume of solution after dilution during analysis and hydrolysis of samples (86.73 ml)

E = the lignin wavelength-dependent molar absorptivity coefficient (25 ml mg^{-1} cm^{-1})

ODW = Oven dry weight (determined by the removal of moisture content from biomass and is reported in milligrams; sample weight of biomass was taken as 100 mg for lignin calculations)

l = path length taken as 1 cm

AIL was obtained from the recovered solid after acid hydrolysis. The solid was filtered after the addition of hot 50 ml of deionised water for a shorter filtration time. The solids were transferred to a filtering crucible and dried at 105 ± 5 °C for 6 h. The crucibles were weighed before and after oven drying using the analytical balance (Kern ABS-N/ABJ-NM, Germany).

Equation 3.5 was used to calculate AIL, whereby the acid insoluble residue (AIR) was the remaining solids after oven drying.

$$\% \mathbf{AIL} = \frac{\boldsymbol{acid\ insoluble\ residue\ (AIR)}}{\mathbf{ODW}} \times \mathbf{100}\% \qquad \mathbf{(3.5)}$$

The total lignin amount was the sum of ASL and AIL in percentages.

A NIST SCB standard sample was used to verify the method used for the determining the ASL and the AIL.

3.2.2.3 Pre-treatment of SCB with ILs

3.2.2.3.1 Pre-treatment of SCB with [bmim][$MeSO_4$] or [bmim][HSO_4]

Ground SCB (1 g) was weighed on an analytical balance where the mass was recorded accurately using a weighing boat. The SCB was transferred to a round-bottom flask where 20 ml of either [bmim][$MeSO_4$] or [bmim][HSO_4] was added to the SCB. A stirrer bar was placed in the flask to ensure thorough mixing of the contents. The round-bottom flask was placed on a hot plate equipped with a stirrer function and the contents stirred at 200 rpm for the required time and temperature. The pre-treatment time was 4, 8 and 12 h respectively at 120 °C. The samples prepared with [bmim][HSO_4] were denoted by [bmim][HSO_4]-4, [bmim][HSO_4]-8 and [bmim][HSO_4]-12 for the pre-treatment time of 4, 8 and 12 h, respectively. The samples prepared with [bmim][$MeSO_4$]were denoted by [bmim][$MeSO_4$]-4, [bmim][$MeSO_4$]-8 and [bmim][$MeSO_4$]-12 for the pre-treatment time of 4, 8 and 12 h, respectively.

After the desired time was reached, 20 ml of ethanol was added to the round-bottom flask before the contents were transferred to a 50 ml beaker to wash the pulp. The contents were left to cool at room temperature. Repeated washing with the ethanol was done using 10 ml

quantities of ethanol to ensure the washing was properly done and the ILs was completely removed. The solid precipitate was recovered by centrifugation and filtered using a Munktel (AHLSTROM, Germany) 150 mm filter papers on a vacuum filtration. The mass of the precipitate was obtained using an analytical balance (Kern ABS-N/ABJ-NM, Germany). All IL-treated solids were dried overnight at 105 °C in a vacuum oven prior to analysis. The solids were analysed for sugars using HPLC, and IL insoluble lignin (ILIL) using Uv-Vis spectroscopy. ILIL was quantified based on the amount of lignin that was hydrolysed during acid hydrolysis. The conditions were similar to Section 3.2.2.2.2. The samples were analysed using an HPLC SEDEX Model 75 ELSD (Evaporative Light Scattering detector, SEDERE, France) detector. AIL was not quantified.

3.2.2.3.2 Pre-treatment of pulp with [bmim][HSO_4]

The recovered pulp obtained from the IL pre-treatment at different times was further pre-treated with IL [bmim][HSO_4] to obtained CNCs. However, the yield of the recovered pulp was drastically affected by the long reaction time of the SCB with both ILs, and it was not viable to add the IL for the extraction of CNCs. The discussion of the results are given in Section 4.2.2.

3.2.2.3.3 Pre-treatment of SCB using IL/DMSO mixtures

The SCB sample were first pre-treated separately with each of the ILs/DMSO mixtures: [bmim][$MeSO_4$]/DMSO or [bmim][HSO_4]/DMSO. Following the pre-treatment with IL/DMSO mixtures, the samples were bleached with 20 % H_2O_2 and 4 % NaOH solution for 3 h at 45 °C. Thereafter, the pre-treated samples, the recovered solids which contained the cellulose, were characterized for nanocellulose.

The IL/DMSO pre-treatment was done at 120 °C for 30, 45 and 60 min at varied DMSO concentrations (50, 25, 10 and 0 mass %) using an autoclave. The solid to IL ratio was 1: 20. Ethanol was used to wash the recovered solids until the IL was no longer present (Brandt *et al.* 2011); i.e. after washing with 5 x 10 ml of ethanol and until washing was clear. The recovered solids were dried overnight at 105 °C and weighed on an analytical balance to determine the mass recovered. About ~0.5 g of the recovered pulp was bleached with 20 % H_2O_2 and 4 % NaOH mixture (1:1 ratio) for 3 hours at 45 ˚C. After the desired time, the pulp was washed through centrifugation with deionised water until the pH was neutral (4 times washing with 20 ml deionised water). The solution was sonicated using a sonicator (Model UMC5, Integral Systems, South Africa) for 10 min at 10 °C. The aqueous suspension was quickly frozen by pouring liquid nitrogen (N_2) into the sample container and then freeze dried for 3 days using a SP SCIENTIFIC VirTis Pro freeze dryer (New York, USA) to remove excess water while maintaining the sample nature. The samples were kept in a desiccator for carbohydrate and lignin quantification; and CNC characterisation and quantification. The solid sample was analysed for sugars, while soluble lignin quantities were determined using the method in Section 3.2.2.2.2. The mass of the sample was determined using an analytical balance.

The samples pre-treated with [bmim][$MeSO_4$]/DMSO were denoted by [bmim][$MeSO_4$]-50, [bmim][$MeSO_4$]-75, [bmim][$MeSO_4$]-90 and [bmim][$MeSO_4$]-100 for the IL/DMSO concentrations of 50/50, 75/25; 90/10 and 100/0, respectively. The pre-treatment time was added at the end of the sample name in brackets i.e. [bmim][$MeSO_4$]-50 (30), [bmim][$MeSO_4$]-50 (45), and [bmim][$MeSO_4$]-50 (60) for the pre-treatment time of 30, 45 and 60 min in an autoclave, respectively.

The samples pre-treated with [bmim][HSO_4]/DMSO were denoted by [bmim][HSO_4]-50, [bmim][HSO_4]-75, [bmim][HSO_4]-90 and [bmim][HSO_4]-100 for the IL/DMSO concentrations of 50/50, 75/25; 90/10 and 100/0, respectively. The pre-treatment time was added at the end of the sample name in brackets i.e. [bmim][HSO_4]-50 (30), [bmim][HSO_4]-50 (45), and [bmim][HSO_4]-50 (60) for the pre-treatment time of 30, 45 and 60 min in an autoclave, respectively.

Bleached samples were denoted by a letter B after the time the sample reacted in the autoclave. The notation used was [bmim][$MeSO_4$]-50 (30-B), [bmim][$MeSO_4$]-75 (30-B), [bmim][$MeSO_4$]-90 (30-B), and [bmim][$MeSO_4$]-100 (30-B) for bleached 30 min pre-treated samples. The notation used was [bmim][$MeSO_4$]-50 (45-B), [bmim][$MeSO_4$]-75 (45-B), [bmim][$MeSO_4$]-90 (45-B), and [bmim][$MeSO_4$]-100 (45-B) for bleached 45 min pre-treated samples. The notation used was [bmim][$MeSO_4$]-50 (60-B) for bleached 60 min pre-treated sample, [bmim][$MeSO_4$]-75 (60-B) for bleached 60 min pre-treated sample, [bmim][$MeSO_4$]-90 (60-B) for bleached 60 min pre-treated sample, and [bmim][$MeSO_4$]-100 (60-B) for bleached 60 min pre-treated samples.

Bleached samples were denoted by a letter B after the time the sample reacted in the autoclave. The notation used was [bmim][HSO_4]-50 (30-B), [bmim][HSO_4]-75 (30-B), [bmim][HSO_4]-90 (30-B), and [bmim][HSO_4]-100 (30-B) for bleached 30 min pre-treated samples. The notation used was [bmim][HSO_4]-50 (45-B), [bmim][HSO_4]-75 (45-B), [bmim][HSO_4]-90 (45-B), and [bmim][HSO_4]-100 (45-B) for bleached 45 min pre-treated samples. The notation used was [bmim][HSO_4]-50 (60-B), [bmim][HSO_4]-75 (60-B), [bmim][HSO_4]-90 (60-B), and [bmim][HSO_4]-100 (60-B) for bleached 60 min pre-treated samples.

3.2.2.4 Characterisation techniques

Characterisation using a range of analytical techniques was done on the IL/DMSO SCB samples pre-treated for 60 min. The samples were characterised after bleaching was done.

3.2.2.4.1 Scanning electron microscopy (SEM)

Surface morphology of the IL/DMSO bleached freeze dried cellulose/nanocellulose sample was studied using a scanning electron microscope JEOL SEM (Model JSM-7500F, JEOL USA, Inc., USA) at an accelerating voltage of 3 kV. The samples were deposited on carbon tape mounted on sample stubs under vacuum at 20 mA for 2 min (Bio-Rad SEM coating system) and sputter coated with carbon to avoid charging during analysis. All samples were observed and imaged at 5 kV accelerating voltage at different magnifications.

3.2.2.4.2 Transmission electron microscopy (TEM)

To determine the fibre length, width, aspect ratio (length to width) and to indicate the aggregation state of the fibrils/crystals, highly diluted samples (in water) of the hydrolysed suspension of cellulose nanocrystals were analysed by Transmission Electron Microscopy (JEOL USA, Inc., USA). A 10 µl drop of the CNC suspension was dispensed onto a carbon coated copper grid, allowed to stand for 15 minutes and the excess fluid was wiped off with a Whatman No. 1 filter paper. The grid was air dried and viewed in the bright field mode at 80 kV.

3.2.2.4.3 Powder X-ray diffraction (P-XRD)

Powder X-ray diffraction (P-XRD) determinations were done on the CNC samples using a X-ray diffractometer (XPERT PRO PANalytical, Netherland) for crystal phase identification. The samples were run with Cu Kα radiation with a secondary monochromator ($\lambda = 0.1545$ nm) at 45 kV and 40 mA. The diffraction measurements were conducted at room temperature

in a Bragg-Brenton geometry with a scan range of 2Θ = 5-60^{o} using continuous scanning at a rate of 0.02 ^{o}/s. The crystalline structure was attributed according to literature (Sugiyama, Persson and Chanzy, 1991). The relative amount of crystallinity of the specimens was evaluated using Segal's crystallinity index (*CrI*) (Segal *et al.*, 1959). It is defined in Equation 3.6 below:

$$\% \boldsymbol{CrI} = \frac{\boldsymbol{I_{200} - I_{am}}}{\boldsymbol{I_{200}}} \times \mathbf{100} \qquad \textbf{(3.6)}$$

where I_{200} is the main peak at 2Θ = ~22.5˚ for cellulose I, whereas I_{am} is the diffraction intensity caused by the amorphous portion of cellulose at 2Θ = ~18˚.

3.2.2.4.4 Attenuated total reflection-Fourier transform infrared (ATR-FTIR) spectroscopy

The ATR-FTIR spectra for samples were recorded on a Spectrum 100 FT-IR spectrometer equipped with ATR sampling accessory (Perkin-Elmer instrument, USA). The spectra were collected in the transmittance mode from an accumulation of 32 scans at 8 cm^{-1} resolution over 4000-600 cm^{-1} range.

3.2.2.4.5 Thermogravimetric analysis (TGA)

The thermal stability of the cellulose samples were determined by TGA Q500 (TA instruments, USA). Samples were heated from 25 ˚C to 600 ˚C at a heating rate of 10 ˚C/min with a nitrogen flow rate of 25 ml/min. Measurements were performed under an inert nitrogen atmosphere to prevent any thermooxidative degradation of the materials.

3.2.2.4.6 Dynamic light scattering (DLS)

Particle size distribution was determined using a HORIBA LB 550 nanoparticle size analyser (HORIBA, Ltd. Kyoto Japan). The turbid aqueous sample suspension of nanocellulose (± 5 ml) was shaken and transferred to a quartz cuvette for analysis.

The CNC yield was calculated from the percentages of nanoparticle sizes obtained from DLS analysis. The freeze dried samples were weighed after analysis and the mass was recorded. The CNC yield was calculated using the recovered yield and the particle size distributed in DLS below 500 nm (Fan and Li, 2012) using Equation 3.7 below:

$$\% \text{ CNC Yield} = \frac{\mathrm{m}n}{\mathrm{M}} \times 100\ \% \qquad \textbf{(3.7)}$$

where:

m is the mass of total CNC obtained after freeze drying suspension.

n is the percentage of CNC particles size less than 500 nm analysed using DLS.

M is the initial mass of untreated SCB.

CHAPTER 4

RESULTS AND DISCUSSION

The IL pre-treatment process involved a mixture of IL with milled dried biomass at a certain temperature as a dissolution mechanism (Dibble *et al.*, 2011). In this chapter, the results for the compositional analysis, the extraction of cellulose from SCB and characterisation of CNCs are given. The effectiveness of time at a constant temperature using two ILs; [bmim][HSO_4] and [bmim][$MeSO_4$] are discussed for the yield of cellulose. The production of nanocellulose from cellulose using the IL/DMSO and bleaching procedure, and the amount of lignin removed will also be discussed for each IL.

Swatloski *et al.* (2002) stated that "ILs are capable of dissolving complex macromolecules and polymeric materials with high efficiency by breaking the extensive hydrogen bonding network of polysaccharides and promoting their dissolution". One of the cellulose-rich fractions obtained can be regenerated by water, an alcohol and acetone (Mäki-Arvela *et al.* 2010; Brandt *et al.* 2011; Dibble *et al.* 2011; Lan, Liu and Sun 2011; Sathitsuksanoh *et al.* 2014). In this work, the solvent used to regenerate cellulose was ethanol. The choice of solvent was based on the presence of hydroxyl ions. Water has hydroxyl ions; however, water molecules shield the IL molecules from cellulose by forming hydrodynamic shells around the IL (Mäki-Arvela *et al.* 2010; Minnick *et al.* 2016). Thus hindering direct interactions between cellulose and IL molecules, prohibiting the cellulose intra- and intermolecular hydrogen bonds to reintegrate (Mäki-Arvela *et al.* 2010; Minnick *et al.* 2016).

"IL pre-treatment has been shown to reduce the cellulose crystallinity, and the hemicellulose and lignin content of biomass" (Dibble *et al.* 2011).

In this work, during the IL pre-treatment, the solutions became dark indicating deconstruction of lignocellulosic biomass by solubilisation of lignin. Wang *et al.* (2011) and Sathitsuksanoh *et al.* (2014) observed similar results in the extraction of cellulose from wood chips using the IL 1-allyl-3-methylimidazolium chloride/dimethylsulphoxide (AmimCl/DMSO) mixtures and 1-ethyl-3-methylimidazolium acetate (emimAcO), respectively.

4.1 Compositional analysis

4.1.1 Moisture and ash content

Computrac software was used to calculate the moisture and ash content, which was reported to 4 decimal places for all runs. The mass, moisture and ash content for all samples is reported in Table 4-1. The average moisture content was 6.80 ± 0.13 % and the average ash content was 4.33 ± 0.45 %. These values are similar to literature values (Sun *et al.* 2004; Mandal and Chakrabarty 2011). The standard deviation was calculated using Equation 4.1.

$$\boldsymbol{Standard\ deviation} = \sqrt{\frac{\sum (\boldsymbol{x}-\boldsymbol{\mu})^2}{\boldsymbol{N}}} \qquad \textbf{(4.1)}$$

whereby $\sum$ means "sum of", x is a value in the data set, μ is the mean of the data set, and N is the number of data points in the population.

Table 4-1. Sample mass, moisture and ash content of SCB before pre-treatment.

	Sample mass (mg)	Moisture content (%)	Ash content (%)
Run 1	3.4406	6.93	4.43
Run 2	3.8878	6.63	3.68
Run 3	3.4243	6.87	4.20
Run 4	3.5956	6.86	4.43
Run 5	3.4931	6.69	4.93
Mean value	**3.5683**	**6.80**	**4.33**
Standard deviation	**0.19**	**0.13**	**0.45**

4.1.2 Carbohydrate quantification

4.1.2.1 Cellulose

The glucose and glucan content of cellulose was reported in Table 4-2. The initial cellulose was 55.6 % for untreated SCB which was also reported by other researchers (Mandal and Chakrabarty 2011; Loh *et al.* 2013; Sofla *et al.* 2016). The glucose and glucan content was calculated using Equation 3.1.

Table 4-2. Glucan content of untreated SCB and NIST standard SCB.

Sample ID	Concentration of glucose (%)	Sample mass (mg)	Glucose (mg) in 86.73 ml	Glucan content (%)
Untreated SCB	0.1016	300.6	88.13	**55.6**
NIST Standard SCB	0.09012	300.8	78.16	**49.3**
SRS	0.1157	300.5	100.4	**31.7**

4.1.2.2 Hemicellulose

The amount of hemicellulose was quantified to be 27.8 % for untreated SCB and 24.6 % for NIST SCB standard. Hemicellulose amount in SCB was similar to literature values of 20-30 % (Sun *et al.* 2004; Mandal and Chakrabarty 2011). Hemicellulose was calculated using Equation 3.2.

Table 4-3. Xylan content of untreated SCB and NIST standard SCB.

Sample ID	Concentration of xylose (%)	Sample mass (mg)	Xylose (mg) in 86.73 ml	Xylan content (%)
Untreated SCB	0.1095	300.6	94.9	**27.8**
NIST Standard SCB	0.09692	300.8	84.1	**24.6**

4.1.3 Lignin content before pre-treatment

The amount of acid soluble lignin (ASL) on the untreated SCB was 24.80 ± 0.012 % and for the NIST SCB standard sample the ASL was 24.40 ± 0.012 % with respect to the whole biomass. The AIL of the untreated SCB was 1.06 ± 0.019 % and for NIST SCB standard 1.03 ± 0.019 %. The total lignin for untreated SCB was 25.9 % and 25.4 % for the untreated SCB and NIST SCB standard samples, respectively. The amount of lignin in untreated SCB has been reported in literature to be between 24-28 % (Sasaki, Adschiri and Arai 2003; Cerqueira, Rodrigues Filho and da Silva Meireles 2007; Mandal and Chakrabarty 2011; Karatzos, Edye and Doherty 2012). The results obtained for lignin in this work is within the acceptable values for the NIST SCB standard sample as shown in Table 4-4 below. The total lignin was the sum of ASL and AIL which was 25.9 % for untreated SCB and 25.4 % for the NIST SCB sample. ASL was calculated using Equation 4.4, while for AIL, Equation 4.5 was used.

Table 4-4. ASL, AIL and total lignin of untreated SCB and NIST standard SCB.

	UV_{abs}	% ASL	% Acid insoluble residue	% AIL	Total lignin
Untreated SCB (run 1)	0.68	25.31	1.0103	1.09	26.4
Untreated SCB (run 2)	0.66	24.57	0.9815	1.06	25.6
Untreated SCB (run 3)	0.66	24.57	0.9786	1.05	25.6
Mean	**0.67**	**24.82**	**0.9901**	**1.06**	**25.9**
Standard deviation	**0.012**	**0.012**	**0.02**	**0.019**	**-**
NIST SCB (run 1)	0.65	24.20	0.9601	1.03	25.2
NIST SCB (run 2)	0.67	24.94	0.9422	1.01	26.0
NIST SCB (run 3)	0.65	24.20	0.9779	1.05	25.3
Mean	**0.66**	**24.40**	**0.96**	**1.03**	**25.4**
Standard deviation	**0.011**	**0.012**	**0.018**	**0.019**	**-**

4.2 Pre-treatment of SCB with ILs

4.2.1 Pre-treatment of SCB using IL [bmim][$MeSO_4$] or [bmim][HSO_4]

4.2.1.1 Pulp recovery after IL pre-treatment

The mass percentage of pulp recovered after the IL: [bmim][$MeSO_4$] pre-treatment was 38.4 %, 32.8 % and 26.1 % for the pre-treatment time of 4 h, 8 h and 12 h, respectively, as shown in Table 4-5. The mass percentage loss was due to the removal of lignin, hemicellulose and some of the pulp while the latter was due to loss of pulp during the washing of the pulp (Sun

et al. 2005; Watkins *et al.* 2015; Liu *et al.* 2016). The maximum mass of pulp recovered was 38.4 % for the 4 h pre-treatment time.

The mass percentage of pulp recovered after pre-treatment with the IL: [bmim][HSO_4] at 4 h, 8 h and 12 h was 32.0 %, 29.1 % and 23.0 %, respectively (Table 4-5). The maximum mass of cellulose recovered was 32.0 % which was also for the 4 h pre-treatment time. The values for the pulp recovery for IL [bmim][HSO_4] was less than that for [bmim][$MeSO_4$] probably due to $[HSO_4]^-$ anion being more acidic than the $[MeSO_4]^-$ anion (Isik, Sardon and Mecerreyes 2014).

Prolonging the pre-treatment time resulted in a greater loss of the SCB cellulose yield. After 4 h of pre-treatment, a mass loss of 61.6 % and 68.0 % was observed for [bmim][$MeSO_4$]-4 and [bmim][HSO_4]-4, respectively. After 6 hours of pre-treatment, a mass loss of 67.2 % and 70.9 % was observed for [bmim][$MeSO_4$]-8 and [bmim][HSO_4]-8, respectively. After 12 hours of pre-treatment, a mass loss of 73.9 % and 77.0 % for [bmim][$MeSO_4$]-12 and [bmim][HSO_4]-12, respectively. The loss was due to the removal of lignin and hemicellulose and the washing of the pulp (Sun *et al.* 2005; Watkins *et al.* 2015; Liu *et al.* 2016). The mass of the pre-treated SCB was recorded in duplicate. The experimental values are recorded in Table 4-5.

Table 4-5. Mass percentage of the recovered pulp after pre-treatment with each IL at varied times.

Pre-treatment with [bmim][$MeSO_4$]							
Sample ID	**I_{SCB} mass (g) (run 1)**	**I_{SCB} mass (g) (run 2)**	**Mean I_{SCB} mass (g)**	**F_{pulp} mass (g) (run 1)**	**F_{pulp} mass (g) (run 2)**	**Mean F_{pulp} mass (g)**	**% Mass recovered**
[bmim][$MeSO_4$]-4	1.001	1.001	1.001	0.3700	0.3982	0.3841	**38.4**
[bmim][$MeSO_4$]-8	1.002	1.001	1.002	0.3194	0.3388	0.3291	**32.8**
[bmim][$MeSO_4$]-12	1.002	1.000	1.001	0.2711	0.2504	0.2608	**26.1**
Pre-treatment with [bmim][HSO_4]							
Sample ID	**I_{SCB} mass (g) (run 1)**	**I_{SCB} mass (g) (run 2)**	**Mean I_{SCB} mass (g)**	**F_{pulp} mass (g) (run 1)**	**F_{pulp} mass (g) (run 2)**	**Mean F_{pulp} mass (g)**	**% Mass recovered**
[bmim][HSO_4]-4	1.000	1.000	1.000	0.3186	0.3211	0.3199	**32.0**
[bmim][HSO_4]-8	1.000	1.002	1.001	0.3008	0.2816	0.2912	**29.1**
[bmim][HSO_4]-12	1.001	1.002	1.001	0.2361	0.2250	0.2306	**23.0**

I_{SCB} = initial SCB mass and F_{pulp} = final pulp mass.

4.2.1.2 Lignin removed after IL pre-treatment

The results for ionic liquid insoluble lignin (ILIL) after pre-treatment with [bmim][$MeSO_4$] or [bmim][HSO_4] was given in Table 4-6 and Table 4-7, respectively.

ILIL was reduced from 24.8 % in the untreated SCB to 12.0 %, 8.62 % and 6.55 % for [bmim][$MeSO_4$]-4, [bmim][$MeSO_4$]-8 and [bmim][$MeSO_4$]-12, respectively. The percent

reduction was 53.7 %, 66.7 % and 74.7 % for [bmim][$MeSO_4$]-4, [bmim][$MeSO_4$]-8 and [bmim][$MeSO_4$]-12, respectively, with respect to the initial lignin content.

Table 4-6. ILIL after pre-treatment with [bmim][$MeSO_4$] at varied pre-treatment times.

Pre-treatment with [bmim][$MeSO_4$]				
Sample ID	**UV_{abs} (run 1)**	**UV_{abs} (run 2)**	**Mean UV_{abs}**	**% ILIL**
[bmim][$MeSO_4$]-4	0.33	0.32	0.32	**12.0**
[bmim][$MeSO_4$]-8	0.22	0.25	0.23	**8.62**
[bmim][$MeSO_4$]-12	0.18	0.17	0.18	**6.55**

ILIL after pre-treatment with [bmim][HSO_4] was given in Table 4-7. ILIL was reduced from 24.8 % in the untreated SCB to 8.20 %, 6.30 % and 6.01 % for [bmim][HSO_4]-4, [bmim][HSO_4]-8 and [bmim][HSO_4]-12, respectively. The percent reduction was 68.3 %, 75.7 % and 76.8 % for [bmim][HSO_4]-4, [bmim][HSO_4]-8 and [bmim][HSO_4]-12, respectively, with respect to the initial lignin content. The IL [bmim][HSO_4]-12 gave the pulp with the lowest amount of lignin which was 6.01 %. Moreover, a longer pre-treatment time for the pulp resulted in the lower lignin content, an indication that the pulp was of higher purity.

Table 4-7. ILIL after pre-treatment with bmim[HSO_4] at varied pre-treatment times.

Pre-treatment with IL bmim[HSO_4]				
Sample ID	**UV_{abs} (run 1)**	**UV_{abs} (run 2)**	**Mean UV_{abs}**	**% ILIL**
[bmim][HSO_4]-4	0.23	0.21	0.22	**8.20**
[bmim][HSO_4]-8	0.16	0.18	0.17	**6.30**
[bmim][HSO_4]-12	0.17	0.15	0.16	**6.01**

In literature, lignin removal from sugarcane bagasse with ionic liquid 1-butyl-3-methylimidazolium alkylbenzenesulfonate [C_2C_1im][ABS], has been achieved with the effective removal of more than 93 % of lignin (Tan *et al.* 2009). Pu, Jiang and Ragauskas (2007) removed 80 % lignin after pre-treatment of biomass with IL, 1-ethyl-3-methylimidazolium acetate, [C_2C_1im][$MeCO_2$], while Sun *et al.* (2009) removed 60-70 % lignin using the same IL. The goal for a successful removal of lignin lies within 5-8 % of lignin remaining on the pulp (McDonough 1992). In this work this was achieved for the following pre-treatment conditions: for [bmim][$MeSO_4$]-12, [bmim][HSO_4]-8 and [bmim][HSO_4]-12.

4.2.1.3 Carbohydrate yield after IL pre-treatment

4.2.1.3.1 Cellulose

The pulp cellulose content decreased from 55.6 % to 49.1 % for [bmim][$MeSO_4$]-4. The pulp cellulose content increased from 55.6 % to 58.3 % and 62.8 % for [bmim][$MeSO_4$]-8 and [bmim][$MeSO_4$]-12, respectively. The amount of recovered cellulose was increased with prolonged pre-treatment time as shown in Table 4-8 with an exception of 4 h pre-treatment time.

Table 4-8. Glucan content after pre-treatment of SCB with [bmim][$MeSO_4$] at varied times.

Sample ID	Concentration (%)	Sample mass (mg)	Glucose (mg) in 86.73 ml	Glucan content (%)
[bmim][$MeSO_4$]-4	0.04692	300.1	20.2	**49.1**
[bmim][$MeSO_4$]-8	0.05110	300.1	22.5	**58.3**
[bmim][$MeSO_4$]-12	0.05750	300.9	31.4	**62.8**

The pulp cellulose content increased from 55.6 % to 61.1 %, 73.5 % and 74.1 % for [bmim][HSO_4]-4, [bmim][HSO_4]-8 and [bmim][HSO_4]-12, respectively. There was an increase for [bmim][HSO_4]-4, [bmim][HSO_4]-8 and [bmim][HSO_4]-12 with respect to the initial cellulose content of the pulp after first pre-treatment. The amount of cellulose was increased with prolonged pre-treatment time with [bmim][HSO_4]-12 giving the highest amount of recovered cellulose.

Table 4-9. Glucan content after pre-treatment of SCB with [bmim][HSO_4] at varied times.

Sample ID	Concentration (%)	Sample mass (mg)	Glucose (mg) in 86.73 ml	Glucan content (%)
[bmim][HSO_4]-4	0.05574	300.1	30.5	**61.1**
[bmim][HSO_4]-8	0.06715	300.2	36.8	**73.5**
[bmim][HSO_4]-12	0.06774	300.6	37.1	**74.1**

In literature, Qiu, Aita and Walker (2012) recovered 87 % cellulose after pre-treatment of energy cane bagasse with IL, 1-ethyl-3-methylimidazolium acetate ([emim][OAc]). Moreover, da Silva *et al.* (2011) found 99.7 % cellulose recovered after pre-treatment with the same IL. In this study, the IL [bmim][HSO_4] had the highest cellulose recovery of 74.1 % after 12 h.

4.2.1.3.2 Hemicellulose

The amount of hemicellulose recovered was reduced with prolonged pre-treatment time. The pulp hemicellulose content of 27.8 % was reduced to 15.4 %, 12.2 % and 9.08 % for [bmim][$MeSO_4$]-4, [bmim][$MeSO_4$]-8 and [bmim][$MeSO_4$]-12, respectively (Table 4-10). This was a reduction by 23.1 %, 32.7 % and 36.9 % for [bmim][$MeSO_4$]-4, [bmim][$MeSO_4$]-8 and [bmim][$MeSO_4$]-12 with respect to the initial hemicellulose content of the pulp after first pre-treatment. The [bmim][$MeSO_4$]-12 had the highest amount of removed hemicellulose after pre-treatment. The xylan content after pre-treatment of SCB with ILs at varied times is shown in Table 4-10.

Table 4-10. Xylan content after pre-treatment of SCB with [bmim][$MeSO_4$] at varied times.

Sample ID	Concentration (%)	Sample mass (mg)	Xylose (mg) in 86.73 ml	Xylan content (%)
[bmim][$MeSO_4$]-4	0.06061	300.5	52.6	**15.4**
[bmim][$MeSO_4$]-8	0.04807	300.8	41.7	**12.2**
[bmim][$MeSO_4$]-12	0.03570	300.2	31.0	**9.08**

The amount of hemicellulose recovered was reduced with prolonged time. The pulp had hemicellulose content which was reduced to 12.5 %, 10.0 % and 6.52 % for [bmim][HSO_4]-4, [bmim][HSO_4]-8 and [bmim][HSO_4]-12, respectively (Table 4-11). This was a reduction by 26.9 %, 39.8 % and 43.8 % for [bmim][HSO_4]-4, [bmim][HSO_4]-8 and [bmim][HSO_4]-12 with respect to the initial hemicellulose content of the pulp after first pre-treatment. The IL [bmim][HSO_4] had the lowest amount of reduced hemicellulose after 12 h with 6.52 % hemicellulose remaining on the pulp.

Table 4-11. Xylan content after pre-treatment of SCB with [bmim][HSO_4] at varied times.

Sample ID	Concentration (%)	Sample mass (mg)	Xylose (mg) in 86.73 ml	Xylan content (%)
[bmim][HSO_4]-4	0.04913	300.1	42.6	**12.5**
[bmim][HSO_4]-8	0.03927	299.8	34.1	**10.0**
[bmim][HSO_4]-12	0.02565	300.4	22.2	**6.52**

Hemicellulose content was reduced after pre-treatment using ILs and the reduction was due to the disruption of lignocellulose structure during prolonged pre-treatment (Brandt *et al.* 2011; Zhuo *et al.* 2015). In literature, Qiu, Aita and Walker (2012) removed 14 % hemicellulose when IL: 1-ethyl-3-methylimidazolium acetate ([EMIM][OAc]) was used to pre-treat energy cane bagasse at a short reaction time.

4.2.2 Pre-treatment of pulp with [bmim][HSO_4]

The CNC yield is usually below 30 % when biomass is the starting material. In literature, the most common acid that is used to extract CNCs is sulfuric acid. Phanthong *et al.* (2016) and Filson, Dawson-Andoh and Schwegler-Berry (2009) extracted a CNC yield of 47 % and 29 % respectively. Moreover, the extraction of CNCs is a very tedious process which usually results in poor yields (Yu *et al.* 2013; Mao *et al.* 2015; Tan, Hamid and Lai 2015). Recently, IL [bmim][HSO_4] has been used to extract CNCs, however, the starting material was either wood pulp or MCC, and hence the CNCs were extracted successfully. Mao *et al.* (2015) extracted 76 % CNCs from MCC as starting material using the IL [bmim][HSO_4]. Man *et al.* (2011) and Tan, Hamid and Lai (2015) did not report any CNC yields. Considering the poor CNC yield and the starting material being MCC, therefore the recovered pulp was not treated

in this part of the experiment with IL [bmim][HSO_4] for the extraction of CNCs due to the low yield of pulp.

4.2.3 Pre-treatment of SCB using IL/DMSO mixtures

The long pre-treatment time using ILs is a major disadvantage in industrial applications (Mohtar *et al.* 2017). The particle sizes of recovered pulp were in the micro-scale therefore no nanocellulose was produced from using ILs at a longer pre-treatment time. The objective of the study was to produce nanocellulose from SCB using ILs. The above results were not satisfactory in accordance to the objectives of this study for the long pre-treatment time. An alternative method was used whereby DMSO was added to the ILs for a shorter pre-treatment time and the resulting pulp was bleached to disrupt linkages between cellulose, hemicellulose and lignin before the extraction of CNCs.

This section presents the results for the simultaneous production of cellulose nanocrystals (CNCs) and cellulose nanofibrils (CNFs) from SCB using IL/DMSO mixture. The first part involves the IL/DMSO pre-treatment followed by the bleaching of the pulp due to the presence of residual lignin to produce both CNFs and CNCs simultaneously. In the process of cellulose extraction from biomass, hemicellulose is easily removed due to its low molecular weight and branched structure, whereas lignin's highly crosslinked structure makes it difficult for its removal from the pulp (Lee, Hamid and Zain 2014; Sathitsuksanoh *et al.* 2014).

A co-solvent, namely DMSO, was used in this work to reduce the viscosity of the IL. The choice of the co-solvent was based on its ability to react with both the cation and anion of the IL. According to Zhao *et al.* (2015) an aprotic polar solvent (dimethyl sulfoxide, DMSO) is more effective than a protic polar solvent (water). Brandt *et al.* (2011) used water as a co-solvent in their pre-treatment of miscanthus, willow and pine using IL ([bmim][HSO_4]) and

did not use any other antisolvent as a comparative study. The other advantage of using DMSO is its ability to swell cellulose so that the IL can diffuse into the fibres more easily (Mandal and Chakrabarty 2011).

The use of ILs is often followed by enzymatic hydrolysis due to the ILs inability to effectively remove most of the lignin at shorter reaction times. The addition of an oxidant, hydrogen peroxide with sodium hydroxide was used to effectively remove all residual lignin from the pulp after IL-DMSO pre-treatment (McDonough 1992). The advantages of using hydrogen peroxide as a bleaching agent is that it accelerated the delignification process by selectively removing hemicellulose and lignin from the pulp which results in an increased fibre brightness (Hart and Rudie 2012; Watkins *et al.* 2015). Therefore, breaking down the lignin macromolecules to small hydrophilic fragments that are soluble in water and alkali solution (Hart and Rudie 2012).

4.2.3.1 Pulp yield after IL/DMSO pre-treatment

The results for the percentage pulp obtained for the [bmim][$MeSO_4$]/ DMSO pre-treatment are tabulated in Table 4-12, Table 4-13 and Table 4-14.

The percentage of pulp yield after 30 min pre-treatment with [bmim][$MeSO_4$]/DMSO mixtures was 82.9 %, 80.1 %, 81.5 % and 80.6 % for [bmim][$MeSO_4$]-50, [bmim][$MeSO_4$]-75, [bmim][$MeSO_4$]-90 and [bmim][$MeSO_4$]-100, respectively.

Table 4-12. Mass recovered after pre-treatment of SCB with [bmim][$MeSO_4$]/DMSO after 30 min.

Sample ID	I_{SCB} mass (g) (run 1)	I_{SCB} mass (g) (run 2)	Mean I_{SCB} mass (g)	F_{pulp} mass (g) (run 1)	F_{pulp} mass (g) (run 2)	Mean F_{pulp} mass (g)	% Mass recovered
[bmim][$MeSO_4$]-50 (30)	1.002	1.006	1.004	0.8403	0.8163	0.8283	**82.9**
[bmim][$MeSO_4$]-75 (30)	1.005	1.003	1.004	0.8009	0.7995	0.8002	**80.1**
[bmim][$MeSO_4$]-90 (30)	1.004	1.005	1.005	0.8133	0.8150	0.8142	**81.5**
[bmim][$MeSO_4$]-100 (30)	1.010	1.001	1.006	0.8031	0.8068	0.8049	**80.6**

I_{SCB} = initial SCB mass and F_{pulp} = final pulp mass.

The percentage of pulp yield after 45 min pre-treatment was 78.6 %, 79.3 %, 72.0 % and 75.5 % for [bmim][$MeSO_4$]-50, [bmim][$MeSO_4$]-75, [bmim][$MeSO_4$]-90 and [bmim][$MeSO_4$]-100, respectively. There was no clear trend in percent pulp obtained because the IL was not effective for cellulose removal, due to the aprotic anion of IL [bmim][$MeSO_4$]. In the cellulose structure, the O atom of the OH group can form hydrogen bonds with a donor hydrogen atom from the IL. The $[MeSO_4]^-$ anion does not have a hydrogen and therefore the formation of hydrogen bonds with the cellulose is hindered. Therefore, increasing the IL loading did not affect the yield of cellulose which remained constant.

Table 4-13. Mass recovered after pre-treatment of SCB with [bmim][$MeSO_4$]/DMSO after 45 min.

Sample ID	I_{SCB} mass (g) (run 1)	I_{SCB} mass (g) (run 2)	Mean I_{SCB} mass (g)	F_{pulp} mass (g) (run 1)	F_{pulp} mass (g) (run 2)	Mean F_{pulp} mass (g)	% Mass recovered
[bmim][$MeSO_4$]-50 (45)	1.002	1.005	1.004	0.7943	0.7762	0.7853	**78.6**
[bmim][$MeSO_4$]-50 (45)	1.005	1.006	1.006	0.8022	0.7815	0.7919	**79.2**
[bmim][$MeSO_4$]-90 (45)	1.009	1.002	1.006	0.7273	0.7069	0.7185	**72.0**
[bmim][$MeSO_4$]-100 (45)	1.004	1.001	1.003	0.7606	0.7482	0.7544	**75.5**

I_{SCB} = initial SCB mass and F_{pulp} = final pulp mass.

The percentage of pulp yield after 60 min pre-treatment was 76.8 %, 73.9 %, 70.0 % and 68.7 % for [bmim][$MeSO_4$]-50, [bmim][$MeSO_4$]-75, [bmim][$MeSO_4$]-90 and [bmim][$MeSO_4$]-100, respectively. There was no clear trend in percent pulp obtained because the IL was not effective for cellulose removal, due to the aprotic anion of IL [bmim][$MeSO_4$] which was not able to form hydrogen bonds with cellulose.

Table 4-14. Mass recovered after pre-treatment of SCB with [bmim][$MeSO_4$]/DMSO after 60 min.

Sample ID	I_{SCB} mass (g) (run 1)	I_{SCB} mass (g) (run 2)	Mean I_{SCB} mass (g)	F_{pulp} mass (g) (run 1)	F_{pulp} mass (g) (run 2)	Mean F_{pulp} mass (g)	% Mass recovered
[bmim][$MeSO_4$]-50 (60)	1.005	1.008	1.007	0.7720	0.761	0.7665	**76.8**
[bmim][$MeSO_4$]-75 (60)	1.001	1.006	1.004	0.7339	0.7423	0.7381	**73.9**
[bmim][$MeSO_4$]-90 (60)	1.007	1.005	1.006	0.7097	0.6871	0.6984	**70.0**
[bmim][$MeSO_4$]-100 (60)	1.000	1.004	1.002	0.6975	0.6752	0.6864	**68.7**

I_{SCB} = initial SCB mass and F_{pulp} = final pulp mass.

A similar pattern was obtained for the pulp yield. The percentage pulp yield reduced with an increase in both pre-treatment time and concentration of the DMSO co-solvent. The highest pulp yield (82.9 %) was obtained for the pre-treatment condition of 30 min for [bmim][$MeSO_4$]-50. The results for the percentage pulp obtained for the [bmim][HSO_4]/DMSO pre-treatment are tabulated in Table 4-15, Table 4-16 and Table 4-17.

The percentage of pulp remaining after the [bmim][HSO_4]/DMSO pre-treatment after 30 min was 76.5 %, 74.3 %, 71.9 % and 69.8 % for [bmim][HSO_4]-50, [bmim][HSO_4]-75, [bmim][HSO_4]-90 and [bmim][HSO_4]-100, respectively.

Table 4-15. Mass recovered after pre-treatment of SCB with [bmim][HSO_4]/DMSO after 30 min.

Sample ID	I_{SCB} mass (g) (run 1)	I_{SCB} mass (g) (run 2)	Mean I_{SCB} mass (g)	F_{pulp} mass (g) (run 1)	F_{pulp} mass (g) (run 2)	Mean F_{pulp} mass (g)	% Mass recovered
[bmim][HSO_4]-50 (30)	1.005	1.002	1.004	0.7732	0.7552	0.7642	**76.5**
[bmim][HSO_4]-75 (30)	1.003	1.008	1.006	0.7464	0.7368	0.7416	**74.3**
[bmim][HSO_4]-90 (30)	1.007	1.002	1.005	0.7260	0.7095	0.7177	**71.9**
[bmim][HSO_4]-100 (30)	1.009	1.005	1.007	0.7083	0.6835	0.6959	**69.8**

I_{SCB} = initial SCB mass and F_{pulp} = final pulp mass.

The percentage of pulp remaining after 45 minutes was 74.8 %, 73.9 %, 70.0 % and 65.7 % for [bmim][HSO_4]-50, [bmim][HSO_4]-75, [bmim][HSO_4]-90 and [bmim][HSO_4]-100, respectively.

Table 4-16. Mass recovered after pre-treatment of SCB with [bmim][HSO_4]/DMSO after 45 min.

Sample ID	I_{SCB} mass (g) (run 1)	I_{SCB} mass (g) (run 2)	Mean I_{SCB} mass (g)	F_{pulp} mass (g) (run 1)	F_{pulp} mass (g) (run 2)	Mean F_{pulp} mass (g)	% Mass recovered
[bmim][HSO_4]-50 (45)	1.001	1.004	1.003	0.7567	0.7380	0.7474	**74.8**
[bmim][HSO_4]-75 (45)	1.006	1.004	1.005	0.7525	0.7229	0.7377	**73.9**
[bmim][HSO_4]-90 (45)	1.004	1.002	1.003	0.7119	0.6863	0.6991	**70.0**
[bmim][HSO_4]-100 (45)	1.004	1.006	1.005	0.6644	0.6462	0.6553	**65.7**

I_{SCB} = initial SCB mass and F_{pulp} = final pulp mass.

The percentage of pulp remaining after 60 min was 68.5 %, 58.6 %, 51.3 % and 49.4 % for [bmim][HSO_4]-50, [bmim][HSO_4]-75, [bmim][HSO_4]-90 and [bmim][HSO_4]-100, respectively.

Table 4-17. Mass recovered after pre-treatment of SCB with [bmim][HSO_4]/DMSO after 60 min.

Sample ID	I_{SCB} mass (g) (run 1)	I_{SCB} mass (g) (run 2)	Mean I_{SCB} mass (g)	F_{pulp} mass (g) (run 1)	F_{pulp} mass (g) (run 2)	Mean F_{pulp} mass (g)	% Mass recovered
[bmim][HSO_4]-50 (60)	1.002	1.009	1.006	0.6963	0.6702	0.6833	**68.5**
[bmim][HSO_4]-75 (60)	1.006	1.007	1.007	0.5736	0.5930	0.5833	**58.6**
[bmim][HSO_4]-90 (60)	1.008	1.002	1.005	0.5223	0.4988	0.5106	**51.3**
[bmim][HSO_4]-100 (60)	1.002	1.006	1.004	0.5095	0.4745	0.4920	**49.4**

I_{SCB} = initial SCB mass and F_{pulp} = final pulp mass.

The percent pulp yield reduced with an increase in both pre-treatment time and concentration of the IL for both ILs. The highest pulp yield (76.5 %) was obtained for the pre-treatment condition of 30 min for [bmim][HSO_4]-50. The pulp yield for the [bmim][HSO_4]-100 at 30 min pre-treatment was higher than for the results obtained above for the long IL pre-treatment times clearly indicating that a shorter pre-treatment time resulted in higher yield of pulp for only IL pre-treatment.

IL [bmim][$MeSO_4$]-50 gave the best results with 82.9 % for 30 min pre-treatment time. Moreover, the IL/DMSO ratio of 1:1 gave the highest yield at different times compared to the IL only samples for the shorter pre-treatment time.

4.2.3.2 Pulp yield after bleaching (IL/DMSO samples)

After the IL/DMSO pre-treatment, the pulp was bleached to extract CNCs. The mass recovery of pulp was recorded. The yield was based on the ability of IL/DMSO mixtures to dissolve cellulose and the acidity of the IL (Liu *et al.* 2016).

The freeze dried samples were weighed and recorded in Table 4-18, Table 4-19 and Table 4-20 with respect to [bmim][$MeSO_4$]-50, [bmim][$MeSO_4$]-75, [bmim][$MeSO_4$]-90 and [bmim][$MeSO_4$]-100, respectively, after 30, 45 and 60 min.

The percent pulp yield reduced with an increase in both pre-treatment time and concentration of the IL. The highest pulp yield (40.1 %) was obtained for the pre-treatment condition of 30 min for [bmim][$MeSO_4$]-50. Bleaching with hydrogen peroxide degraded the lignin molecules by being dissolved in solution and easily removed by washing the pulp (Watkins *et al.* 2015). Moreover, bleaching cleaved the bonds between lignin and hemicellulose thus reducing the amount of pulp recovered (Watkins *et al.* 2015).

Table 4-18. Mass recovered after bleaching ([bmim][$MeSO_4$]/DMSO-30 min pre-treated samples).

Sample ID	I_{pulp} mass (g) (run 1)	I_{pulp} mass (g) (run 2)	Mean I_{pulp} mass (g)	F_{pulp} mass (g) (run 1)	F_{pulp} mass (g) (run 2)	Mean F_{pulp} mass (g)	% Mass recovered
[bmim][$MeSO_4$]-50 (30-B)	0.5005	0.5001	0.5003	0.2510	0.1502	0.2006	**40.1**
[bmim][$MeSO_4$]-75 (30-B)	0.5003	0.5004	0.5004	0.2504	0.1459	0.1981	**39.6**
[bmim][$MeSO_4$]-90 (30-B)	0.5002	0.5005	0.5004	0.2222	0.1371	0.1796	**35.9**
[bmim][$MeSO_4$]-100 (30-B)	0.5001	0.5004	0.5003	0.1856	0.1146	0.1501	**30.0**

I_{pulp} = initial pulp mass and F_{pulp} = final pulp mass.

Table 4-19. Mass recovered after bleaching ([bmim][$MeSO_4$]/DMSO-45 min pre-treated samples).

Sample ID	I_{pulp} mass (g) (run 1)	I_{pulp} mass (g) (run 2)	Mean I_{pulp} mass (g)	F_{pulp} mass (g) (run 1)	F_{pulp} mass (g) (run 2)	Mean F_{pulp} mass (g)	% Mass recovered
[bmim][$MeSO_4$]-50 (45-B)	0.4998	0.5003	0.5001	0.2412	0.1258	0.1835	**36.7**
[bmim][$MeSO_4$]-75 (45-B)	0.5002	0.5002	0.5002	0.2229	0.1092	0.1661	**33.2**
[bmim][$MeSO_4$]-90 (45-B)	0.5006	0.5009	0.5008	0.1989	0.0955	0.1472	**29.4**
[bmim][$MeSO_4$]-100 (45-B)	0.5004	0.5004	0.5004	0.1822	0.076	0.1291	**25.8**

I_{pulp} = initial pulp mass and F_{pulp} = final pulp mass.

Table 4-20. Mass recovered after bleaching ([bmim][$MeSO_4$]/DMSO-60 min pre-treated samples).

Sample ID	I_{pulp} mass (g) (run 1)	I_{pulp} mass (g) (run 2)	Mean I_{pulp} mass (g)	F_{pulp} mass (g) (run 1)	F_{pulp} mass (g) (run 2)	Mean F_{pulp} mass (g)	% Mass recovered
[bmim][$MeSO_4$]-50 (60-B)	0.5008	0.5007	0.5008	0.1338	0.1126	0.1232	**24.6**
[bmim][$MeSO_4$]-75 (60-B)	0.5009	0.4999	0.5004	0.1192	0.1090	0.1141	**22.8**
[bmim][$MeSO_4$]-90 (60-B)	0.5001	0.5002	0.5002	0.1199	0.1112	0.1155	**23.1**
[bmim][$MeSO_4$]-100 (60-B)	0.5004	0.5005	0.5005	0.0870	0.1152	0.1011	**20.2**

I_{pulp} = initial pulp mass and F_{pulp} = final pulp mass.

Even after bleaching, the samples pre-treated with IL [bmim][$MeSO_4$] showed no clear trend due to the presence of an aprotic anion.

The freeze dried samples were weighed and recorded in Table 4-21, Table 4-22 and Table 4-23, with respect to [bmim][HSO_4]-50, [bmim][HSO_4]-75, [bmim][HSO_4]-90 and [bmim][HSO_4]-100 respectively, after 30, 45 and 60 min.

Table 4-21. Mass recovered after bleaching ([bmim][HSO_4]/DMSO-30 min pre-treated samples).

Sample ID	I_{pulp} mass (g) (run 1)	I_{pulp} mass (g) (run 2)	Mean I_{pulp} mass (g)	F_{pulp} mass (g) (run 1)	F_{pulp} mass (g) (run 2)	Mean F_{pulp} mass (g)	% Mass recovered
[bmim][HSO_4]-50 (30-B)	0.5015	0.5002	0.5009	0.1513	0.1502	0.1508	**30.1**
[bmim][HSO_4]-75 (30-B)	0.4999	0.5001	0.5000	0.1231	0.1459	0.1345	**26.9**
[bmim][HSO_4]-90 (30-B)	0.5006	0.5002	0.5004	0.1251	0.1371	0.1311	**26.2**
[bmim][HSO_4]-100 (30-B)	0.5008	0.5006	0.5007	0.1107	0.1146	0.1127	**22.5**

I_{pulp} = initial pulp mass and F_{pulp} = final pulp mass.

Table 4-22. Mass recovered after bleaching ([bmim][HSO_4]/DMSO-45 min pre-treated samples).

Sample ID	I_{pulp} mass (g) (run 1)	I_{pulp} mass (g) (run 2)	Mean I_{pulp} mass (g)	F_{pulp} mass (g) (run 1)	F_{pulp} mass (g) (run 2)	Mean F_{pulp} mass (g)	% Mass recovered
[bmim][HSO_4]-50 (45-B)	0.5001	0.5004	0.5003	0.1273	0.1258	0.1266	**25.3**
[bmim][HSO_4]-75 (45-B)	0.5009	0.5006	0.5008	0.1071	0.1092	0.1082	**21.6**
[bmim][HSO_4]-90 (45-B)	0.5002	0.5001	0.5002	0.0941	0.076	0.0850	**17.0**
[bmim][HSO_4]-100 (45-B)	0.5003	0.5003	0.5003	0.0726	0.0955	0.0841	**16.8**

I_{pulp} = initial pulp mass and F_{pulp} = final pulp mass.

Table 4-23. Mass recovered after bleaching ([bmim][HSO_4]/DMSO-60 min pre-treated samples).

Sample ID	I_{pulp} mass (g) (run 1)	I_{pulp} mass (g) (run 2)	Mean I_{pulp} mass (g)	F_{pulp} mass (g) (run 1)	F_{pulp} mass (g) (run 2)	Mean F_{pulp} mass (g)	% Mass recovered
[bmim][HSO_4]-50 (60-B)	0.5009	0.5001	0.5005	0.0885	0.0896	0.0891	**17.8**
[bmim][HSO_4]-75 (60-B)	0.5003	0.5003	0.5003	0.0818	0.0836	0.0828	**16.5**
[bmim][HSO_4]-90 (60-B)	0.5005	0.5006	0.5006	0.0767	0.0855	0.0811	**16.2**
[bmim][HSO_4]-100 (60-B)	0.5006	0.5003	0.5005	0.0702	0.0699	0.0701	**14.0**

I_{pulp} = initial pulp mass and F_{pulp} = final pulp mass.

The IL [bmim][$MeSO_4$] had the highest pulp recovery yield of 40.1 % after 30 min pre-treatment time followed by bleaching. While the highest pulp yield for IL [bmim][HSO_4] was 30.1 % after 30 min pre-treatment time followed by bleaching. The percent pulp yield reduced with an increase in both pre-treatment time and concentration of the IL. The highest pulp yield (30.1 %) was obtained for the pre-treatment condition of 30 min for [bmim][HSO_4]-50. The pulp percentage recovered after [bmim][HSO_4]/DMSO at 60 min of pre-treatment time was not any better than the pulp obtained for the long pre-treatment time with DMSO.

The drastic reduction of pulp percentage mass was due to degradation of the lignin molecules by dissolving the lignin molecules in solution (Watkins *et al.* 2015). The delignification process is accelerated by the oxidising agents by cleaving the ether bonds between lignin and hemicellulose (Xu *et al.* 2006; Watkins *et al.* 2015). Fernández-Rodríguez *et al.* (2017) selectively removed 90 % lignin after bleaching bagasse. The bleaching process drastically reduces the pulp yield due to the degradation of lignin and the cleavage of ether bonds between lignin and hemicellulose (Hart and Rudie 2012; Watkins *et al.* 2015; Fernández-

Rodríguez *et al.* 2017). Thus the solubility of lignin and hemicellulose through ether bond cleavage reduces the pulp yield after bleaching (Watkins *et al.* 2015). The bleaching agent, hydrogen peroxide has a poor selectivity which resulted in the random degradation of cellulose polymerization degree which contributed to the severe mass loss (Mussatto, Rocha and Roberto 2008).

4.2.3.3 Lignin removal

The initial amount of ASL present in the untreated SCB was 24.8 % of the original biomass. After pre-treatment of SCB with [bmim][HSO_4]/DMSO or [bmim][$MeSO_4$]/DMSO mixtures, ionic liquid insoluble lignin (ILIL) was calculated using UV-Vis. The amount of lignin removed from the pulp and ILIL was recorded in Table 2-24, Table 2-25 and Table 2-26.

Table 4-24. ILIL with respect to bleached pulp after pre-treatment (30 min) with [bmim][$MeSO_4$]/DMSO at varied DMSO concentrations.

Sample ID	UV_{abs} (run 1)	UV_{abs} (run 2)	Mean UV_{abs}	% ILIL
[bmim][$MeSO_4$]-50 (30-B)	0.37	0.3	0.34	**12.5**
[bmim][$MeSO_4$]-75 (30-B)	0.32	0.34	0.33	**12.3**
[bmim][$MeSO_4$]-90 (30-B)	0.30	0.33	0.32	**11.8**
[bmim][$MeSO_4$]-100 (30-B)	0.31	0.31	0.31	**11.5**

Table 4-25. ILIL with respect to bleached pulp after pre-treatment (45 min) with [bmim][$MeSO_4$]/DMSO at varied DMSO concentrations.

Sample ID	UV_{abs} (run 1)	UV_{abs} (run 2)	Mean UV_{abs}	% ILIL
[bmim][$MeSO_4$]-50 (45-B)	0.26	0.24	0.25	**9.30**
[bmim][$MeSO_4$]-75 (45-B)	0.23	0.25	0.24	**8.95**
[bmim][$MeSO_4$]-90 (45-B)	0.26	0.21	0.23	**8.68**
[bmim][$MeSO_4$]-100 (45-B)	0.19	0.21	0.20	**7.49**

Table 4-26. ILIL with respect to bleached pulp after pre-treatment (60 min) with [bmim][$MeSO_4$]/DMSO at varied DMSO concentrations.

Sample ID	UV_{abs} (run 1)	UV_{abs} (run 2)	Mean UV_{abs}	% ILIL
[bmim][$MeSO_4$]-50 (60-B)	0.18	0.22	0.20	**7.44**
[bmim][$MeSO_4$]-75 (60-B)	0.19	0.15	0.17	**6.37**
[bmim][$MeSO_4$]-90 (60-B)	0.15	0.17	0.16	**5.93**
[bmim][$MeSO_4$]-100 (60-B)	0.16	0.17	0.17	**6.15**

The amount of lignin removed was a function of both reaction time and the concentration of IL. The longer reaction time (60 min) and higher IL concentration removed more lignin. The structure of lignin and the IL cation have delocalised π electrons leading to possible π-π interactions that promote the extraction of lignin.

A longer reaction time (60 min) and 90 % IL concentration gave the highest removal of lignin. Thus, the remaining ILIL in the pulp was 5.93 %. The amount of lignin removed from the pulp and ILIL was recorded in Table 4-27, Table 4-28 and Table 4-29.

Table 4-27. ILIL with respect to bleached pulp after pre-treatment (30 min) with [bmim][HSO_4]/DMSO at varied DMSO concentrations.

Sample ID	UV_{abs} (run 1)	UV_{abs} (run 2)	Mean UV_{abs}	% ILIL
[bmim][HSO_4]-50 (30-B)	0.30	0.33	0.32	**11.7**
[bmim][HSO_4]-75 (30-B)	0.27	0.31	0.29	**10.7**
[bmim][HSO_4]-90 (30-B)	0.24	0.27	0.26	**9.57**
[bmim][HSO_4]-100 (30-B)	0.25	0.20	0.23	**8.43**

Table 4-28. ILIL with respect to bleached pulp after pre-treatment (45 min) with [bmim][HSO_4]/DMSO at varied DMSO concentrations.

Sample ID	UV_{abs} (run 1)	UV_{abs} (run 2)	Mean UV_{abs}	% ILIL
[bmim][HSO_4]-50 (45-B)	0.17	0.19	0.18	**6.77**
[bmim][HSO_4]-75 (45-B)	0.16	0.18	0.17	**6.37**
[bmim][HSO_4]-90 (45-B)	0.15	0.17	0.16	**5.93**
[bmim][HSO_4]-100 (45-B)	0.13	0.11	0.12	**4.54**

Table 4-29. ILIL with respect to bleached pulp after pre-treatment (60 min) with [bmim][HSO_4]/DMSO at varied DMSO concentrations.

Sample ID	UV_{abs} (run 1)	UV_{abs} (run 2)	Mean UV_{abs}	% ILIL
[bmim][HSO_4]-50 (60-B)	0.10	0.11	0.11	**3.94**
[bmim][HSO_4]-75 (60-B)	0.08	0.10	0.09	**3.42**
[bmim][HSO_4]-90 (60-B)	0.09	0.05	0.07	**2.58**
[bmim][HSO_4]-100 (60-B)	0.05	0.05	0.05	**1.91**

The amount of lignin removed was a function of both reaction time and the concentration of IL. A longer reaction time (60 min) and higher concentration of IL (100) gave the highest removal of lignin. The optimised lignin removal (1.91 %) occurred for the pre-treatment condition 60 min and [bmim][HSO_4]-100. This is 92 % of the lignin present in the biomass.

A lignin amount after biomass pre-treatment with ILs in the range of 13-19 % has been previously reported (Brandt *et al.* 2011; Dibble *et al.* 2011; Prado, Erdocia and Labidi 2013). Prado, Erdocia and Labidi (2013), Brandt *et al.* (2011) and (Dibble *et al.* 2011) recovered 10 %, 19 % and 14 % of lignin remaining after IL pre-treatment, respectively.

The results were reported based on the amount of lignin with respect to the initial total acid soluble lignin of 24.8 % This is due the high delignification efficiency of the oxidative

hydrogen peroxide and hydrolysing sodium hydroxide during the bleaching process under mild conditions that the active species in solution eliminates the chromophores of lignin which leads to the dissolution of lignin (Sun *et al.* 2001). The effective removal of lignin from biomass was achieved with [bmim][HSO_4]-100 with optimum results at the maximum time of 60 min. The IL [bmim][HSO_4] was much more effective than IL [bmim][$MeSO_4$] in terms of the removal of lignin from SCB.

4.2.3.4 Carbohydrates

For the bleaching step only the 60 min IL/DMSO pre-treatment condition was used. Equation (3.1) was used to calculate the percentage cellulose as glucan. The results are shown in Table 4-30 and Table 4-31.

Table 4-30. Glucan content amount for the [bmim][$MeSO_4$]/DMSO pre-treated samples (60 min) quantified after bleaching.

Sample ID	Concentration of glucose (%)	Sample mass (mg)	Glucose (mg) in 86.73 ml	Glucan content (%)	Corrected glucan content (%)
Pre-treatment with IL [bmim][$MeSO_4$]/DMSO mixtures (60 min)					
[bmim][$MeSO_4$]-50 (60-B)	0.05472	299.9	48.3	76.32	**44.7**
[bmim][$MeSO_4$]-75 (60-B)	0.06724	300.4	59.1	93.26	**61.6**
[bmim][$MeSO_4$]-90 (60-B)	0.07561	300.4	65.6	103.45	**71.8**
[bmim][$MeSO_4$]-100 (60-B)	0.2013	300.9	174.6	109.98	**78.3**

The highest purity cellulose (92.1 %) was obtained for the IL [bmim][HSO_4]-100. The protic IL [bmim][HSO_4], was able to form hydrogen bonds with the cellulose and remove lignin and hemicellulose effectively.

Table 4-31. Glucan content amount for the [bmim][HSO_4]/DMSO pre-treated samples (60 min) quantified after bleaching.

Sample ID	Concentration of glucose (%)	Sample mass (mg)	Glucose (mg) in 86.73 ml	Glucan content (%)	Corrected glucan content (%)
Pre-treatment with IL [bmim][HSO_4]/DMSO mixtures (60 min)					
[bmim][HSO_4]-50 (60-B)	0.03113	300.7	27	85.1	**53.4**
[bmim][HSO_4]-75 (60-B)	0.03115	300.4	27.9	88.05	**56.4**
[bmim][HSO_4]-90 (60-B)	0.04698	300.1	41.6	105.13	**73.5**
[bmim][HSO_4]-100 (60-B)	0.04425	300.2	39.2	123.92	**92.1**

Equations (3.2) was used to calculate the hemicellulose content after bleaching and are given in Table 4-32 and Table 4-33.

The IL [bmim][HSO_4] gave the greatest decrease in hemicellulose. The results obtained have a similar pattern to the IL pre-treatments by Doherty *et al.* (2010) and Brandt *et al.* (2011) where the acidity of IL was able to disrupt the lignocellulosic structure by a slightly removal of lignin at a short reaction time.

The xylan results are shown in Table 4-32 and Table 4-33.

Table 4-32. Xylan content for the [bmim][$MeSO_4$]/DMSO pre-treated samples (60 min) quantified after bleaching.

Sample ID	Concentration (%)	Sample mass (mg)	Xylose (mg) in 86.73 ml	Xylan content (%)
Pre-treatment with IL [bmim][$MeSO_4$]/DMSO mixtures (60 min)				
[bmim][$MeSO_4$]-50 (60-B)	0.05472	299.9	48.3	**14.6**
[bmim][$MeSO_4$]-75 (60-B)	0.06724	300.4	59.1	**10.1**
[bmim][$MeSO_4$]-90 (60-B)	0.07561	300.4	65.6	**0**
[bmim][$MeSO_4$]-100 (60-B)	0.2013	300.9	174.6	**0**

Table 4-33. Xylan content for the [bmim][HSO_4]/DMSO pre-treated samples (60 min) quantified after bleaching.

Sample ID	Concentration (%)	Sample mass (mg)	Xylose (mg) in 86.73 ml	Xylan content (%)
Pre-treatment with IL [bmim][HSO_4]/DMSO mixtures (60 min)				
[bmim][HSO_4]-50 (60-B)	0.03113	300.7	27	**4.77**
[bmim][HSO_4]-75 (60-B)	0.03115	300.4	27.9	**4.77**
[bmim][HSO_4]-90 (60-B)	0.04698	300.1	41.6	**11.3**
[bmim][HSO_4]-100 (60-B)	0.04425	300.2	39.2	**5.59**

4.2.3.5 Extraction of CNCs

Abushammala, Krossing and Laborie (2015) recently studied the direct extraction of CNCs from wood with an ionic liquid which simultaneously dissolves lignin, swell cellulose and catalyse cellulose hydrolysis to nanocellulose. Extraction of cellulose nanocrystals from cellulose using an ionic liquid is a new approach which is made to replace the use of strong acids during hydrolysis. The use of 1-butyl-3-methyimidazolium hydrogen sulphate has similar properties to hydrogen sulphate in terms of removing the amorphous regions of cellulose and increasing the yield of crystalline portion of cellulose (Man *et al.* 2011; Mao *et al.* 2015; Tan, Hamid and Lai 2015).

4.3 Characterisation and quantification of CNCs

The characterisation and quantification of nanocellulose from bleached pulp where the highest amount of cellulose was recovered and with the least lignin was undertaken. The results given in the next section are of the SCB pre-treated with [bmim][$MeSO_4$] or [bmim][HSO_4]/DMSO- mixtures at 60 min followed by bleaching.

In some instances the untreated SCB sample was analysed for comparison purposes.

A range of characterisation techniques was used to confirm the existence of CNCs.

The morphologies of freeze dried cellulose suspension after bleaching the pulp was studied with scanning electron microscopy (SEM) and transmission electron microscopy (TEM).

The crystallinity index of nanocellulose was calculated from the X-ray diffraction (XRD) diffractograms.

Attenuated total reflection Fourier transform infrared (ATR-FTIR) was used to confirm the absence of lignin and hemicellulose in nanocellulose.

Thermograms of the CNCs was obtained from thermogravimetric analysis (TGA) to investigate thermal stability or decomposition.

To analyse the nanoparticle size and calculate the amount of CNCs, dynamic light scattering (DLS) was used.

4.3.1 Scanning electron microscopy (SEM)

The untreated SCB showed sheets of fibres as seen in Figure 4-1. The fibres were clustered. After the pre-treatment with IL/DMSO mixtures, the SCB bundles started to dismantle and the fibres became detached from others (Rezende *et al.*, 2011).

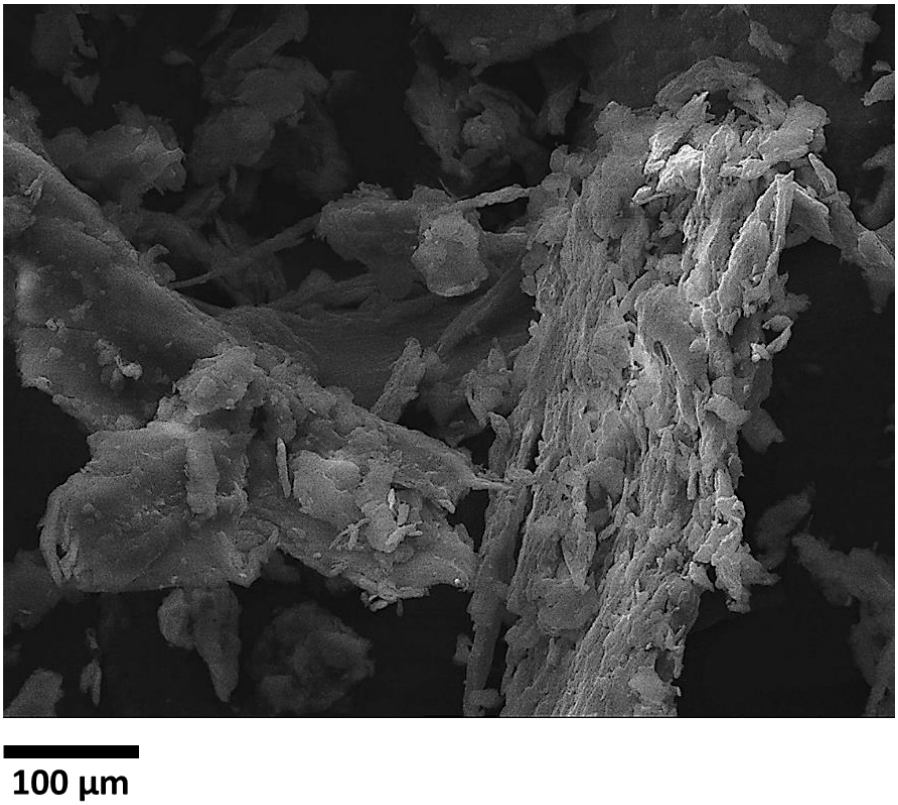

Figure 4-1. SEM image of untreated SCB.

DMSO swells cellulose which was observed on the SEM images (Mendes *et al.*, 2015). Samples showed sheet like structures for all SEM images as shown in Figure 4-2. The [bmim][HSO_4]-100 with only the IL present on the mixture resulted in more rods observed on rougher surfaces as evident in Figure 4-2 (h). This means that the presence of DMSO as a co solvent exposed the SCB fibres to pre-treatment but however limited the direct extraction of nanocellulose from bagasse.

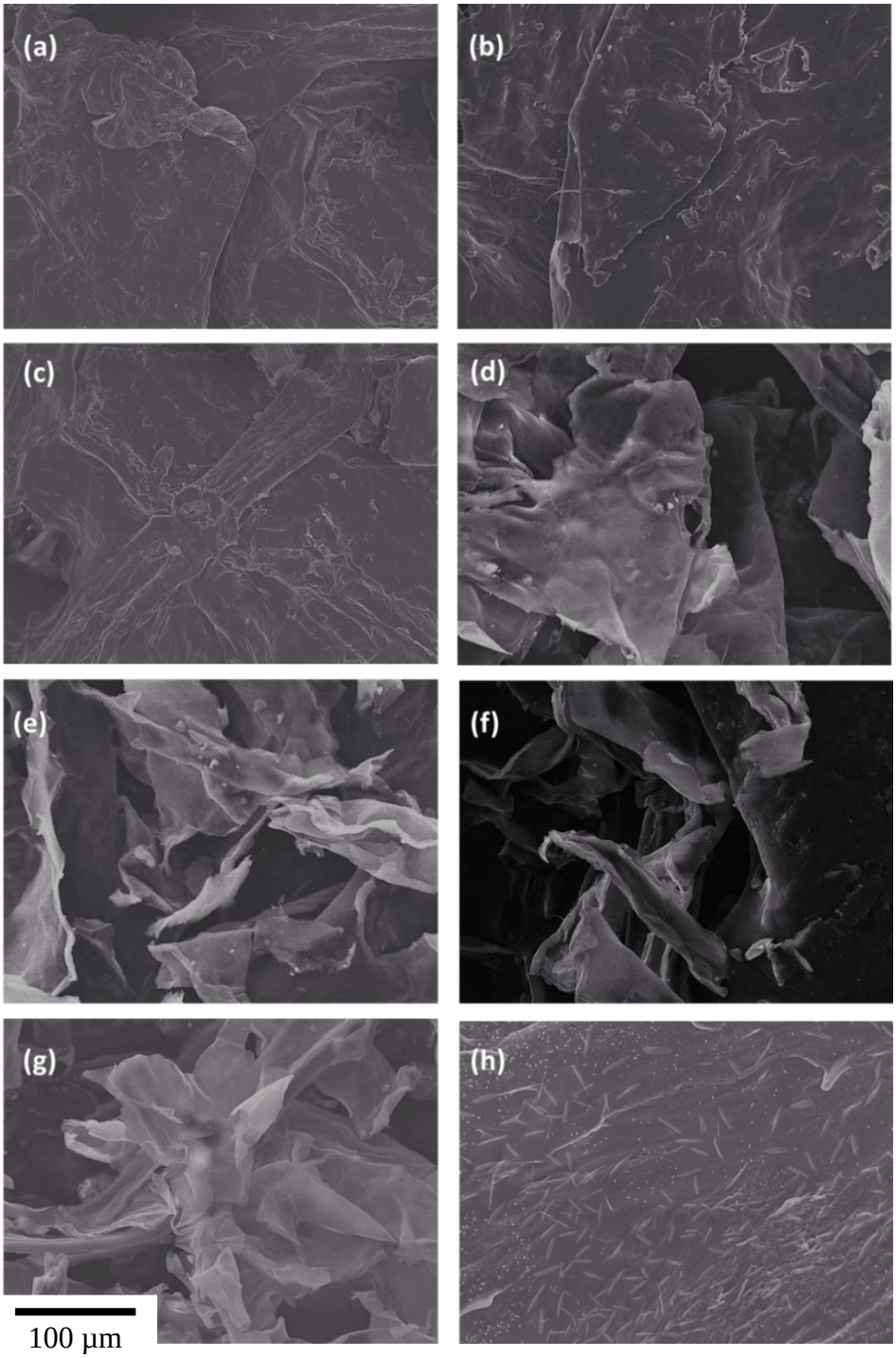

Figure 4-2. SEM images of (a) [bmim][$MeSO_4$]-50 (60-B), (c) [bmim][$MeSO_4$]-75 (60-B), (e) [bmim][$MeSO_4$]-90 (60-B) and (g) [bmim][$MeSO_4$]-100 (60-B) respectively; and (b) [bmim][HSO_4]-50 (60-B), (d) [bmim][HSO_4]-75 (60-B), (f) [bmim][HSO_4]-90 (60-B) and (h) [bmim][HSO_4]-100 (60-B), respectively.

DMSO as co-solvent exposed the SCB fibres to pre-treatment hut however, limited the direct extraction of nanocellulose from SCB (Abushammala, Krossing and Laborie 2015). The disruption of the tissue network was observed as sheets where DMSO swelled the fibres, thus limiting the ability of nanocellulose extraction directly from SCB. Wang and co-workers found no DMSO effects on the solubility of wood chips but the swelling of the fibres (Wang *et al.,* 2011) as shown in Figure 4-2 (a-c). Binod *et al.* (2012) also observed similar SEM images where a smooth and continuous surface in the higher DMSO content resulted from the use of a co-solvent, whereas the higher the IL concentration has a rough surface (Figure 4-2 h). The other reason for the inability of IL/DMSO mixtures to produce CNCs directly from biomass is the cellulose insolubility in DMSO which hinders the removal of amorphous regions of cellulose (Xiao *et al.*, 2014).

The pure IL, [bmim][HSO_4], effectively remove the amorphous region of cellulose due to its cellulose solubility properties without any assistance from any solvent as this IL has similar properties with H_2SO_4. IL hydrolysis of the amorphous cellulose rearranges the interlinking glycosidic bonds in anhydroglucose units of cellulose, thus releasing internal strain in cellulose molecule (Man *et al.*, 2011). The IL [bmim][HSO_4]-100 where there was no DMSO present, showed distinct CNCs with a needle like morphology. This meant that the pure IL was more effective for the conversion of cellulose to CNCs. However, the IL [bmim][$MeSO_4$] did not result in needle-like rods due to the presence of $[MeSO_4]^-$ anion.

Mohtar *et al.* (2017) reported that the pre-treatment of biomass with ILs shatters the network between cellulose, hemicellulose and lignin. The removal of both lignin and hemicellulose results in rough morphology compared to SCB fibres. Moreover, the increase of crystallinity increased the roughness of the pulp. The pre-treatment of SCB with ILs resulted in a formation of hydrogen bond, dipole-dipole interactions and van der Waals interactions

(Mohtar *et al.*, 2017). The bleaching method did not only swell cellulose, but assisted in the removal of lignin and hemicellulose by disrupting the hydrogen bonds of carbohydrates and ester bonds of lignin (Mohtar *et al.*, 2017).

4.3.2 Transmission electron microscopy (TEM)

TEM images of both [bmim][HSO_4]-90 and [bmim][HSO_4]-100 are shown in Figure 4-3 indicating nanocellulose fibrils (>500 nm) and cellulose nanocrystals (<500 nm) respectively. In TEM analyses only a section of the sample is used unlike DLS which analyses the whole sample. The other samples did not show any fibrils nor CNCs due to no nanocellulose produced. The TEM images produced quality of measurement of CNCs length which was similar to the work done by Lu and Hsieh (2012) and further confirmed by the nanoparticle sizes under DLS characterisation technique.

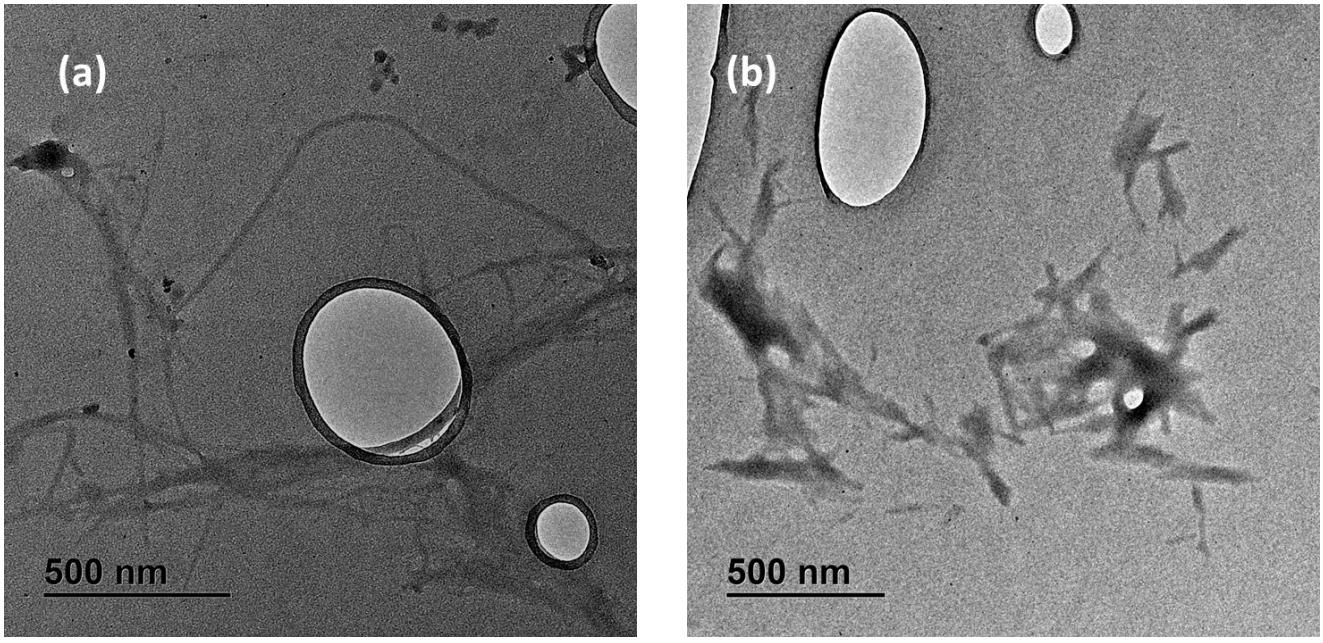

Figure 4-3. TEM images of [bmim][HSO_4]-90 showing nanocellulose fibrils; and (b) [bmim][HSO_4]-100 showing CNCs.

4.3.3 Powder-X-ray diffraction (P-XRD)

XRD was used to monitor the change of cellulose crystalline structures of untreated SCB and MCC (Figure 4-4). MCC was used as a reference material with respect to untreated SCB. The diffraction patterns for cellulosic material exhibits characteristic convoluted peaks of cellulose I at 2Θ equal to 14.8˚ corresponds to the crystallographic plane [110], the peak at 2Θ equal to 16.3˚ with [110], 2Θ equal to 20.4˚ corresponds to the plane [102], the peak at 2Θ equal to 22.4˚ corresponds to the [200] plane and the 2Θ equal to 34.5˚ corresponds the plane [004] (Abushammala, Krossing and Laborie, 2015) all shown in Figure 4-4. The absence of cellulose I peak around 12˚ meant that there was no cellulose regeneration into cellulose II (Jin *et al.*, 2016).

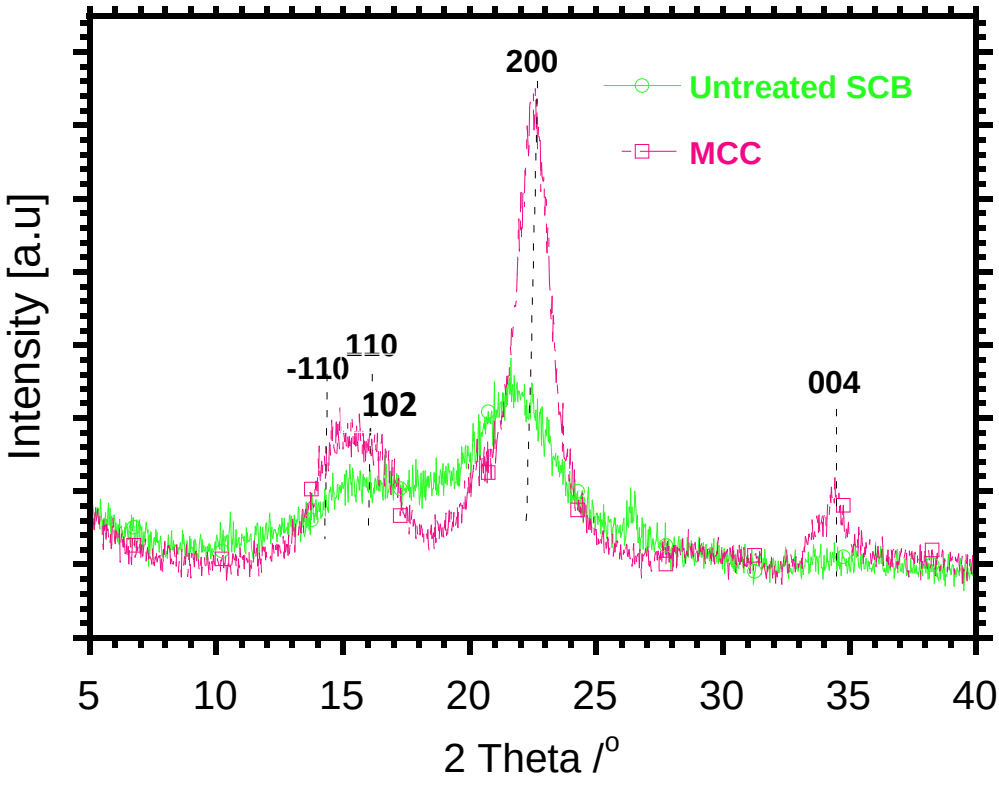

Figure 4-4. XRD diffractogram of untreated SCB and MCC.

The pulp which was pre-treated with IL/DMSO mixtures for 60 min pre-treatment and bleaching is shown on the diffractograms (Figure 4-5 a and b).

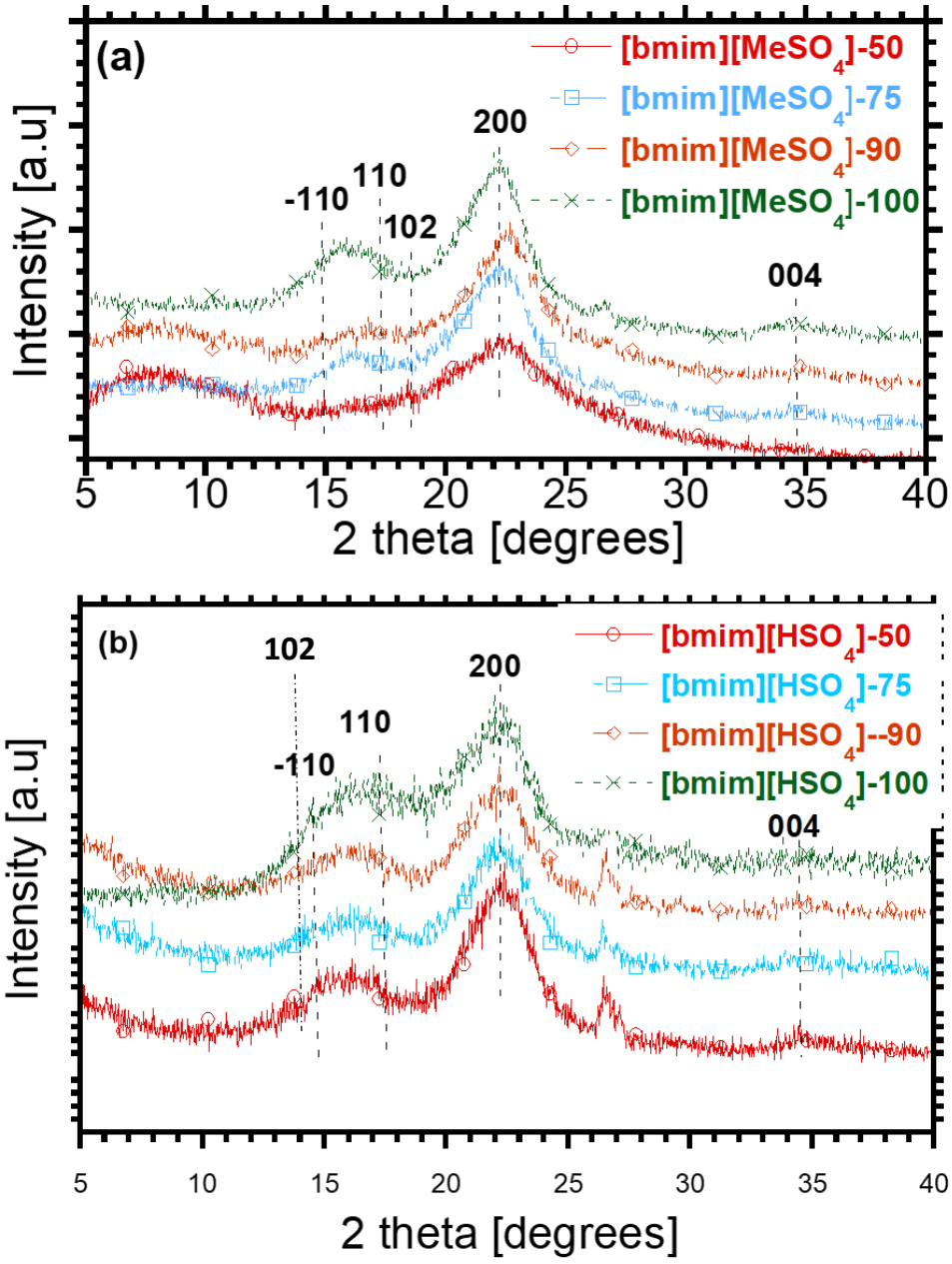

Figure 4-5. XRD diffractograms of IL/DMSO mixtures; (a) [bmim][$MeSO_4$]/DMSO (60-B) mixtures; and (b) [bmim][HSO_4]/DMSO (60-B) after pre-treatment time of 60 min bleaching.

The CrI was calculated using equation (3.6). CrI (%) of MCC was 84.1 % and for untreated SCB was 41.7 %. CrI (%) for bleached samples is shown in Table 4-34.

Table 4-34. CrI (%) for untreated SCB, MCC and SCB pre-treated samples.

Sample ID	CrI (%)
Untreated SCB	41.7
MCC	84.1
[bmim][$MeSO_4$]-50 (60-B)	48.7
[bmim][$MeSO_4$]-75 (60-B)	47.3
[bmim][$MeSO_4$]-90 (60-B)	45.2
[bmim][$MeSO_4$]-100 (60-B)	36.1
[bmim][HSO_4]-50 (60-B)	74.0
[bmim][HSO_4]-75 (60-B)	70.0
[bmim][HSO_4]-90 (60-B)	67.0
[bmim][HSO_4]-100 (60-B)	40.1

For both IL, the CrI was greatest for the pulp with the higher DMSO concentration in the IL/DMSO pre-treatment, which decreased with increasing IL concentration.

The ILs were able to fractionate the SCB biomass by removing lignin and affecting the crystallinity of cellulose (Cuissinat, Navard and Heinze 2008; Isik, Sardon and Mecerreyes 2014).

However, at 100 % IL there was the greatest decrease in CrI. This was due to the effectiveness of the IL [bmim][HSO_4] in the removal of lignin and hemicellulose and also the production of CNCs (Man *et al.* 2011).

The [bmim][$MeSO_4$]/DMSO pre-treated pulp which has a higher amount of lignin compared to [bmim][HSO_4]/DMSO had a minor increase in the amounts of CrI. This is due to the DMSO which swells cellulose but is not able to dissolve it (Brandt *et al.* 2011; Mandal and Chakrabarty 2011; Isik, Sardon and Mecerreyes 2014) and the ineffective anion of the [bmim][$MeSO_4$] IL.

4.3.4 Attenuated total reflection-Fourier transform infrared (ATR-FTIR)

Absorption band at 3600-3200 cm^{-1} for OH (stretch) was expected in the wavenumbers for all sample spectra. The bands at 1432 cm^{-1} (CH_2 scissoring) and 1340 cm^{-1} (CH bending) were expected to decrease in intensity with any decrease in crystalline content of the sample, whilst that at 1022 cm^{-1} (C_1 group vibrations) increases (Roberts, 1991). SCB microfibrils also result in less uniform nanocellulose as reported by (Bhattacharya, Germinario and Winter, 2008). The ATR-FTIR spectra of SCB, MCC and lignin are shown in Figure 4-6 (a and b).

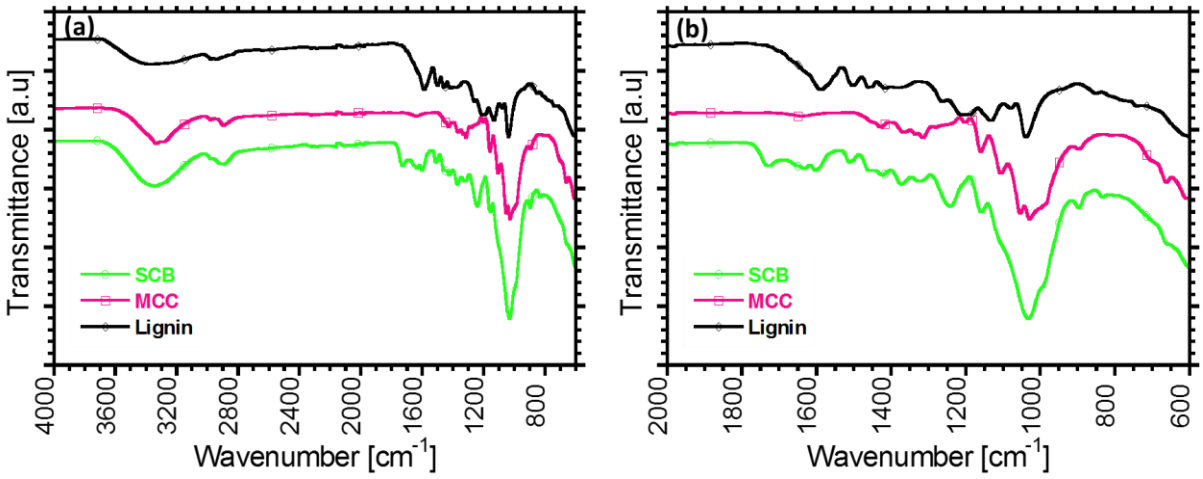

Figure 4-6. ATR-FTIR spectra of SCB, MCC and lignin; (a) at the wavenumbers 4000-600 cm^{-1}; and (b) at the wavenumbers 2000-600 cm^{-1}.

The FTIR spectra of [bmim][HSO4]/DMSO samples after 60 min pre-treatment and bleaching is shown in Figure 4-7.

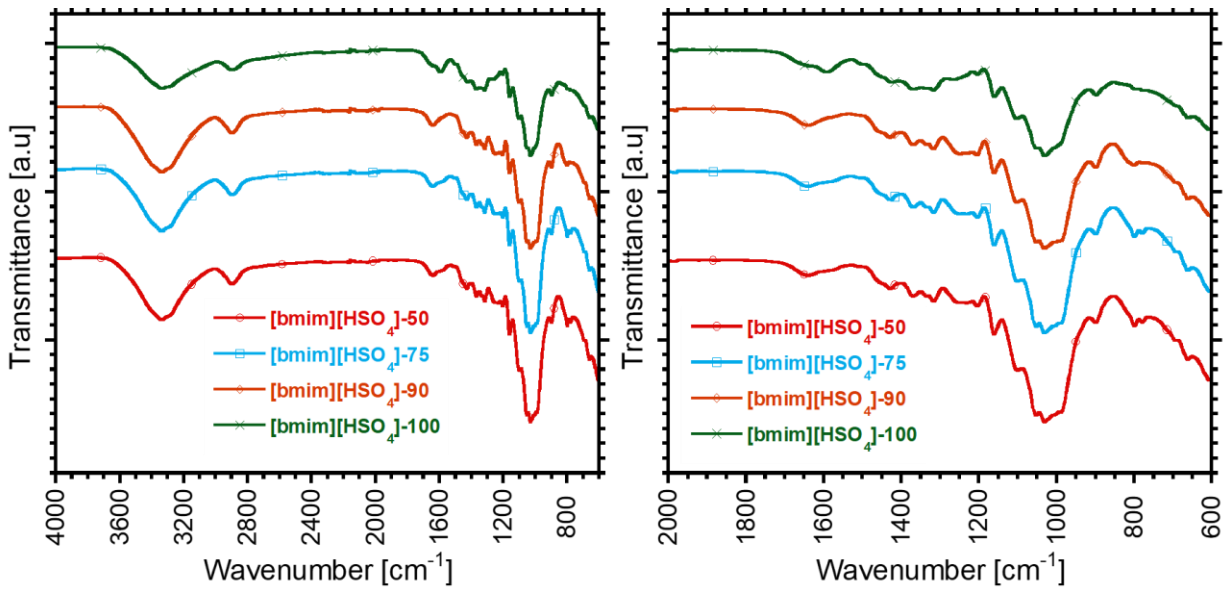

Figure 4-7. ATR-FTIR spectra of [bmim][HSO_4] samples after bleaching of 60 min pre-treatment time; ; (a) at the wavenumbers 4000-600 cm^{-1}; and (b) at the wavenumbers 2000-600 cm^{-1}.

The bands assigned at 1160 and 1111 cm^{-1} are C-O-C stretching and glucose ring stretching, respectively has a decrease in intensity from [bmim][HSO_4]-50 (60-B) to [bmim][HSO_4]-100 (60-B). The lack of bands at 1239 cm^{-1} implies the effective removal of lignin and hemicelluloses during pre-treatment of SCB. The sharp peak observed at 1313 cm^{-1} indicates –C-H asymmetric deformations of lignin which were absent in the [bmim][HSO_4]-50 (60-B) sample.

The FTIR spectra of [bmim][$MeSO_4$] samples after 60 min autoclave and bleaching is shown in Figure 4-8.

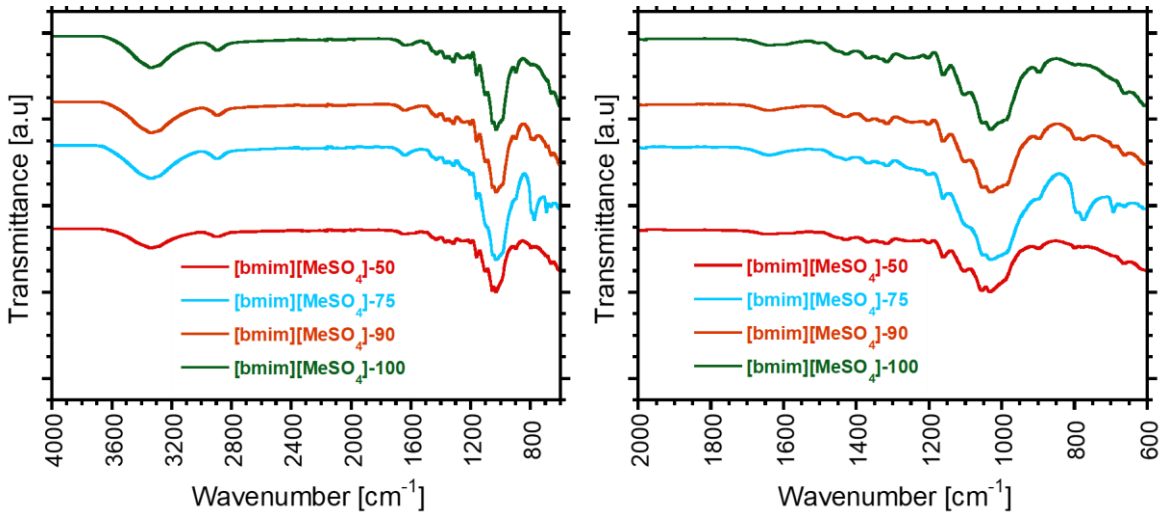

Figure 4-8. ATR-FTIR spectra of [bmim][$MeSO_4$] samples after bleaching of 60 min pre-treatment time; (a) at the wavenumbers 4000-600 cm^{-1}; and (b) at the wavenumbers 2000-600 cm^{-1}.

The prominent peak at 1731 cm^{-1} that is seen in the spectrum of the samples (Figure 4-7 and Figure 4-8) can be attributed either to the acetyl and uronic ester groups of the hemicelluloses or to the ester linkage of the carboxylic group of ferulic and p-coumarins of lignin and/or hemicelluloses (Elanthikkal *et al.*, 2010; Mandal and Chakrabarty, 2011). The peak is reduced in the MCC and the pre-treated samples spectra due to removal of these compounds.

The lack of bands at 1239 cm^{-1} implies the effective removal of lignin and hemicelluloses during pre-treatment of SCB. The sharp peak observed at 1313 cm^{-1} indicates –C-H asymmetric deformations. The increase in intensity of the band at 1022 cm^{-1} shows an increase in the cellulose content. The small sharp peak at 893 cm^{-1} band in the spectrum represents glycosidic –C_1-H deformation with a ring vibration contribution and –O-H bending. These features are characteristic of β-glycosidic linkages between the anhydroglucose units (Elanthikkal *et al.* 2010; Mandal and Chakrabarty 2011).

The assignments of broad bands at 1432 and 897 cm^{-1} are a result of HOC in plane bending of alcohol groups and glucose ring stretching, respectively (Schwanninger *et al.* 2004). The IL-DMSO mixtures disrupts the inter and intramolecular hydrogen bonds of cellulose by resulting in cellulose structural disorder (Oh *et al.* 2005).

The bands at 1340 and 1317 cm^{-1} are a result of O-H in plane deformation and CH_2 rocking vibration, respectively. The bands assigned at 1160 and 1111 cm^{-1} are C-O-C stretching and glucose ring stretching, respectively.

The bands at 1059 and 1030 cm^{-1} are from C-O stretching and C-O deformations in primary alcohols (Casas *et al.* 2012). The spectra also clearly confirmed the absence of 1596 cm^{-1} peak, which represents the aromatic skeletal vibrations with C=O stretching. A band at 1510 cm^{-1}, which represents the C-H deformations asymmetry. Two bands at 1463 and 1423 cm^{-1}, which represents C-H in plane deformation of lignin (Casas *et al.* 2012). A carbonyl stretching at 1729 cm^{-1} was also absent in the resulting nanocellulose which signals hemicellulose removal (Lu and Hsieh 2012).

4.3.5 Thermogravimetric analysis (TGA)

The samples were dried prior to thermal analysis. The thermograms of MCC and SCB are shown in Figure 4-9. The first thermal degradation peak for SCB was the instrument stabilisation. There was a plateau up to 240 ^{o}C for SCB, while for MCC there a 10 % initial gradual loss, the latter due slow degradation of cellulose. After 260 ^{o}C for both samples there is a rapid mass loss due to complete degradation of cellulose for MCC and for SCB complete degradation of cellulose, hemicellulose and lignin.

SCB had a thermal degradation of hemicellulose at 287.5 °C followed by a last thermal degradation of cellulose and lignin at 357.5 °C (Mandal and Chakrabarty, 2011; Yu *et al.*,

2013) as shown in Table 4-32. The SCB was the most thermally stable due to the presence of lignin which has anti-oxidant properties thus improves the thermal stability (Faruk and Sain 2015). SCB had ± 75 % mass loss at 400 °C and no further mass loss up to 500 °C whereas MCC had a 100 % mass loss at 500 °C which was a total thermal degradation of cellulose.

The thermal degradation properties of untreated SCB and MCC are shown in Table 4-35.

Table 4-35. Thermal degradation properties of SCB and MCC onset temperatures at 5 % mass loss ($T_{0.05}$), char (%) at 500 °C and maximum degradation temperatures from the first derivative curves (dTGA).

Sample ID	DTG (°C)	DTG (°C)	T_{char} (%)
Untreated SCB	287.5	357.5	15.8
MCC	323.4	none	2.37

The percentage char is the remaining inorganic matter and impurities after the pre-treatment of SCB with IL/DMSO that requires a higher temperature to absorb energy and thermally degrade. This usually takes place at temperatures above 600 °C (Watkins *et al.* 2015).

The percentage char was 15.8 % for untreated SCB, which was very higher compared to that of MCC which was 2.37 %. This was due to the presence of waxes, inorganic matter and impurities on untreated SCB and the IL/DMSO pre-treatment technique. Residual IL can also increase the amount of char (Mandal and Chakrabarty, 2011). Two step decomposition process resulted in a high percentage of char due to different decomposition and gasification processes and a low degree of crystallinity (41.7 %) (Tan, Hamid and Lai 2015).

The mass derivative indicated that the MCC was more thermally stable than the SCB.

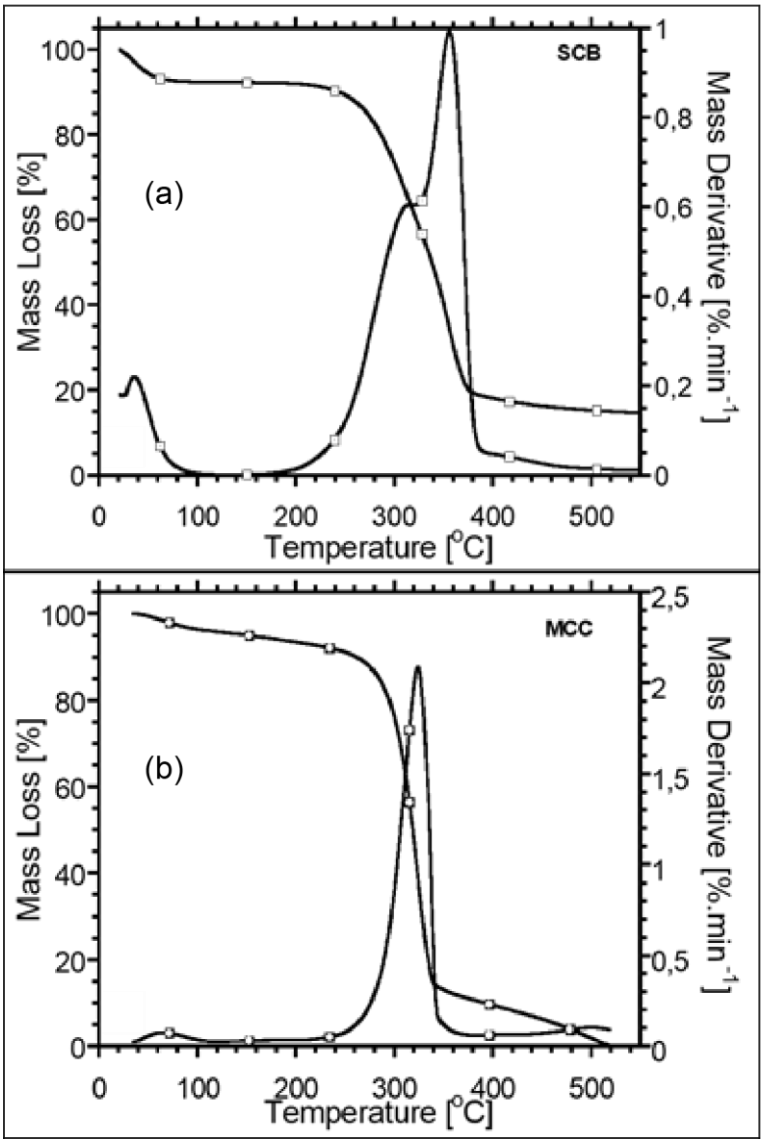

Figure 4-9. The thermogram of the mass loss as a function of temperature; and the maximum degradation temperatures from the first derivative curves (dTGA) of (a) untreated SCB; and (b) MCC.

The maximum thermal degradation of [bmim][$MeSO_4$]-50 (60-B) was at 269.4 °C and for [bmim][HSO_4]-50 (60-B) it was at 289.7 °C (Figure 4-10). Moreover, both gave an extra degradation peak at 426.0 °C and 390.5 °C for [bmim][$MeSO_4$]-50 (60-B) and [bmim][HSO_4]-50 (60-B), respectively. IL pre-treated pulp samples might have had impurities which resulted in % char above 20 %.

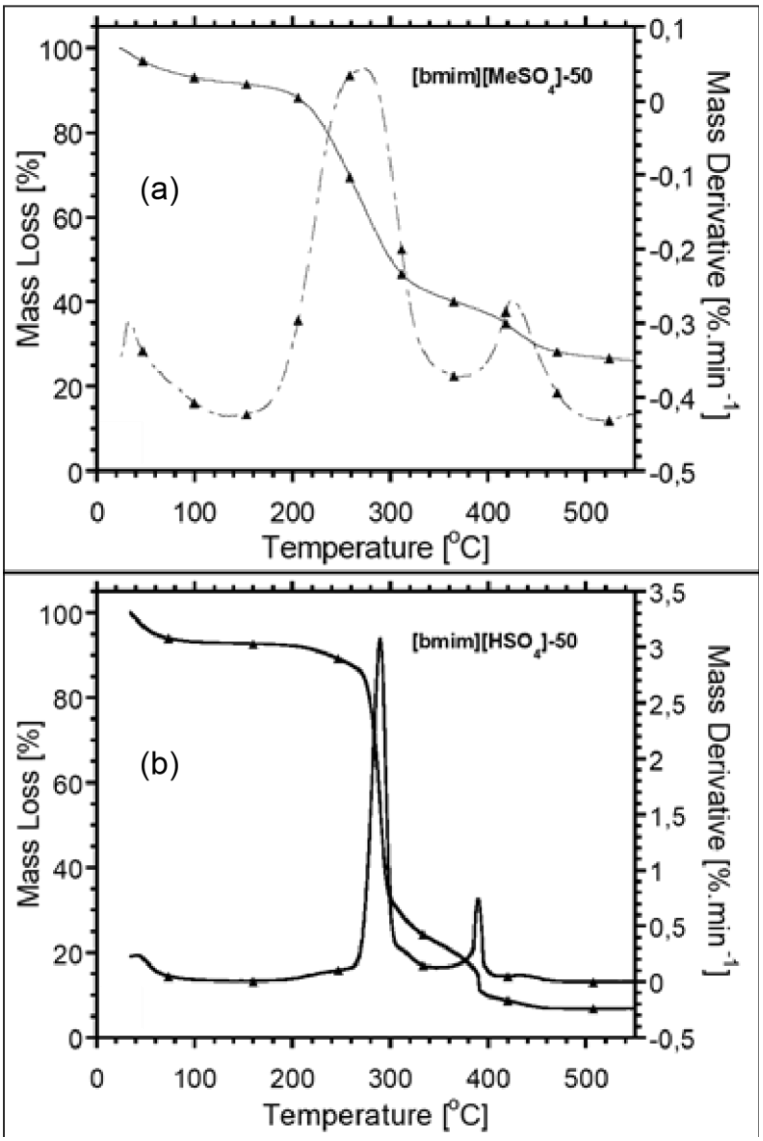

Figure 4-10. The thermogram of the mass loss as a function of temperature; and the maximum degradation temperatures from the first derivative curves (dTGA) of (a) [bmim][$MeSO_4$]-50 (60-B); and (b) [bmim][HSO_4]-50 (60-B).

The sample [bmim][$MeSO_4$]-75 (60-B) had a better thermal stability of 294.1 °C than [bmim][HSO_4]-75 (60-B) with 280.6 °C (Figure 4-11). However, these samples both resulted in two extra degradation peaks which was as a result of impurities (inorganic matter) in treated samples (Mandal and Chakrabarty 2011).

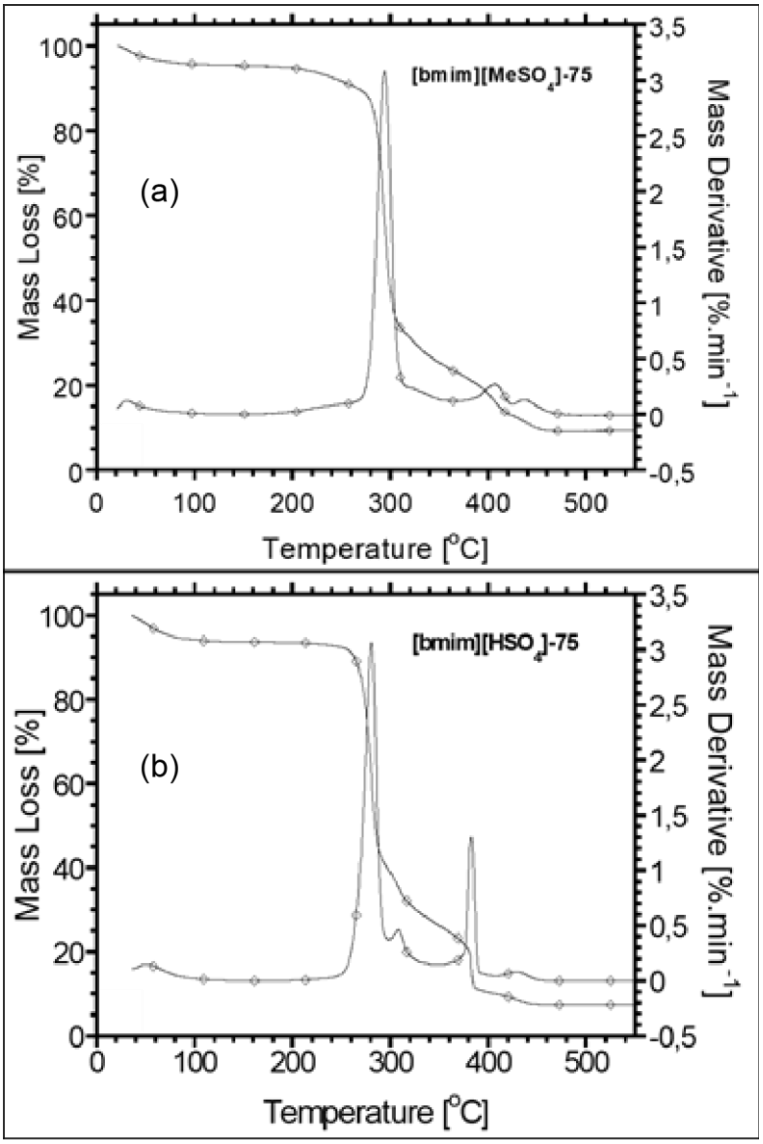

Figure 4-11. The thermogram of the mass loss as a function of temperature; and the maximum degradation temperatures from the first derivative curves (dTGA) of (a) [bmim][$MeSO_4$]-75 (60-B); and (b) [bmim][HSO_4]-75 (60-B).

The maximum thermal degradation of [bmim][$MeSO_4$]-90 (60-B) was 289.9 °C and [bmim][HSO_4]-90 (60-B) with 288.6 °C (Figure 4-12). There was no difference in the thermal degradation temperatures. Moreover, these samples resulted in two extra degradation peaks which was a result of inorganic impurities (Mandal and Chakrabarty 2011).

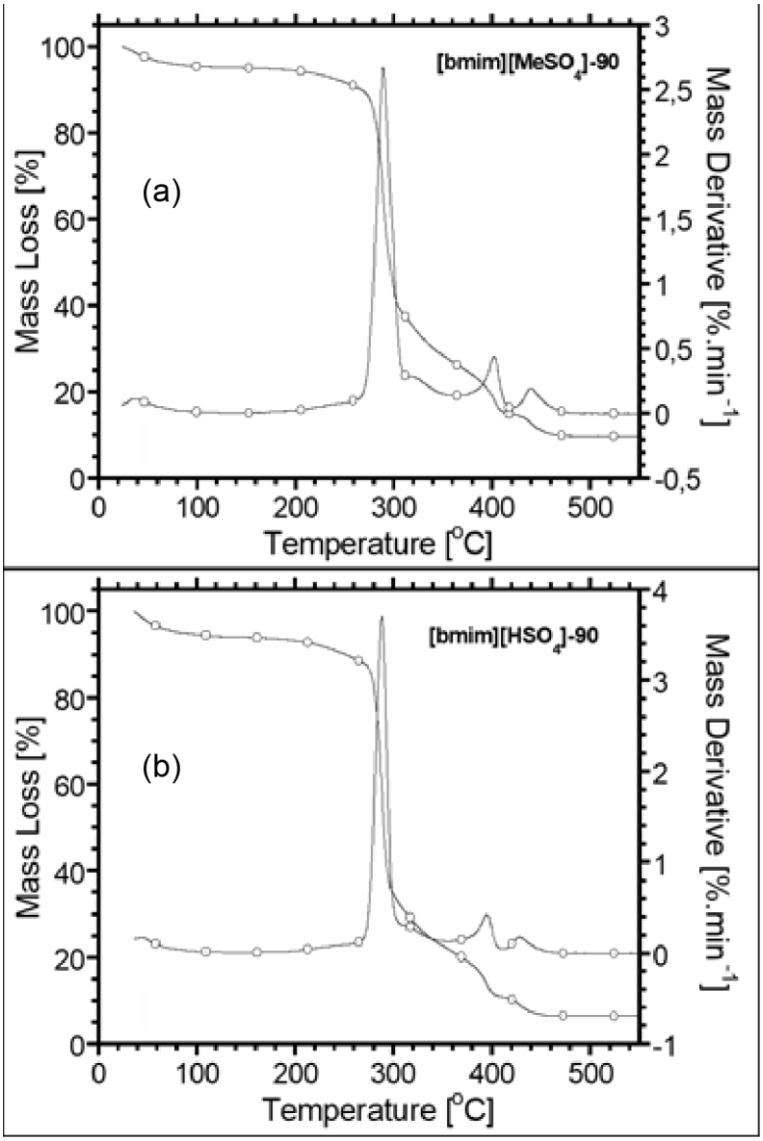

Figure 4-12. The thermogram of the mass loss as a function of temperature; and the maximum degradation temperatures from the first derivative curves (dTGA) of (a) [bmim][$MeSO_4$]-90 (60-B); and (b) [bmim][HSO_4]-90 (60-B).

The thermal properties of 100 % ILs were maximum thermal degradation of [bmim][$MeSO_4$]-100 (60-B) was 299.0 °C and [bmim][HSO_4]-100 (60-B) with 303.4 °C (Figure 4-13). Residual char was due to inorganic impurities present after pre-treatment.

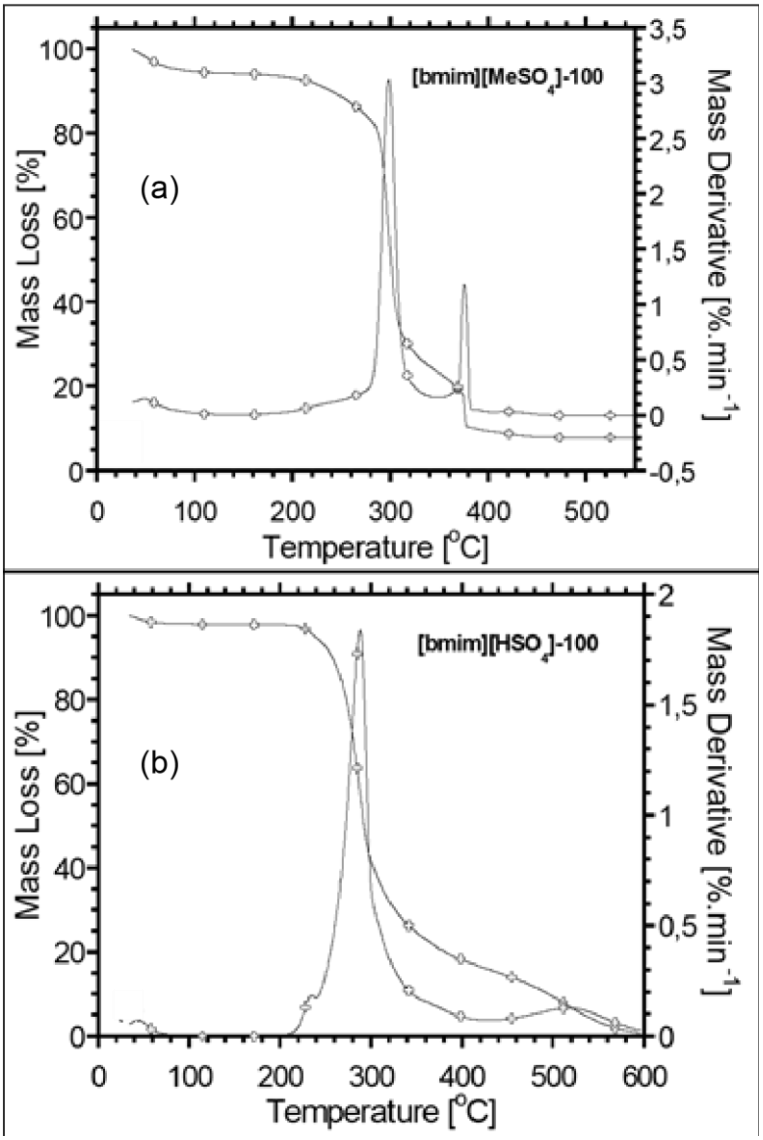

Figure 4-13. The thermogram of the mass loss as a function of temperature; and the maximum degradation temperatures from the first derivative curves (dTGA) of (a) [bmim][$MeSO_4$]-100 (60-B); and (b) [bmim][HSO_4]-100 (60-B).

The thermal properties of samples had a thermal degradation below 300 ℃ was the pyrolysis process. The only exception was for the sample [bmim][HSO_4]-100 (60-B). The thermal degradation pyrolysis process was due to the glucose dehydration of the glycosidic bonds of cellulose molecule which was broken down to –C-C- and –C-O- (Huang *et al.* 2017).

Table 4-36. The thermal degradation properties of IL/DMSO (60 min pre-treated and bleached samples) showing the onset temperatures at 5 % mass loss ($T_{0.05}$), char (%) at 500 ˚C and maximum degradation temperatures from the first derivative curves (DTG).

Pre-treatment with [bmim][$MeSO_4$]/DMSO (60-B)					
Sample ID	**$T_{0.05}$**	**DTG (°C)**	**DTG (°C)**	**DTG (°C)**	**T_{char} (%)**
[bmim][$MeSO_4$]-50 (60-B)	64.2	269.4	426	none	25.8
[bmim][$MeSO_4$]-75 (60-B)	127.8	294.1	406.8	436.8	9.32
[bmim][$MeSO_4$]-90 (60-B)	91.2	289.9	403.2	441.4	9.85
[bmim][$MeSO_4$]-100 (60-B)	77.6	299	376.2	none	7.96

Table 4-37. The thermal degradation properties of IL/DMSO (60 min pre-treated and bleached samples) showing the onset temperatures at 5 % mass loss ($T_{0.05}$), char (%) at 500 ˚C and maximum degradation temperatures from the first derivative curves (DTG).

Pre-treatment with [bmim][HSO_4]/DMSO (60-B)					
Sample ID	**$T_{0.05}$**	**DTG (°C)**	**DTG (°C)**	**DTG (°C)**	**T_{char} (%)**
[bmim][HSO_4]-50 (60-B)	60	289.7	390.5	none	6.82
[bmim][HSO_4]-75 (60-B)	69.7	280.6	309	383.1	7.49
[bmim][HSO_4]-90 (60-B)	78.1	288.6	396.4	430.3	6.51
[bmim][HSO_4]-100 (60-B)	59.8	303.4	none	none	10.4

The amount of char was reduced for the IL [bmim][$MeSO_4$] compared to the IL [bmim][HSO_4]. The IL [bmim][HSO_4] had a reduced char compared to the other IL. The MCC due to purity had the minimal char %. The difference was observed between the two ILs with [bmim][HSO_4]-50 (60-B) giving a better thermal stability compared to [bmim][$MeSO_4$]-50 (60-B). The sample [bmim][$MeSO_4$]-75 (60-B) had a better thermal stability than [bmim][HSO_4]-75. [bmim][HSO_4]-100 (60-B) was the most thermally stable with less impurities present. The percentage char was at 10 % (mass/mass) or below 10 % (m/m) for all samples excluding [bmim][$MeSO_4$]-50 (60-B).

The presence of DMSO disrupted cellulose structure, thus reducing thermal stability of nanocellulose materials. However, it should be noted that there was no drastic differences in all samples DTG due to cellulose degradation which occurs within the same region. The thermal stability of cellulose increases with the content of ILs presence during pre-treatment while cellulose decomposition started at 250 °C and persisted until 400 °C (Abraham *et al.* 2011; Saelee *et al.* 2016). Thus followed by another thermal degradation peak around 290 to 300 ˚C for nanocellulose and 335 ˚C for SCB due to "the cleavage of chemical bonds of glycosidic linkages of cellulose" (Luz *et al.* 2008) which shifted to the lower value for all samples. The extra degradation peaks were due to impurities a tar formation of levoglucosan through the pyrolysis of cellulose which further thermally degraded nanocellulose (Brown, Dayton and Daily 2001). The last thermal degradation of nanocellulose is carbonaceous residues in the region of 400 to 450 ˚C (Luz *et al.* 2008).

4.3.6 Dynamic light scattering (DLS)

4.3.6.1 Particle size analysis

The DLS scans are given in particle counts as a function of nanoparticle size in nanometers.

Figure 4-14, Figure 4-15, Figure 4-16 and Figure 4-17 are the particle size distribution for [bmim][$MeSO_4$]-50 (60-B), [bmim][$MeSO_4$]-75 (60-B), [bmim][$MeSO_4$]-90 (60-B) and [bmim][$MeSO_4$]-100 (60-B), respectively.

The results obtained from IL [bmim][$MeSO_4$] did not indicate any nanocellulose present. It should be noted that the samples still had lignin present which may also resulted in micro particles instead of nanoparticles. The smallest particle size for [bmim][$MeSO_4$]-50 (60-B) was 2900 nm, which was not in the nano-range.

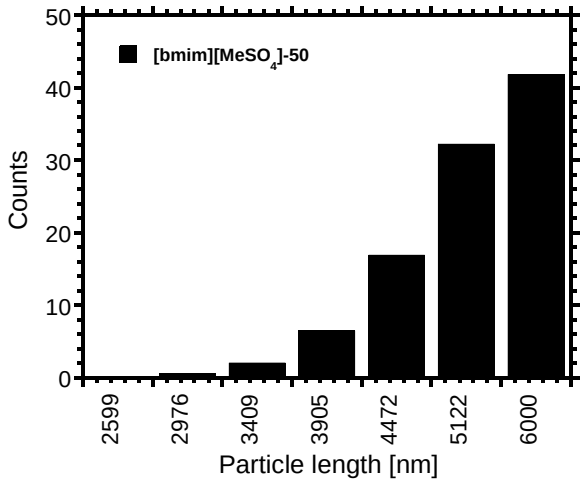

Figure 4-14. Particle size distribution of [bmim][$MeSO_4$]-50 (60-B).

The average particles size length for [bmim][$MeSO_4$]-75 (60-B) was 4400 nm. There was no nanoparticles present.

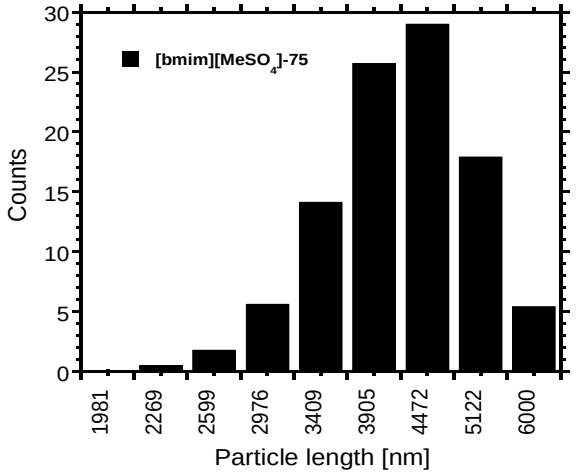

Figure 4-15. Particle size distribution of [bmim][$MeSO_4$]-75 (60-B).

The average particles size length for [bmim][$MeSO_4$]-90 (60-B) was 2900 nm. There was no nanoparticles present. However, the presence of lignin meant that the samples had lignin nanoparticles present.

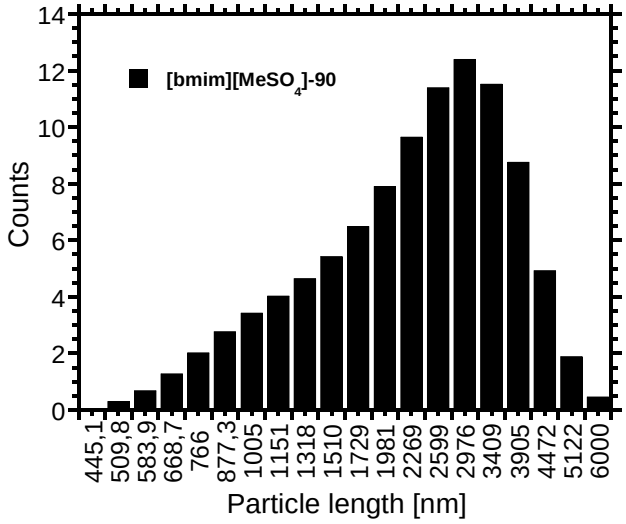

Figure 4-16. Particle size distribution of [bmim][$MeSO_4$]-90 (60-B).

The average particles size length for [bmim][$MeSO_4$]-100 (60-B) was not easy to determine since there were particle sizes below 1000 nm present. However, none resulted in CNCs. It

should also be noted that lignin was still present so it meant that the particles did not only represent cellulose particles but lignin too.

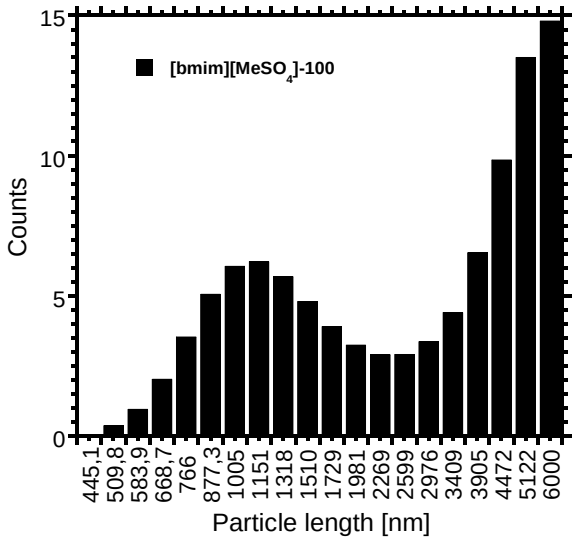

Figure 4-17. Particle size distribution of [bmim][MeSO4]-100.

Figure 4-18, Figure 4-19, Figure 4-20 and Figure 4-21 are the particle size distribution for [bmim][HSO4]-50 (60-B), [bmim][HSO4]-75 (60-B), [bmim][HSO4]-90 (60-B) and [bmim][HSO4]-100 (60-B), respectively.

The average particles size length for [bmim][HSO4]-50 (60-B) was not evenly distributed. There were no nanoparticles present. The 50 % (m/m) DMSO resulted in no nano particles (Figure 4-18).

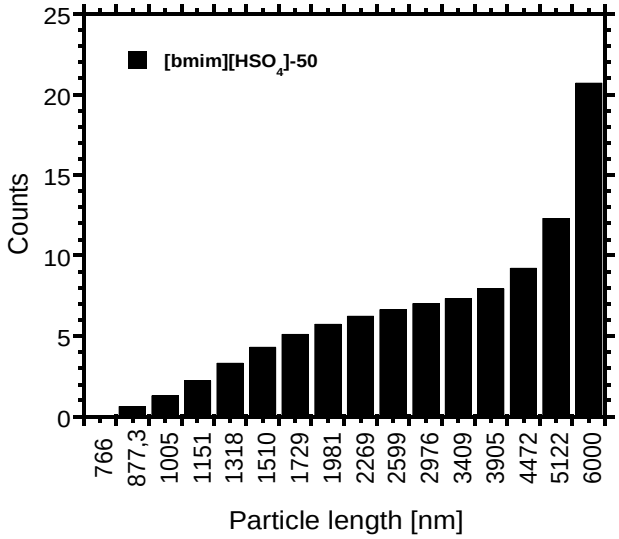

Figure 4-18. Particle size distribution of [bmim][HSO_4]-50 (60-B).

The average particles size length for [bmim][HSO_4]-75 (60-B) was 2000 nm with no nanoparticles present (Figure 4-19).

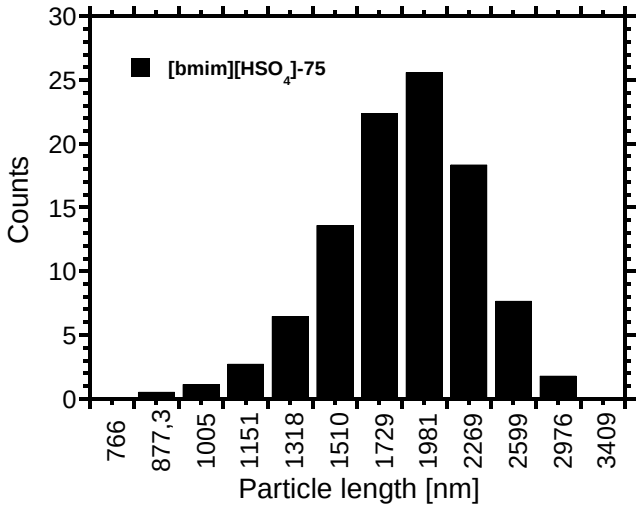

Figure 4-19. Particle size distribution of [bmim][HSO_4]-75 (60-B).

The average particles size length for [bmim][HSO_4]-90 (60-B) was 440 nm with a few particles above 500 nm. These was also observed in TEM images as nanofibrils. The percentage nanoparticles less than 500 nm (Figure 4-20) was 78.7 %.

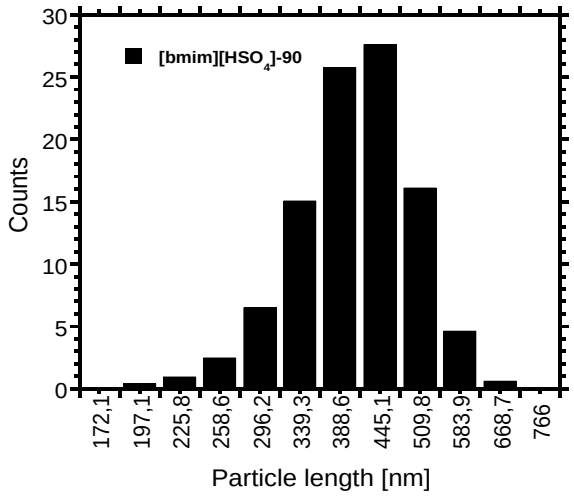

Figure 4-20. Particle size distribution of [bmim][HSO_4]-90 (60-B).

The [bmim][HSO_4]-100 sample resulted in only nanocellulose particles since lignin was reduced after pre-treatment and bleaching. As observed on the TEM images (Figure 4-3), there was CNCs which correspond to the particle size distribution of nanocellulose (Figure 4-21). The percentage nano particles less than 500 nm (Figure 4-21) was 100 %.

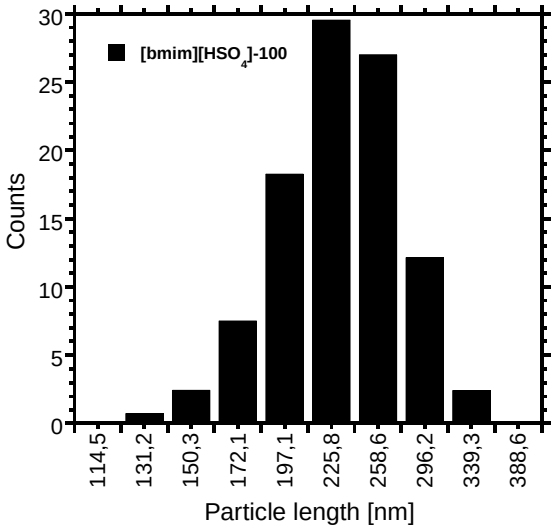

Figure 4-21. Particle size distribution of [bmim][HSO4]-100 (60-B).

4.3.6.2 Yield of nanocellulose

Equation 3.7 was used to calculate the percentage yield of nanocellulose.

There were no CNCs for all samples except [bmim][HSO4]-90 and [bmim][HSO4]-100 samples. The effect of IL [bmim][HSO4] on SCB resulted in the extraction of CNCs from SCB when no DMSO was present. Moreover, there was an extraction even at 90 % IL due to the strong acidic properties of [bmim][HSO4]. The CNC yield of [bmim][HSO4]-90 was 12.6 % from the initial SCB which was almost 80 % conversion. The [bmim][HSO4]-100, there was a complete extraction of CNCs from SCB which was a complete conversion of cellulose to CNCs. The amount of hydrolysed cellulose resulted in the direct extraction of CNCs from biomass. The DLS measurement for particle size is more accurate than the TEM analyses and the DLS analyses confirms that for [bmim][HSO4]-90 and [bmim][HSO4]-100 CNCs were obtained.

Table 4-38. Amount (%) of nanoparticles and yield (%) of CNCs.

Sample ID	I_{SCB} mass (g)	Mean particle size (nm)	Mass of recovered suspension (g)	*n** (%)	CNC Yield (%)
[bmim][$MeSO_4$]-50 (60-B)	1.005	> 6000	-	-	-
[bmim][$MeSO_4$]-75 (60-B)	1.001	4472	-	-	-
[bmim][$MeSO_4$]-90 (60-B)	1.007	2976	-	-	-
bmim][$MeSO_4$]-100 (60-B)	1.000	> 6000	-	-	-
[bmim][HSO_4]-50 (60-B)	1.002	> 6000	-	-	-
bmim][HSO_4]-75 (60-B)	1.006	1900	-	-	-
[bmim][HSO_4]-90 (60-B)	1.008	445	0.162	78.7	12.6
[bmim][HSO_4]-100 (60-B)	1.002	225	0.140	100	14.0

***n** = amount of nanoparticles below 500 nm.

I_{SCB} = initial SCB mass weighed before pre-treatment.

The mass of recovered suspension of samples with particle size above 500 nm was not recorded in Table 4-38, due to no nanocellulose particles present.

CHAPTER 5

CONCLUSION

5.1 Summary

SCB was pretreated with ILs: [bmim][$MeSO_4$] or [bmim][HSO_4] at varied times for the extraction of CNCs. The pre-treatment consumed up to 12 hours without a successful extraction of CNCs. For the [bmim][$MeSO_4$] samples, the amount of lignin and hemicellulose was reduced including the amount of cellulose. The yield of pulp after pre-treatment was drastically reduced. The [bmim][HSO_4] samples had a reduced lignin and hemicellulose similar to the [bmim][$MeSO_4$] samples. A significant difference between both ILs was that the amount of cellulose was increased for the [bmim][HSO_4] samples. Thus the IL [bmim][HSO_4] was capable of cellulose dissolution compared to the IL [bmim][$MeSO_4$]. The longer the pre-treatment with both ILs, the more lignin and hemicellulose removal from SCB.

Pre-treatment of biomass with ILs is tedious and time consuming so incorporation of ILs with another delignifying technique, bleaching process minimises the pretrtreatment time while retaining the crystallinity of cellulose. In this study, [bmim][HSO_4]/DMSO or [bmim][$MeSO_4$]/DMSO mixtures with 50%, 75%, 90% and 100% IL were used to delignify sugarcane bagasse. The results showed that bleaching removes most lignin and retain cellulose. The presence of DMSO affected the removal of both lignin and hemicellulose, thus decreasing solubility of cellulose. The resulting CNCs were produced when there was 10 % and no DMSO present with IL [bmim][HSO_4]. All samples resulted in a drastic redmoval of lignin and hemicellulose. The cellulose was increased due to more exposure when lignin and hemicellulose were removed. The only samples that resulted in CNCs were [bmim][HSO_4]-

90 and [bmim][HSO_4]-100 where the [bmim][HSO_4]/DMSO was the mixture used. [bmim][HSO_4]-90 resulted in 80 % CNC conversion with [bmim][HSO_4]-100 resulting in 100 % conversion of cellulose to CNCs.

The IL was successfully used for the production of CNCs.

5.2 Recommendation

The CNCs produced in this study can be used in the biocomposites as a reinforcement agent. However, this does not limit the application of CNCs as they can be used in other several fields of study.

5.3 Future work

Research into reinforcement of nanocellulose and functionalised nanocellulose in composite applications.

BIBLIOGRAPHY

Abe, M., Fukaya, Y. and Ohno, H. 2012. Fast and facile dissolution of cellulose with tetrabutylphosphonium hydroxide containing 40 wt% water. *Chemical Communications*, 48 (12): 1808-1810.

Abitbol, T., Rivkin, A., Cao, Y., Nevo, Y., Abraham, E., Ben-Shalom, T., Lapidot, S. and Shoseyov, O. 2016. Nanocellulose, a tiny fiber with huge applications. *Current Opinion in Biotechnology*, 39: 76-88.

Abraham, E., Deepa, B., Pothan, L., Jacob, M., Thomas, S., Cvelbar, U. and Anandjiwala, R. 2011. Extraction of nanocellulose fibrils from lignocellulosic fibres: A novel approach. *Carbohydrate Polymers*, 86 (4): 1468-1475.

Abushammala, H., Krossing, I. and Laborie, M.-P. 2015. Ionic liquid-mediated technology to produce cellulose nanocrystals directly from wood. *Carbohydrate Polymers*, 134: 609-616.

Agbor, V. B., Cicek, N., Sparling, R., Berlin, A. and Levin, D. B. 2011. Biomass pretreatment: fundamentals toward application. *Biotechnology Advances*, 29 (6): 675-685.

Akhtar, N., Gupta, K., Goyal, D. and Goyal, A. 2016. Recent advances in pretreatment technologies for efficient hydrolysis of lignocellulosic biomass. *Environmental Progress & Sustainable Energy*, 35 (2): 489-511.

Akin, D. and Benner, R. 1988. Degradation of polysaccharides and lignin by ruminal bacteria and fungi. *Applied and Environmental Microbiology*, 54 (5): 1117-1125.

Alvira, P., Tomás-Pejó, E., Ballesteros, M. and Negro, M. 2010. Pretreatment technologies for an efficient bioethanol production process based on enzymatic hydrolysis: a review. *Bioresource Technology*, 101 (13): 4851-4861.

Anastas, P. T. and Beach, E. S. 2007. Green chemistry: the emergence of a transformative framework. *Green Chemistry Letters and Reviews*, 1 (1): 9-24.

Atalla, R. and VanderHart, D. L. 1999. The role of solid state 13C NMR spectroscopy in studies of the nature of native celluloses. *Solid State Nuclear Magnetic Resonance*, 15 (1): 1-19.

Atalla, R. H. and Vanderhart, D. L. 1984. Native cellulose: a composite of two distinct crystalline forms. *Science*, 223 (4633): 283-285.

Bamdad, H., Hawboldt, K. and MacQuarrie, S. 2017. A review on common adsorbents for acid gases removal: Focus on biochar. *Renewable and Sustainable Energy Reviews*, 81 (Part 2): 1705-1720.

Baurhoo, B., Ruiz-Feria, C. and Zhao, X. 2008. Purified lignin: Nutritional and health impacts on farm animals—A review. *Animal Feed Science and Technology*, 144 (3-4): 175-184.

Berg, R. W., Deetlefs, M., Seddon, K. R., Shim, I. and Thompson, J. M. 2005. Raman and ab initio studies of simple and binary 1-alkyl-3-methylimidazolium ionic liquids. *The Journal of Physical Chemistry B*, 109 (40): 19018-19025.

Börjesson, M. and Westman, G. 2015. Crystalline nanocellulose—preparation, modification, and properties. In: *Cellulose-Fundamental Aspects and Current Trends*. InTech Publishers, 1687–1691.

Brandt, A., Ray, M. J., To, T. Q., Leak, D. J., Murphy, R. J. and Welton, T. 2011. Ionic liquid pretreatment of lignocellulosic biomass with ionic liquid–water mixtures. *Green Chemistry*, 13 (9): 2489-2499.

Brinchi, L., Cotana, F., Fortunati, E. and Kenny, J. 2013. Production of nanocrystalline cellulose from lignocellulosic biomass: technology and applications. *Carbohydrate Polymers*, 94 (1): 154-169.

Brodeur, G., Yau, E., Badal, K., Collier, J., Ramachandran, K. and Ramakrishnan, S. 2011. Chemical and physicochemical pretreatment of lignocellulosic biomass: a review. *Enzyme Research*, 2011

Brown, A. L., Dayton, D. C. and Daily, J. W. 2001. A study of cellulose pyrolysis chemistry and global kinetics at high heating rates. *Energy & Fuels*, 15 (5): 1286-1294.

Casas, A., Palomar, J., Alonso, M. V., Oliet, M., Omar, S. and Rodriguez, F. 2012. Comparison of lignin and cellulose solubilities in ionic liquids by COSMO-RS analysis and experimental validation. *Industrial Crops and Products*, 37 (1): 155-163.

Cele, N. P. 2017. Beneficiation of sugarcane bagasse for materials development and energy generation in South Africa. In: Proceedings of *NMISA celebrates 70 years of accurate scientific measurement (metrology) and 10 years of Institution existence!* . Pretoria, South Africa, NMISA, 1-12.

Cerqueira, D. A., Rodrigues Filho, G. and da Silva Meireles, C. 2007. Optimization of sugarcane bagasse cellulose acetylation. *Carbohydrate Polymers*, 69 (3): 579-582.

Chen, M., Chen, C., Liu, C. and Sun, R. 2013. Homogeneous modification of sugarcane bagasse with maleic anhydride in 1-butyl-3-methylimidazolium chloride without any catalysts. *Industrial Crops and Products*, 46: 380-385.

Contreras, A. M., Rosa, E., Pérez, M., Van Langenhove, H. and Dewulf, J. 2009. Comparative life cycle assessment of four alternatives for using by-products of cane sugar production. *Journal of Cleaner Production*, 17 (8): 772-779.

Cuissinat, C., Navard, P. and Heinze, T. 2008. Swelling and dissolution of cellulose. Part IV: Free floating cotton and wood fibres in ionic liquids. *Carbohydrate Polymers*, 72 (4): 590-596.

Custodis, V. B., Bährle, C., Vogel, F. and van Bokhoven, J. A. 2015. Phenols and aromatics from fast pyrolysis of variously prepared lignins from hard-and softwoods. *Journal of Analytical and Applied Pyrolysis*, 115: 214-223.

da Silva, A. S. A., Lee, S.-H., Endo, T. and Bon, E. P. 2011. Major improvement in the rate and yield of enzymatic saccharification of sugarcane bagasse via pretreatment with the ionic liquid 1-ethyl-3-methylimidazolium acetate ([Emim][Ac]). *Bioresource Technology*, 102 (22): 10505-10509.

de Carvalho Mendes, C. A., Ferreira, N. M. S., Furtado, C. R. G. and de Sousa, A. M. F. 2015. Isolation and characterization of nanocrystalline cellulose from corn husk. *Materials Letters*, 148: 26-29.

de Oliveira, F. B., Bras, J., Pimenta, M. T. B., da Silva Curvelo, A. A. and Belgacem, M. N. 2016. Production of cellulose nanocrystals from sugarcane bagasse fibers and pith. *Industrial Crops and Products*, 93: 48-57.

Dibble, D. C., Li, C., Sun, L., George, A., Cheng, A., Çetinkol, Ö. P., Benke, P., Holmes, B. M., Singh, S. and Simmons, B. A. 2011. A facile method for the recovery of ionic liquid and lignin from biomass pretreatment. *Green Chemistry*, 13 (11): 3255-3264.

Dien, B., Li, X.-L., Iten, L., Jordan, D., Nichols, N., O'Bryan, P. and Cotta, M. 2006. Enzymatic saccharification of hot-water pretreated corn fiber for production of monosaccharides. *Enzyme and Microbial Technology*, 39 (5): 1137-1144.

Ding, Z.-D., Chi, Z., Gu, W.-X., Gu, S.-M., Liu, J.-H. and Wang, H.-J. 2012. Theoretical and experimental investigation on dissolution and regeneration of cellulose in ionic liquid. *Carbohydrate Polymers*, 89 (1): 7-16.

Doherty, T. V., Mora-Pale, M., Foley, S. E., Linhardt, R. J. and Dordick, J. S. 2010. Ionic liquid solvent properties as predictors of lignocellulose pretreatment efficacy. *Green Chemistry*, 12 (11): 1967-1975.

Du, C. and Zhou, J. 2009. Evaluation of Soil Fertility Using Infrared Spectroscopy – A Review. *Environmental Chemistry Letters*, 7: 453-483.

Duran, N., Lemes, A. P., Duran, M., Freer, J. and Baeza, J. 2011. A minireview of cellulose nanocrystals and its potential integration as co-product in bioethanol production. *Journal of the Chilean Chemical Society*, 56 (2): 672-677.

Eichhorn, S. J., Dufresne, A., Aranguren, M., Marcovich, N., Capadona, J., Rowan, S., Weder, C., Thielemans, W., Roman, M. and Renneckar, S. 2010. current international research into cellulose nanofibres and nanocomposites. *Journal of materials science*, 45 (1): 1.

Elanthikkal, S., Gopalakrishnapanicker, U., Varghese, S. and Guthrie, J. T. 2010. Cellulose microfibres produced from banana plant wastes: Isolation and characterization. *Carbohydrate Polymers*, 80 (3): 852-859.

Espinoza-Acosta, J. L., Torres-Chávez, P. I., Carvajal-Millán, E., Ramírez-Wong, B., Bello-Pérez, L. A. and Montaño-Leyva, B. 2014. Ionic liquids and organic solvents for recovering lignin from lignocellulosic biomass. *BioResources*, 9 (2): 3660-3687.

Faix, O. 1992. Fourier transform infrared spectroscopy. In: *Methods in lignin chemistry*. Springer, 83-109.

Fan, L., Lee, Y. H. and Beardmore, D. H. 1980. Mechanism of the enzymatic hydrolysis of cellulose: effects of major structural features of cellulose on enzymatic hydrolysis. *Biotechnology and Bioengineering*, 22 (1): 177-199.

Faruk, O. and Sain, M. 2015. *Lignin in Polymer Composites*. First ed. William Andrew.

Fernández-Rodríguez, J., Gordobil, O., Robles, E., González-Alriols, M. and Labidi, J. 2017. Lignin valorization from side-streams produced during agricultural waste pulping and total chlorine free bleaching. *Journal of Cleaner Production*, 142: 2609-2617.

Filson, P. B. and Dawson-Andoh, B. E. 2009. Sono-chemical preparation of cellulose nanocrystals from lignocellulose derived materials. *Bioresource Technology*, 100 (7): 2259-2264.

Filson, P. B., Dawson-Andoh, B. E. and Schwegler-Berry, D. 2009. Enzymatic-mediated production of cellulose nanocrystals from recycled pulp. *Green Chemistry*, 11 (11): 1808-1814.

Fortunati, E., Puglia, D., Luzi, F., Santulli, C., Kenny, J. M. and Torre, L. 2013. Binary PVA bio-nanocomposites containing cellulose nanocrystals extracted from different natural sources: Part I. *Carbohydrate Polymers*, 97 (2): 825-836.

Gao, X., Kumar, R. and Wyman, C. E. 2014. Fast hemicellulose quantification via a simple one-step acid hydrolysis. *Biotechnology and Bioengineering*, 111 (6): 1088-1096.

Gardare, V. N., Yadav, S., Avhad, D. N. and Rathod, V. K. 2015. Preparation of adsorbent using sugarcane bagasse by chemical treatment for the adsorption of methylene blue. *Desalination and Water Treatment*, 56 (11): 2872-2878.

Gerwert, K. and Kötting, C. 2010. *Fourier Transform Infrared (FTIR) Spectroscopy*. Wiley Online Library.

Ghaffar, S. H. and Fan, M. 2013. Structural analysis for lignin characteristics in biomass straw. *Biomass and Bioenergy*, 57: 264-279.

Habibi, Y., Lucia, L. A. and Rojas, O. J. 2010. Cellulose nanocrystals: chemistry, self-assembly, and applications. *Chemical Reviews*, 110 (6): 3479-3500.

Hart, P. W. and Rudie, A. W. 2012. *The Bleaching of Pulp*. Technical Association of the Pulp & Paper Industry.

Hatton, P. D., Wilkins, S. B., Beale, T. A. W., Johal, T. K., Prabhakaran, D. and Boothroyd, A. T. 2005. Resonant soft X-ray diffraction - in extremis. *Journal of Synchrotron Radiation*, 12 (4): 434-441.

Hill, C. A. 2007. *Wood modification: chemical, thermal and other processes*. John Wiley & Sons.

Hise, R. G. and Hintz, H. L. 1990. Hypochlorite Bleaching. In: *1990 Bleach Plant Operation*. Atlanta, USA: TAPPI, 141-158.

Huang, S., Wang, X., Shen, J., Wu, R., Zhao, H., Wang, Y., Wang, Y. and Xia, Y. 2017. Surface functionalization of cellulose nanocrystals with polymeric ionic liquids during phase transfer. *Carbohydrate Polymers*, 157: 1426-1433.

Hulett, T. 2013. *Sugarcane Potential Food & Energy* South Africa: Tongaat Hulett.

Ibrahim, M. M., Dufresne, A., El-Zawawy, W. K. and Agblevor, F. A. 2010. Banana fibers and microfibrils as lignocellulosic reinforcements in polymer composites. *Carbohydrate Polymers*, 81 (4): 811-819.

Isik, M., Sardon, H. and Mecerreyes, D. 2014. Ionic liquids and cellulose: dissolution, chemical modification and preparation of new cellulosic materials. *International Journal of Molecular Sciences*, 15 (7): 11922-11940.

Jiang, M., Zhao, M., Zhou, Z., Huang, T., Chen, X. and Wang, Y. 2011. Isolation of cellulose with ionic liquid from steam exploded rice straw. *Industrial Crops and Products*, 33 (3): 734-738.

John, M. J. and Thomas, S. 2008. Biofibres and biocomposites. *Carbohydrate Polymers*, 71 (3): 343-364.

Karatzos, S. K., Edye, L. A. and Doherty, W. O. S. 2012. Sugarcane bagasse pretreatment using three imidazolium-based ionic liquids; mass balances and enzyme kinetics. *Biotechnology for Biofuels*, 5 (1): 62.

Kargarzadeh, H., Ahmad, I., Abdullah, I., Dufresne, A., Zainudin, S. Y. and Sheltami, R. M. 2012. Effects of hydrolysis conditions on the morphology, crystallinity, and thermal stability of cellulose nanocrystals extracted from kenaf bast fibers. *Cellulose*, 19 (3): 855-866.

Karimi, K. and Taherzadeh, M. J. 2016. A critical review of analytical methods in pretreatment of lignocelluloses: composition, imaging, and crystallinity. *Bioresource Technology*, 200: 1008-1018.

Kaur, R. and Uppal, S. 2015. Structural characterization and antioxidant activity of lignin from sugarcane bagasse. *Colloid and Polymer Science*, 293 (9): 2585-2592.

Khan, A., Khan, R. A., Salmieri, S., Le Tien, C., Riedl, B., Bouchard, J., Chauve, G., Tan, V., Kamal, M. R. and Lacroix, M. 2012. Mechanical and barrier properties of nanocrystalline cellulose reinforced chitosan based nanocomposite films. *Carbohydrate Polymers*, 90 (4): 1601-1608.

Kirk, T. K. 1971. Effects of microorganisms on lignin. *Annual review of Phytopathology*, 9 (1): 185-210.

Kumar, P., Barrett, D. M., Delwiche, M. J. and Stroeve, P. 2009. Methods for pretreatment of lignocellulosic biomass for efficient hydrolysis and biofuel production. *Industrial & Engineering Chemistry Research*, 48 (8): 3713-3729.

Lam, E., Male, K. B., Chong, J. H., Leung, A. C. and Luong, J. H. 2012. Applications of functionalized and nanoparticle-modified nanocrystalline cellulose. *Trends in Biotechnology*, 30 (5): 283-290.

Lan, W., Liu, C.-F. and Sun, R.-C. 2011. Fractionation of bagasse into cellulose, hemicelluloses, and lignin with ionic liquid treatment followed by alkaline extraction. *Journal of Agricultural and Food Chemistry*, 59 (16): 8691-8701.

Lee, H., Hamid, S. and Zain, S. 2014. Conversion of lignocellulosic biomass to nanocellulose: structure and chemical process. *The Scientific World Journal*, 2014

Li, H.-Y., Chen, X., Wang, C.-Z., Sun, S.-N. and Sun, R.-C. 2016. Evaluation of the two-step treatment with ionic liquids and alkali for enhancing enzymatic hydrolysis of Eucalyptus: chemical and anatomical changes. *Biotechnology for Biofuels*, 9 (1): 166.

Lin, N. and Dufresne, A. 2014. Nanocellulose in biomedicine: Current status and future prospect. *European Polymer Journal*, 59: 302-325.

Liu, C., Sun, R., Zhang, A., Ren, J., Wang, X., Qin, M., Chao, Z. and Luo, W. 2007. Homogeneous modification of sugarcane bagasse cellulose with succinic anhydride using a ionic liquid as reaction medium. *Carbohydrate Research*, 342 (7): 919-926.

Liu, K.-X., Li, H.-Q., Zhang, J., Zhang, Z.-G. and Xu, J. 2016. The effect of non-structural components and lignin on hemicellulose extraction. *Bioresource Technology*, 214: 755-760.

Liu, Y., Wang, H., Yu, G., Yu, Q., Li, B. and Mu, X. 2014. A novel approach for the preparation of nanocrystalline cellulose by using phosphotungstic acid. *Carbohydrate Polymers*, 110: 415-422.

Loh, Y., Sujan, D., Rahman, M. and Das, C. 2013. Sugarcane bagasse—The future composite material: A literature review. *Resources, Conservation and Recycling*, 75: 14-22.

Lu, B., Xu, A. and Wang, J. 2014. Cation does matter: how cationic structure affects the dissolution of cellulose in ionic liquids. *Green Chemistry*, 16 (3): 1326-1335.

Lu, P. and Hsieh, Y.-L. 2012. Preparation and characterization of cellulose nanocrystals from rice straw. *Carbohydrate Polymers*, 87 (1): 564-573.

Luz, S., Del Tio, J., Rocha, G., Gonçalves, A. and Del'Arco Jr, A. 2008. Cellulose and cellulignin from sugarcane bagasse reinforced polypropylene composites: Effect of acetylation on mechanical and thermal properties. *Composites Part A: Applied Science and Manufacturing*, 39 (9): 1362-1369.

Mäki-Arvela, P., Anugwom, I., Virtanen, P., Sjöholm, R. and Mikkola, J.-P. 2010. Dissolution of lignocellulosic materials and its constituents using ionic liquids—a review. *Industrial Crops and Products*, 32 (3): 175-201.

Man, Z., Muhammad, N., Sarwono, A., Bustam, M. A., Kumar, M. V. and Rafiq, S. 2011. Preparation of cellulose nanocrystals using an ionic liquid. *Journal of Polymers and the Environment*, 19 (3): 726-731.

Mandal, A. and Chakrabarty, D. 2011. Isolation of nanocellulose from waste sugarcane bagasse (SCB) and its characterization. *Carbohydrate Polymers*, 86 (3): 1291-1299.

Mao, J., Heck, B., Reiter, G. and Laborie, M.-P. 2015. Cellulose nanocrystals' production in near theoretical yields by 1-butyl-3-methylimidazolium hydrogen sulfate ([Bmim] HSO 4)–mediated hydrolysis. *Carbohydrate Polymers*, 117: 443-451.

Martin, E. M., Bunnell, K. A., Lau, C.-S., Pelkki, M. H., Patterson, D. W., Clausen, E. C., Smith, J. A. and Carrier, D. J. 2011. Hot water and dilute acid pretreatment of high and low specific gravity Populusdeltoides clones. *Journal of Industrial Microbiology & Biotechnology*, 38 (2): 355-361.

Maryana, R., Ma'rifatun, D., Wheni, A., Satriyo, K. and Rizal, W. A. 2014. Alkaline pretreatment on sugarcane bagasse for bioethanol production. *Energy Procedia*, 47: 250-254.

McDonough, T. 1992. Bleaching Agents, Pulp and Paper. *Kirk-Othmer encyclopedia of chemical technology*,

Minnick, D. L., Flores, R. A., DeStefano, M. R. and Scurto, A. M. 2016. Cellulose solubility in ionic liquid mixtures: temperature, cosolvent, and antisolvent effects. *The Journal of Physical Chemistry B*, 120 (32): 7906-7919.

Mohlala, L. M., Bodunrin, M. O., Awosusi, A. A., Daramola, M. O., Cele, N. P. and Olubambi, P. A. 2016. Beneficiation of corncob and sugarcane bagasse for energy generation and materials development in Nigeria and South Africa: a short overview. *Alexandria Engineering Journal*, 55 (3): 3025-3036.

Mohtar, S. S., Busu, T. N. Z. T. M., Noor, A. M. M., Shaari, N. and Mat, H. 2017. An ionic liquid treatment and fractionation of cellulose, hemicellulose and lignin from oil palm empty fruit bunch. *Carbohydrate Polymers*, 166: 291-299.

Moon, D., Shin, S.-J., Choi, J. W., Park, J.-S., Kim, W. and Kwon, M. 2011. Chemical modification of secondary xylem under tensile stress in the stem of Liriodendron tulipifera. *Forest Science and Technology*, 7 (2): 53-59.

Moosavi, F. 2013. The Structure of Supported Ionic Liquids at the Interface. In: *Ionic Liquids-New Aspects for the Future*. InTech.

Mosier, N., Wyman, C., Dale, B., Elander, R., Lee, Y., Holtzapple, M. and Ladisch, M. 2005. Features of promising technologies for pretreatment of lignocellulosic biomass. *Bioresource Technology*, 96 (6): 673-686.

Mussatto, S., Rocha, G. and Roberto, I. 2008. Hydrogen peroxide bleaching of cellulose pulps obtained from brewer's spent grain. *Cellulose*, 15 (4): 641-649.

Narayanaswamy, N., Dheeran, P., Verma, S. and Kumar, S. 2013. Biological pretreatment of lignocellulosic biomass for enzymatic saccharification. In: *Pretreatment Techniques for Biofuels and Biorefineries*. Springer, 3-34.

Ng, H.-M., Sin, L. T., Tee, T.-T., Bee, S.-T., Hui, D., Low, C.-Y. and Rahmat, A. 2015. Extraction of cellulose nanocrystals from plant sources for application as reinforcing agent in polymers. *Composites Part B: Engineering*, 75: 176-200.

Nishiyama, Y., Langan, P. and Chanzy, H. 2002. Crystal structure and hydrogen-bonding system in cellulose Iβ from synchrotron X-ray and neutron fiber diffraction. *Journal of the American Chemical Society*, 124 (31): 9074-9082.

Nishiyama, Y., Sugiyama, J., Chanzy, H. and Langan, P. 2003. Crystal structure and hydrogen bonding system in cellulose Iα from synchrotron X-ray and neutron fiber diffraction. *Journal of the American Chemical Society*, 125 (47): 14300-14306.

Oh, S. Y., Yoo, D. I., Shin, Y. and Seo, G. 2005. FTIR analysis of cellulose treated with sodium hydroxide and carbon dioxide. *Carbohydrate Research*, 340 (3): 417-428.

Orts, W. J., Shey, J., Imam, S. H., Glenn, G. M., Guttman, M. E. and Revol, J.-F. 2005. Application of cellulose microfibrils in polymer nanocomposites. *Journal of Polymers and the Environment*, 13 (4): 301-306.

Pääkkö, M., Ankerfors, M., Kosonen, H., Nykänen, A., Ahola, S., Österberg, M., Ruokolainen, J., Laine, J., Larsson, P. T. and Ikkala, O. 2007. Enzymatic hydrolysis combined with mechanical shearing and high-pressure homogenization for nanoscale cellulose fibrils and strong gels. *Biomacromolecules*, 8 (6): 1934-1941.

Pan, X., Gilkes, N., Kadla, J., Pye, K., Saka, S., Gregg, D., Ehara, K., Xie, D., Lam, D. and Saddler, J. 2006. Bioconversion of hybrid poplar to ethanol and co-products using an organosolv fractionation process: Optimization of process yields. *Biotechnology and Bioengineering*, 94 (5): 851-861.

Pandey, A., Soccol, C. R., Nigam, P. and Soccol, V. T. 2000. Biotechnological potential of agro-industrial residues. I: sugarcane bagasse. *Bioresource Technology*, 74 (1): 69-80.

Peng, B. L., Dhar, N., Liu, H. and Tam, K. 2011. Chemistry and applications of nanocrystalline cellulose and its derivatives: a nanotechnology perspective. *The Canadian Journal of Chemical Engineering*, 89 (5): 1191-1206.

Pereira, A. L., do Nascimento, D. M., Cordeiro, E. M., Morais, J. P., SOUZA FILHO, M. and ROSA, M. d. F. 2010. Characterization of lignocellulosic materials extracted from the banana pseudostem. In: Proceedings of *Embrapa Agroindústria Tropical-Artigo em anais de congresso (ALICE)*. In: INTERNATIONAL SYMPOSIUM ON NATURAL POLYMERS AND COMPOSITES, 7., 2010, Gramado. Proceedings. São Carlos: Associação Brasileira de Polímeros, 2010.,

Phanthong, P., Guan, G., Ma, Y., Hao, X. and Abudula, A. 2016. Effect of ball milling on the production of nanocellulose using mild acid hydrolysis method. *Journal of the Taiwan Institute of Chemical Engineers*, 60: 617-622.

Prado, R., Erdocia, X. and Labidi, J. 2013. Lignin extraction and purification with ionic liquids. *Journal of Chemical Technology and Biotechnology*, 88 (7): 1248-1257.

Pu, Y., Jiang, N. and Ragauskas, A. J. 2007. Ionic Liquid as a Green Solvent for Lignin. *Journal of Wood Chemistry and Technology*, 27 (1): 23-33.

Pulp, T. A. o. t. and Industry, P. 1993. *Tappi Journal*. Technical Association of the Pulp and Paper Industry.

Qin, Z.-Y., Tong, G., Chin, Y. F. and Zhou, J.-C. 2011. Preparation of ultrasonic-assisted high carboxylate content cellulose nanocrystals by TEMPO oxidation. *BioResources*, 6 (2): 1136-1146.

Qiu, Z., Aita, G. M. and Walker, M. S. 2012. Effect of ionic liquid pretreatment on the chemical composition, structure and enzymatic hydrolysis of energy cane bagasse. *Bioresource Technology*, 117: 251-256.

Raymundo, A. S., Zanarotto, R., Belisário, M., Pereira, M. d. G., Ribeiro, J. N. and Ribeiro, A. V. F. N. 2010. Evaluation of sugar-cane bagasse as bioadsorbent in the textile wastewater treatment contaminated with carcinogenic congo red dye. *Brazilian Archives of Biology and Technology*, 53 (4): 931-938.

Rípoli, T. C. C., Molina Jr, W. F. and Rípoli, M. L. C. 2000. Energy potential of sugar cane biomass in Brazil. *Scientia Agricola*, 57 (4): 677-681.

Romero, A., Santos, A., Tojo, J. and Rodriguez, A. 2008. Toxicity and biodegradability of imidazolium ionic liquids. *Journal of Hazardous Materials*, 151 (1): 268-273.

Rowell, R. M. 2005. 14 Chemical Modification of Wood. *Handbook of Wood Chemistry and Wood Composites*, 381

Saelee, K., Yingkamhaeng, N., Nimchua, T. and Sukyai, P. 2016. An environmentally friendly xylanase-assisted pretreatment for cellulose nanofibrils isolation from sugarcane bagasse by high-pressure homogenization. *Industrial Crops and Products*, 82: 149-160.

Samayam, I. P. and Schall, C. A. 2010. Saccharification of ionic liquid pretreated biomass with commercial enzyme mixtures. *Bioresource Technology*, 101 (10): 3561-3566.

Sarkar, N., Ghosh, S. K., Bannerjee, S. and Aikat, K. 2012. Bioethanol production from agricultural wastes: an overview. *Renewable Energy*, 37 (1): 19-27.

Sasaki, M., Adschiri, T. and Arai, K. 2003. Fractionation of sugarcane bagasse by hydrothermal treatment. *Bioresource Technology*, 86 (3): 301-304.

Sathitsuksanoh, N., Holtman, K. M., Yelle, D. J., Morgan, T., Stavila, V., Pelton, J., Blanch, H., Simmons, B. A. and George, A. 2014. Lignin fate and characterization during ionic liquid biomass pretreatment for renewable chemicals and fuels production. *Green Chemistry*, 16 (3): 1236-1247.

Schwanninger, M., Rodrigues, J., Pereira, H. and Hinterstoisser, B. 2004. Effects of short-time vibratory ball milling on the shape of FT-IR spectra of wood and cellulose. *Vibrational Spectroscopy*, 36 (1): 23-40.

Shafiei-Sabet, S., Hamad, W. Y. and Hatzikiriakos, S. G. 2012. Rheology of nanocrystalline cellulose aqueous suspensions. *Langmuir*, 28 (49): 17124-17133.

Sheltami, R. M., Abdullah, I., Ahmad, I., Dufresne, A. and Kargarzadeh, H. 2012. Extraction of cellulose nanocrystals from mengkuang leaves (Pandanus tectorius). *Carbohydrate Polymers*, 88 (2): 772-779.

Silveira, M. H. L., Morais, A. R. C., da Costa Lopes, A. M., Olekszyszen, D. N., Bogel-Łukasik, R., Andreaus, J. and Pereira Ramos, L. 2015. Current pretreatment technologies for the development of cellulosic ethanol and biorefineries. *ChemSusChem*, 8 (20): 3366-3390.

Sindhu, R., Binod, P. and Pandey, A. 2016. Biological pretreatment of lignocellulosic biomass–An overview. *Bioresource Technology*, 199: 76-82.

Sluiter, A., Hames, B., Ruiz, R., Scarlata, C., Sluiter, J., Templeton, D. and Crocker, D. 2008. Determination of structural carbohydrates and lignin in biomass. *Laboratory analytical procedure*, 1617: 1-16.

Sluiter, J. B., Ruiz, R. O., Scarlata, C. J., Sluiter, A. D. and Templeton, D. W. 2010. Compositional analysis of lignocellulosic feedstocks. 1. Review and description of methods. *Journal of Agricultural and Food Chemistry*, 58 (16): 9043-9053.

Sofla, M. R. K., Brown, R. J., Tsuzuki, T. and Rainey, T. J. 2016. A comparison of cellulose nanocrystals and cellulose nanofibres extracted from bagasse using acid and ball milling methods. *Advances in Natural Sciences: Nanoscience and Nanotechnology*, 7 (3): 035004.

Stuart, B. 2005. *Infrared Spectroscopy*. Wiley Online Library.

Šturcová, A., Davies, G. R. and Eichhorn, S. J. 2005. Elastic modulus and stress-transfer properties of tunicate cellulose whiskers. *Biomacromolecules*, 6 (2): 1055-1061.

Sun, J., Sun, X., Sun, R. and Su, Y. 2004. Fractional extraction and structural characterization of sugarcane bagasse hemicelluloses. *Carbohydrate Polymers*, 56 (2): 195-204.

Sun, N., Rahman, M., Qin, Y., Maxim, M. L., Rodriguez, H. and Rogers, R. D. 2009. Complete dissolution and partial delignification of wood in the ionic liquid 1-ethyl-3-methylimidazolium acetate. *Green Chemistry*, 11 (5): 646-655.

Sun, R., Tomkinson, J., Mao, F. and Sun, X. 2001. Physicochemical characterization of lignins from rice straw by hydrogen peroxide treatment. *Journal of Applied Polymer Science*, 79 (4): 719-732.

Sun, X., Xu, F., Sun, R., Fowler, P. and Baird, M. 2005. Characteristics of degraded cellulose obtained from steam-exploded wheat straw. *Carbohydrate Research*, 340 (1): 97-106.

Sun, Y. and Cheng, J. 2002. Hydrolysis of lignocellulosic materials for ethanol production: a review. *Bioresource Technology*, 83 (1): 1-11.

Swatloski, R. P., Spear, S. K., Holbrey, J. D. and Rogers, R. D. 2002. Dissolution of cellose with ionic liquids. *Journal of the American Chemical Society*, 124 (18): 4974-4975.

Taherzadeh, M. J. and Karimi, K. 2007. Acid-based hydrolysis processes for ethanol from lignocellulosic materials: a review. *BioResources*, 2 (3): 472-499.

Taherzadeh, M. J. and Karimi, K. 2008. Pretreatment of lignocellulosic wastes to improve ethanol and biogas production: a review. *International Journal of Molecular Sciences*, 9 (9): 1621-1651.

Tahir, H., Sultan, M., Akhtar, N., Hameed, U. and Abid, T. 2016. Application of natural and modified sugar cane bagasse for the removal of dye from aqueous solution. *Journal of Saudi Chemical Society*, 20: S115-S121.

Tan, S. S. Y., MacFarlane, D. R., Upfal, J., Edye, L. A., Doherty, W. O. S., Patti, A. F., Pringle, J. M. and Scott, J. L. 2009. Extraction of lignin from lignocellulose at atmospheric pressure using alkylbenzenesulfonate ionic liquid. *Green Chemistry*, 11 (3): 339-345.

Tan, X. Y., Hamid, S. B. A. and Lai, C. W. 2015. Preparation of high crystallinity cellulose nanocrystals (CNCs) by ionic liquid solvolysis. *Biomass and Bioenergy*, 81: 584-591.

Tang, Y., Shen, X., Zhang, J., Guo, D., Kong, F. and Zhang, N. 2015. Extraction of cellulose nano-crystals from old corrugated container fiber using phosphoric acid and enzymatic hydrolysis followed by sonication. *Carbohydrate Polymers*, 125: 360-366.

Templeton, D. W., Wolfrum, E. J., Yen, J. H. and Sharpless, K. E. 2016. Compositional Analysis of Biomass Reference Materials: Results from an Interlaboratory Study. *BioEnergy Research*, 9 (1): 303-314.

Urban, M. W. 1996. *Attenuated total reflectance spectroscopy of polymers: theory and practice*. American Chemical Society.

van Heiningen, A., Krothapalli, D., Genco, J. and Justason, A. 2003. A chemical reactor analysis of industrial oxygen delignification. *Pulp & Paper Canada*, 104 (12): T331-T336.

Wada, M., Chanzy, H., Nishiyama, Y. and Langan, P. 2004. Cellulose IIII crystal structure and hydrogen bonding by synchrotron X-ray and neutron fiber diffraction. *Macromolecules*, 37 (23): 8548-8555.

Wada, M., Heux, L., Isogai, A., Nishiyama, Y., Chanzy, H. and Sugiyama, J. 2001. Improved structural data of cellulose IIII prepared in supercritical ammonia. *Macromolecules*, 34 (5): 1237-1243.

Walford, S. N. 2008. Sugarcane Bagasse: How easy is it to measure its constituents? In: Proceedings of *Proceedings of the South African Sugar Technologists Association*. 266-273.

Wang, X., Li, H., Cao, Y. and Tang, Q. 2011. Cellulose extraction from wood chip in an ionic liquid 1-allyl-3-methylimidazolium chloride (AmimCl). *Bioresource Technology*, 102 (17): 7959-7965.

Watkins, D., Nuruddin, M., Hosur, M., Tcherbi-Narteh, A. and Jeelani, S. 2015. Extraction and characterization of lignin from different biomass resources. *Journal of Materials Research and Technology*, 4 (1): 26-32.

Xu, F., Sun, J.-X., Sun, R., Fowler, P. and Baird, M. S. 2006. Comparative study of organosolv lignins from wheat straw. *Industrial Crops and Products*, 23 (2): 180-193.

Yu, H., Qin, Z., Liang, B., Liu, N., Zhou, Z. and Chen, L. 2013. Facile extraction of thermally stable cellulose nanocrystals with a high yield of 93% through hydrochloric acid hydrolysis under hydrothermal conditions. *Journal of Materials Chemistry A*, 1 (12): 3938-3944.

Zaman, M., Xiao, H., Chibante, F. and Ni, Y. 2012. Synthesis and characterization of cationically modified nanocrystalline cellulose. *Carbohydrate Polymers*, 89 (1): 163-170.

Zhang, Y., Du, H., Qian, X. and Chen, E. Y.-X. 2010. Ionic liquid− water mixtures: enhanced K w for efficient cellulosic biomass conversion. *Energy & Fuels*, 24 (4): 2410-2417.

Zhang, Y., Xu, A., Lu, B., Li, Z. and Wang, J. 2015. Dissolution of cellulose in 1-allyl-3-methylimizodalium carboxylates at room temperature: a structure–property relationship study. *Carbohydrate Polymers*, 117: 666-672.

Zhao, Y., Wang, J., Wang, H., Li, Z., Liu, X. and Zhang, S. 2015. Is there any preferential interaction of ions of ionic liquids with DMSO and H2O? A comparative study from MD simulation. *The Journal of Physical Chemistry B*, 119 (22): 6686-6695.

Zheng, Y., Lin, H.-M., Wen, J., Cao, N., Yu, X. and Tsao, G. T. 1995. Supercritical carbon dioxide explosion as a pretreatment for cellulose hydrolysis. *Biotechnology Letters*, 17 (8): 845-850.

Zhong, C., Wang, C., Wang, F., Jia, H., Wei, P. and Zhao, Y. 2016. Application of tetra-n-methylammonium hydroxide on cellulose dissolution and isolation from sugarcane bagasse. *Carbohydrate Polymers*, 136: 979-987.

Zhu, S., Wu, Y., Yu, Z., Wang, C., Yu, F., Jin, S., Ding, Y., Chi, R. a., Liao, J. and Zhang, Y. 2006. Comparison of three microwave/chemical pretreatment processes for enzymatic hydrolysis of rice straw. *Biosystems Engineering*, 93 (3): 279-283.

Zhuo, K., Du, Q., Bai, G., Wang, C., Chen, Y. and Wang, J. 2015. Hydrolysis of cellulose catalyzed by novel acidic ionic liquids. *Carbohydrate Polymers*, 115: 49-53.

APPENDICES

Appendix A: Conference attendance

G. P. Mdletshe, N. Deenadayalu, S. S. Ray. 2017. Preparation and Charaterisation of Cellulose Nanocrsytals (CNCs) FROM SUGARCANE BAGASSE. **Abstract Proceedings** of the South African Sugar Technologists' Association 90th Annual International Conference, ICC, Durban, South Africa, 15-17 August 2017.

Appendix B: HPLC sugar standards

HPLC chromatograms of standards used for the quantification of untreated SCB and NIST standard SCB using RI detector are shown in Figure B-1.

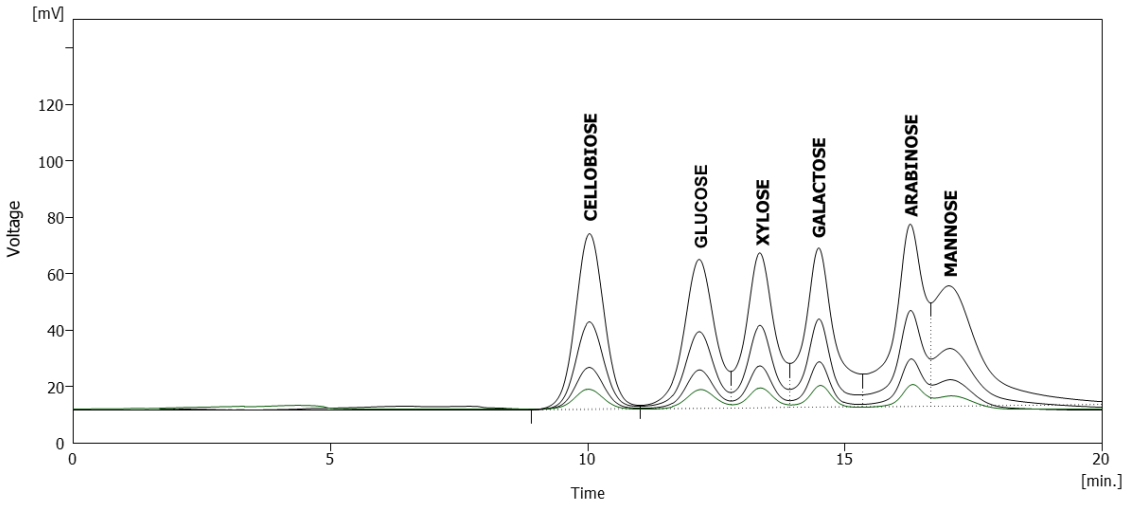

Figure B-1. Chromatograms of sugar standards used for carbohydrate quantification (RI detector).

The linear regression calibration curves of glucose and xylose standards used to calcuate the untretaed SCB and NIST standard SCB cellulose and hemicellulose are show in Figure B-2 and Figure B-3 below.

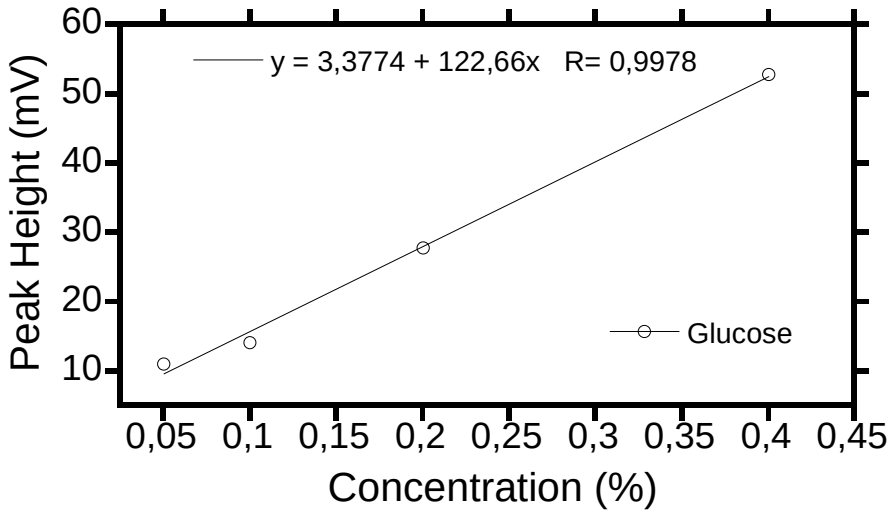

Figure B-2 Glucose standards linear calibration graph.

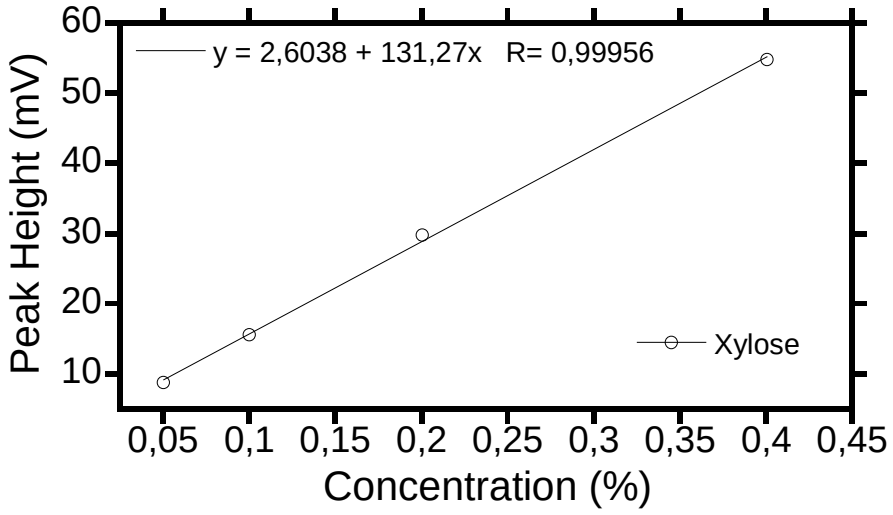

Figure B-3. Xylose standards linear calibration graph.

The chromatograms of untreated SCB and NIST SCB standard are shown in Figure B-4 and Figure B-5 below.

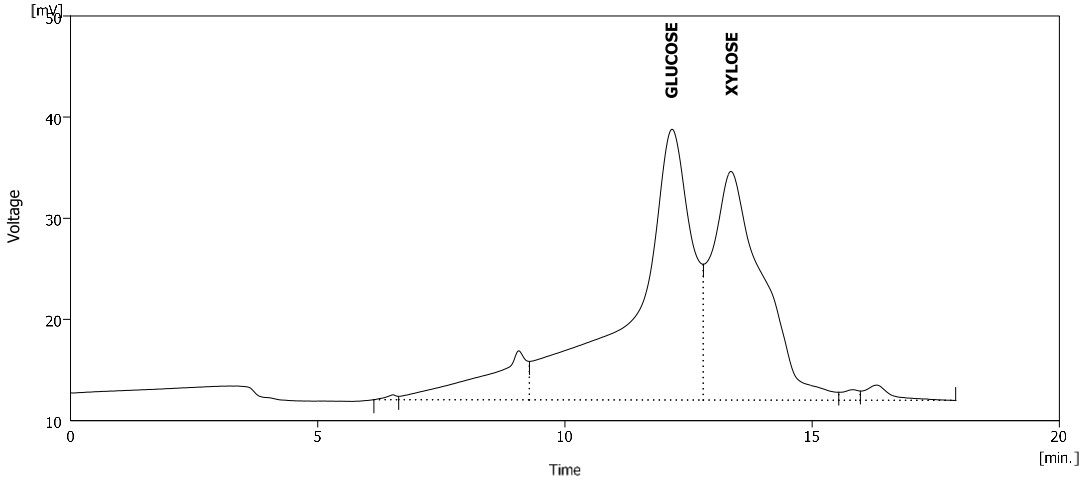

Figure B-4. Untreated SCB chromatogram.

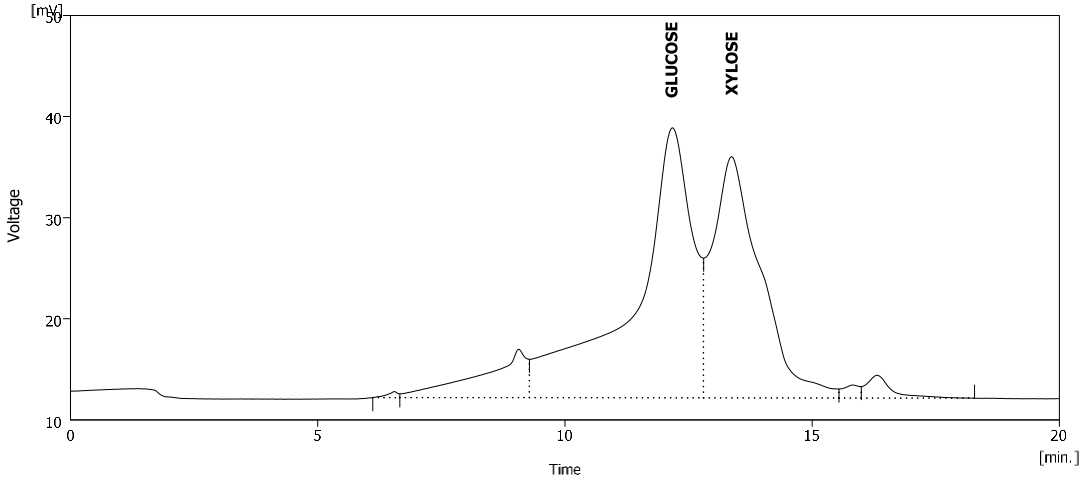

Figure B-5. NIST SCB standard chromatogram.

The HPLC chromatograms of glucose and xylose standards using ELSD detector are shown in Figure B-6 below.

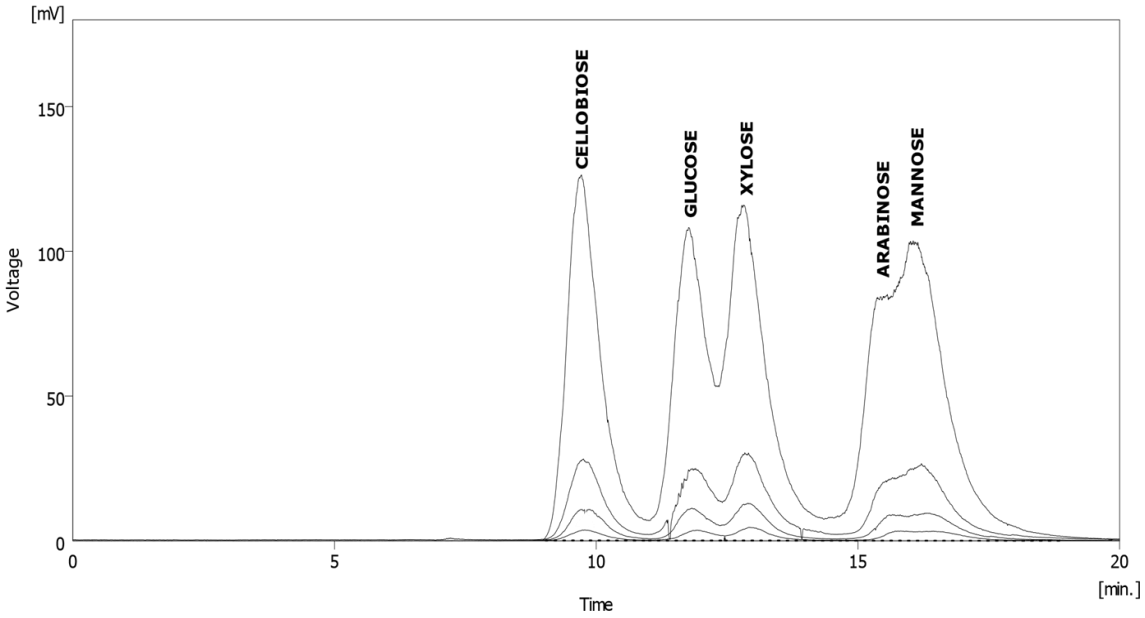

Figure B-6. Chromatograms of sugar standards used for carbohydrate quantification (ELSD detector).

The linear regression calibration curves of the glucose and xylose standards used to calcuate the cellulose and xylose of the ILs and ILs/DMSO pre-treated samples are show in Figure B-7 and Figure B-8 below.

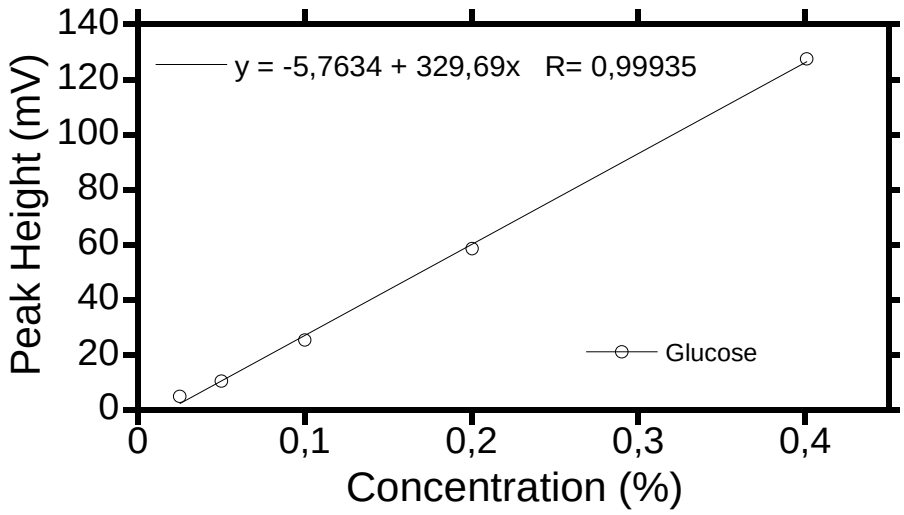

Figure B-7. Glucose standards liner calibration graph.

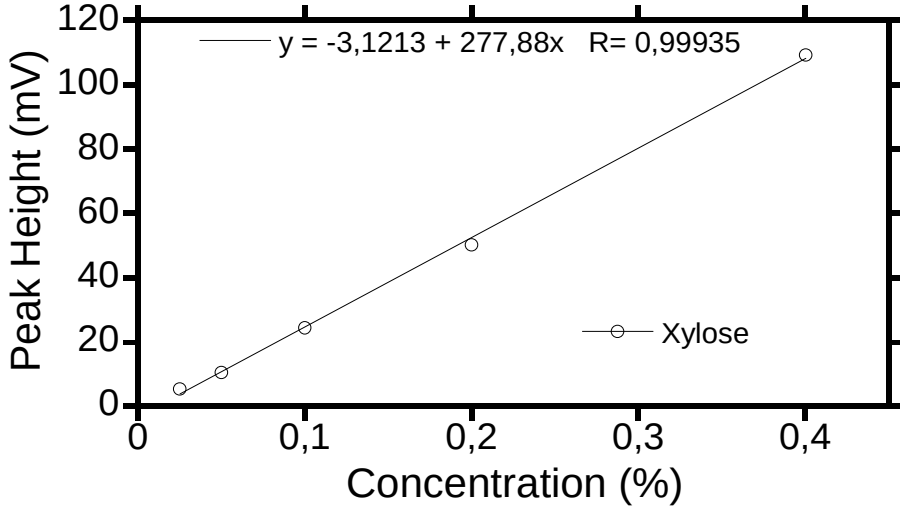

Figure B-8. Xylose standards linear calibration graph.

The glucose sugar recovery standard (SRS) chromatogram is shown in Figure B-9 below. The dilution factor for glucan calculation was 2.

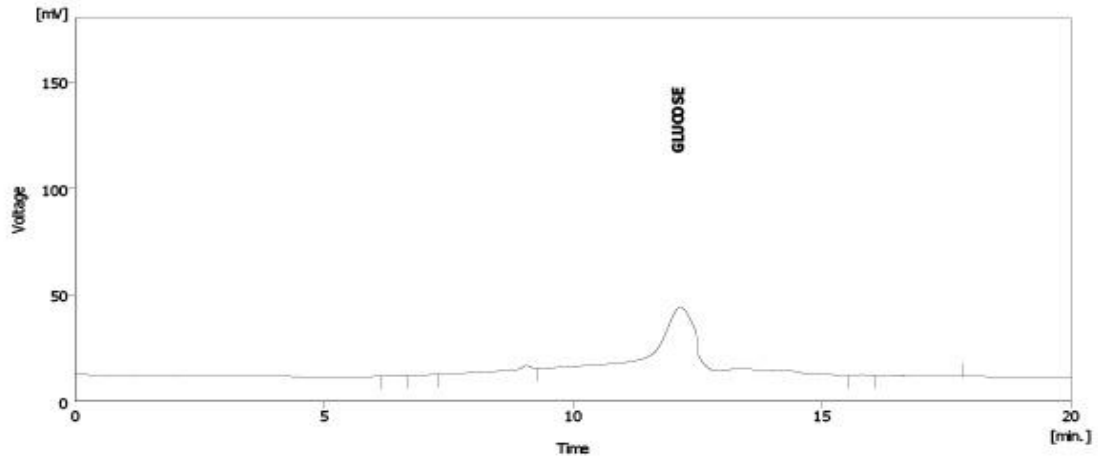

Figure B-9. Glucose SRS chromatogram.

Appendix C: HPLC IL or IL/DMSO results

C1. Pre-treatment of SCB with ILs at varied times

The HPLC chromatograms of SCB pre-treated with ILs at varied pre-treatment time of 4 h, 8 h and 12 h.

The HPLC chromatogram of [bmim][$MeSO_4$]-4 is shown in Figure C1-1 below.

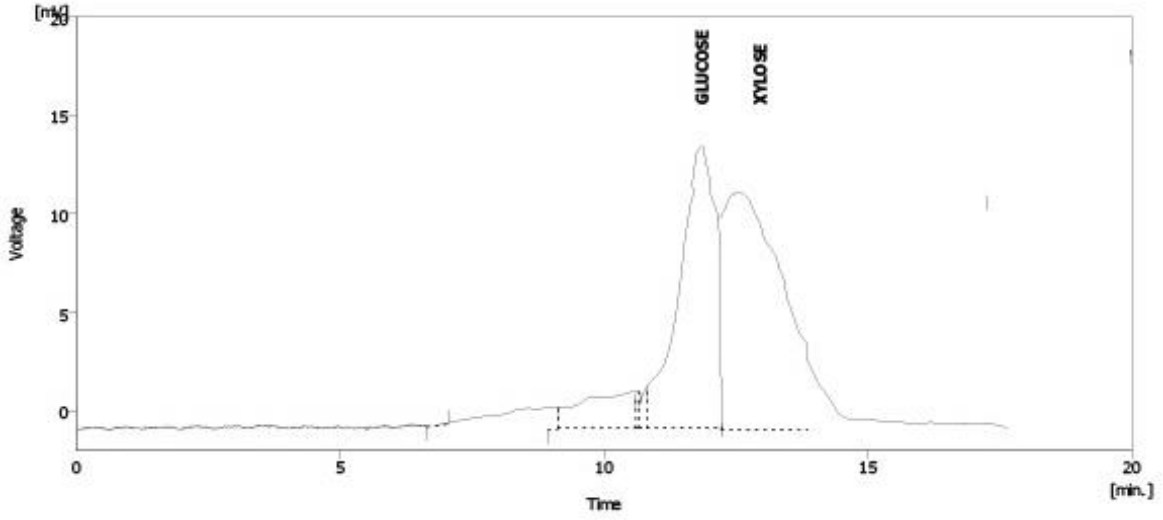

Figure C1-1. Chromatogram of [bmim][$MeSO_4$]-4.

The HPLC chromatogram of [bmim][$MeSO_4$]-8 is shown in Figure C1-2 below.

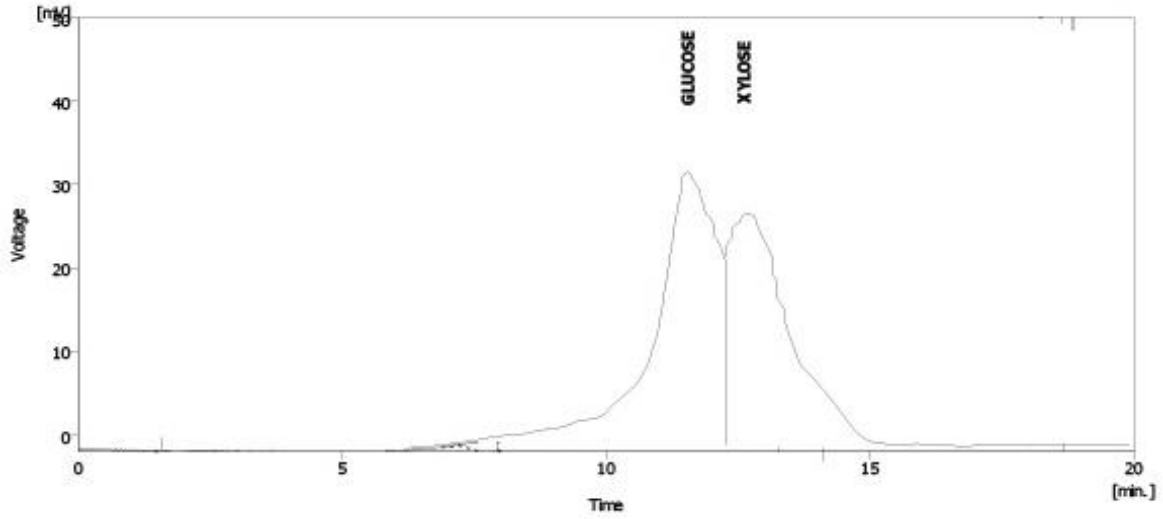

Figure C1-2. Chromatogram of [bmim][$MeSO_4$]-8.

The HPLC chromatogram of [bmim][$MeSO_4$]-12 is shown in Figure C1-3 below.

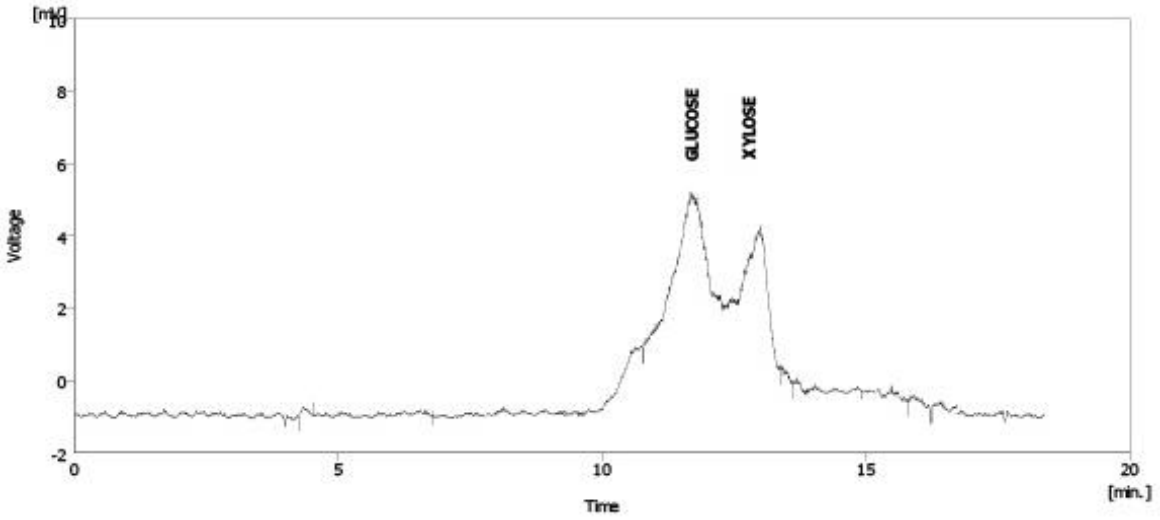

Figure C1-3. Chromatogram of [bmim][$MeSO_4$]-12.

The HPLC chromatogram of [bmim][HSO_4]-4 is shown in Figure C1-4 below.

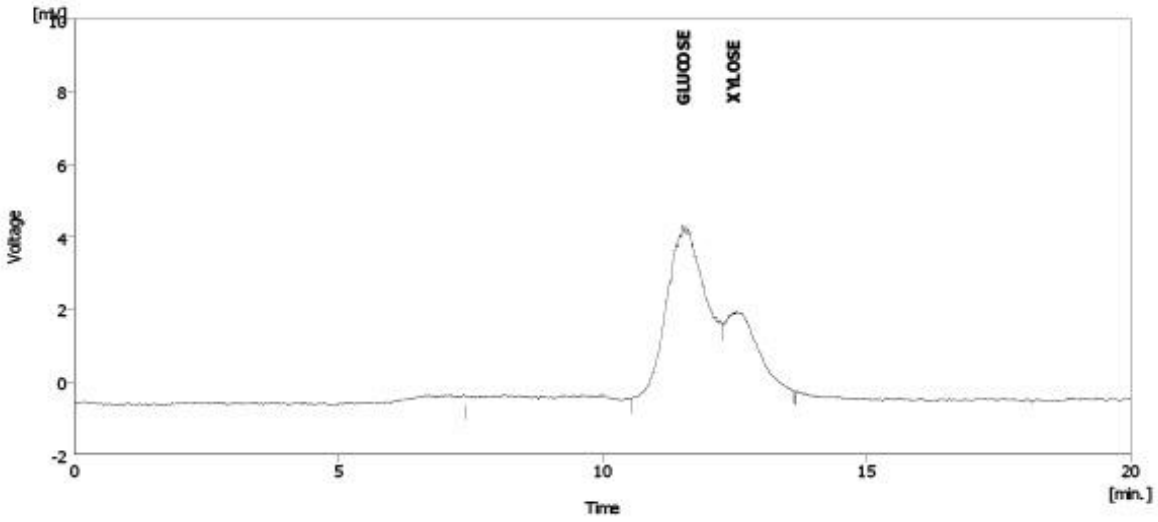

Figure C1-4. Chromatogram of [bmim][HSO_4]-4.

The HPLC chromatogram of [bmim][HSO_4]-8 is shown in Figure C1-5 below.

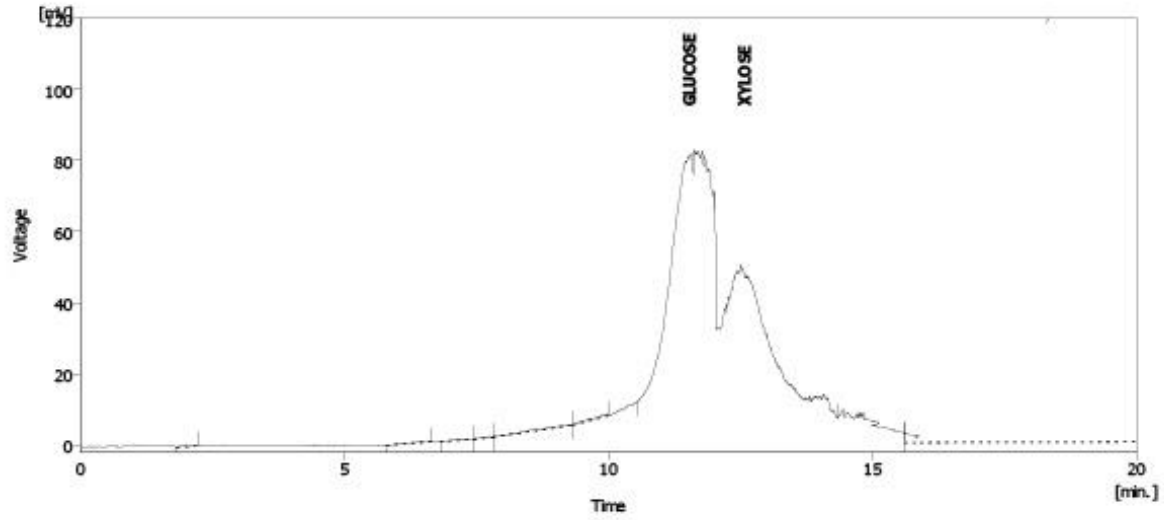

Figure C1-5. Chromatogram of [bmim][HSO_4]-8.

The HPLC chromatogram of [bmim][HSO_4]-12 is shown in Figure C1-6 below

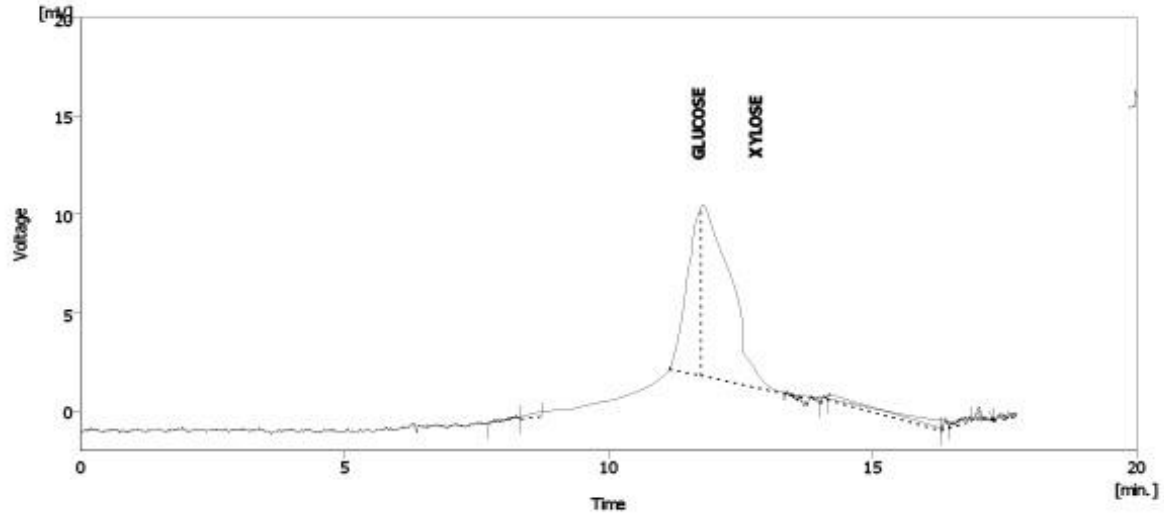

Figure C1-6. Chromatogram of [bmim][HSO_4]-12.

C2. Pre-treatment of SCB with IL/DMSO

The HPLC chromatograms of SCB pre-treated with IL/DMSO followed by bleaching at pre-treatment time of 60 min.

The HPLC chromatogram of [bmim][$MeSO_4$]-50 is shown in Figure C2-1 below.

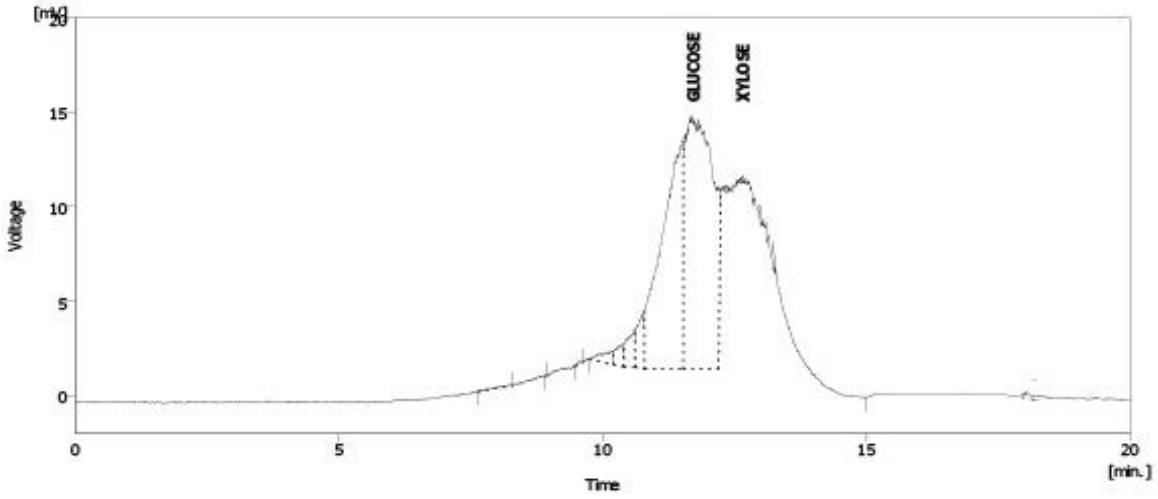

Figure C2-1. Chromatogram of [bmim][$MeSO_4$]-50.

The HPLC chromatogram of [bmim][$MeSO_4$]-75 is shown in Figure C2-2 below.

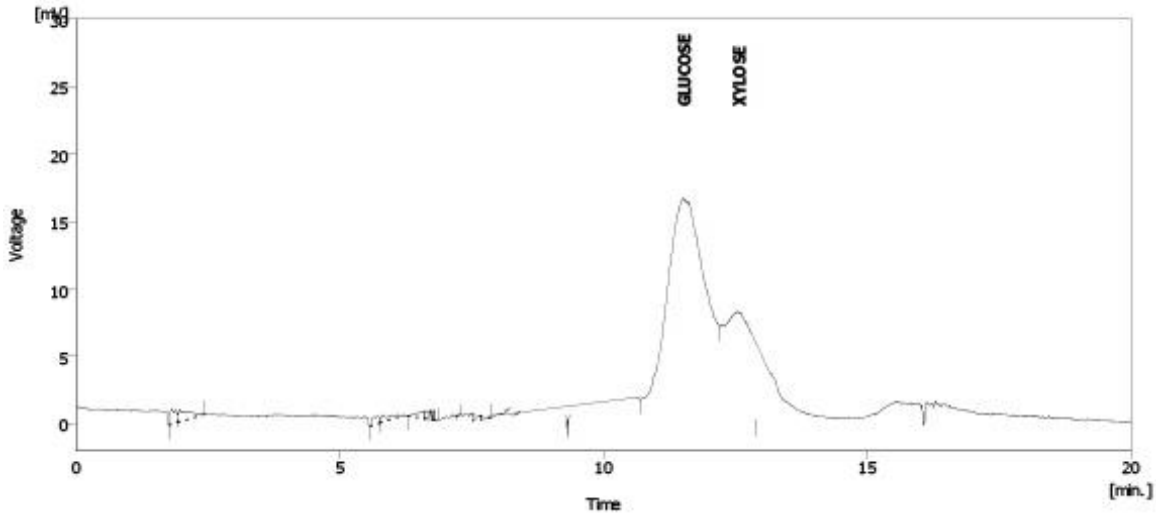

Figure C2-2. Chromatogram of [bmim][$MeSO_4$]-75.

The HPLC chromatogram of [bmim][$MeSO_4$]-90 is shown in Figure C2-3 below.

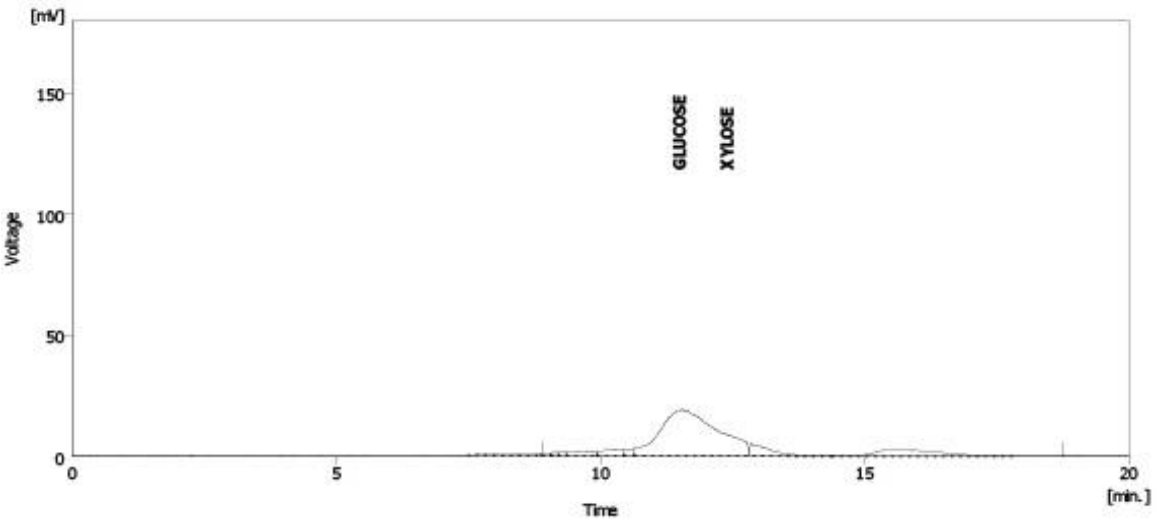

Figure C2-3. Chromatogram of [bmim][$MeSO_4$]-90.

The HPLC chromatogram of [bmim][$MeSO_4$]-100 is shown in Figure C2-4 below.

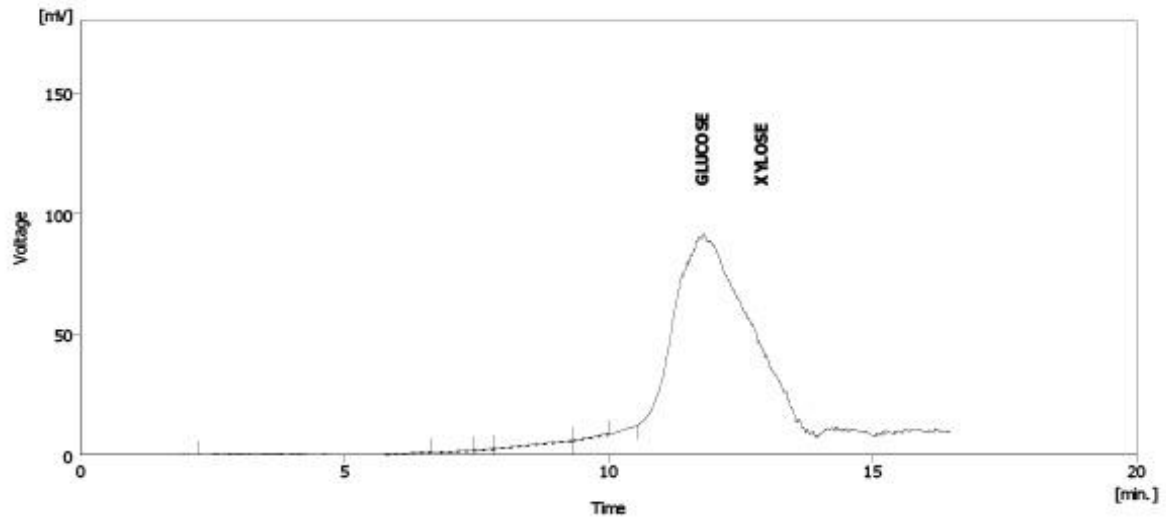

Figure C2-4. Chromatogram of [bmim][$MeSO_4$]-100.

The HPLC chromatogram of [bmim][HSO_4]-50 is shown in Figure C2-5 below.

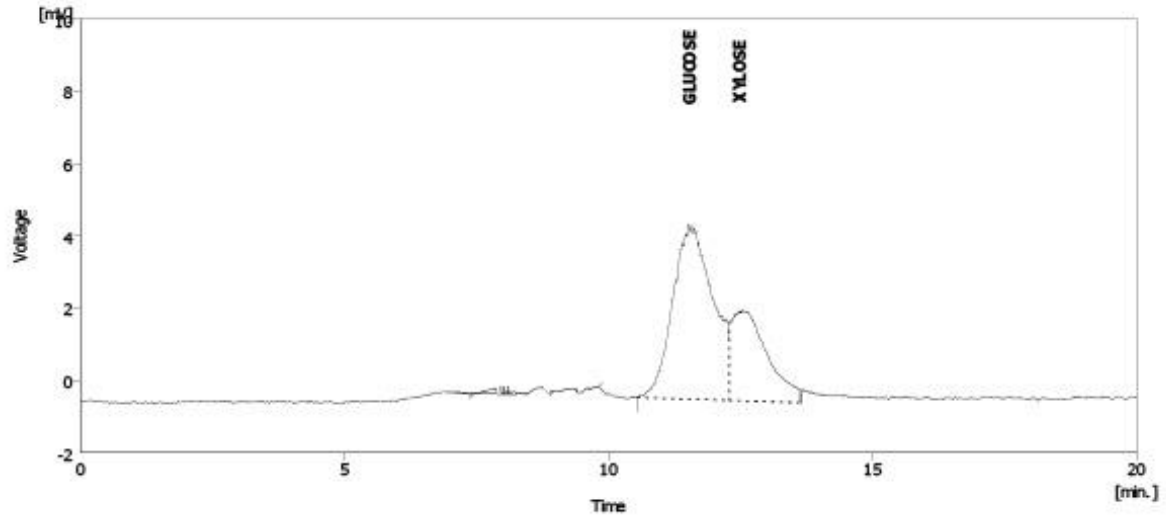

Figure C2-5. Chromatogram of [bmim][HSO_4]-50.

The HPLC chromatogram of [bmim][HSO_4]-75 is shown in Figure C2-6 below.

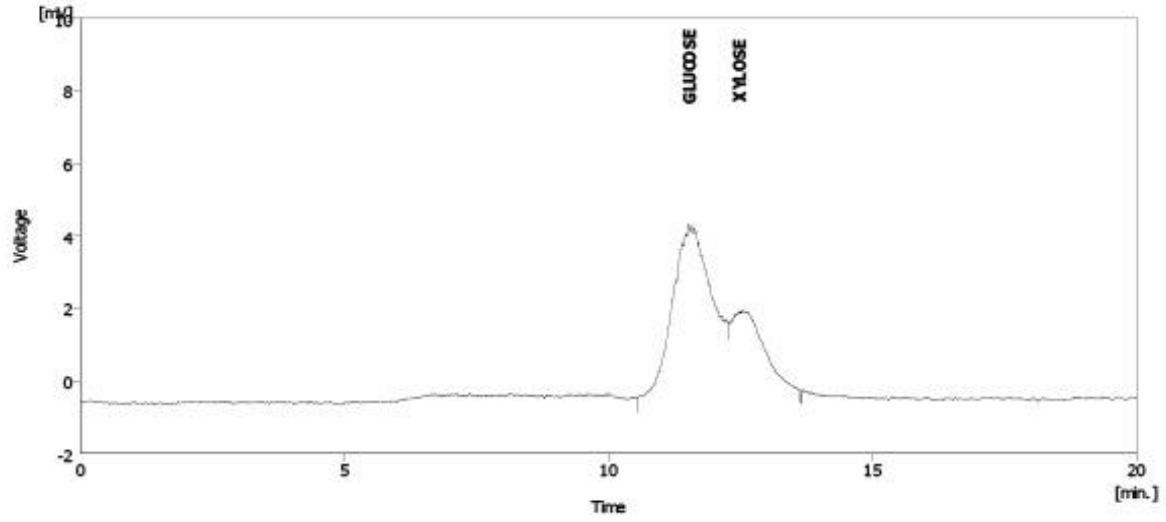

Figure C2-6. Chromatogram of [bmim][HSO_4]-75.

The HPLC chromatogram of [bmim][HSO_4]-90 is shown in Figure C2-7 below.

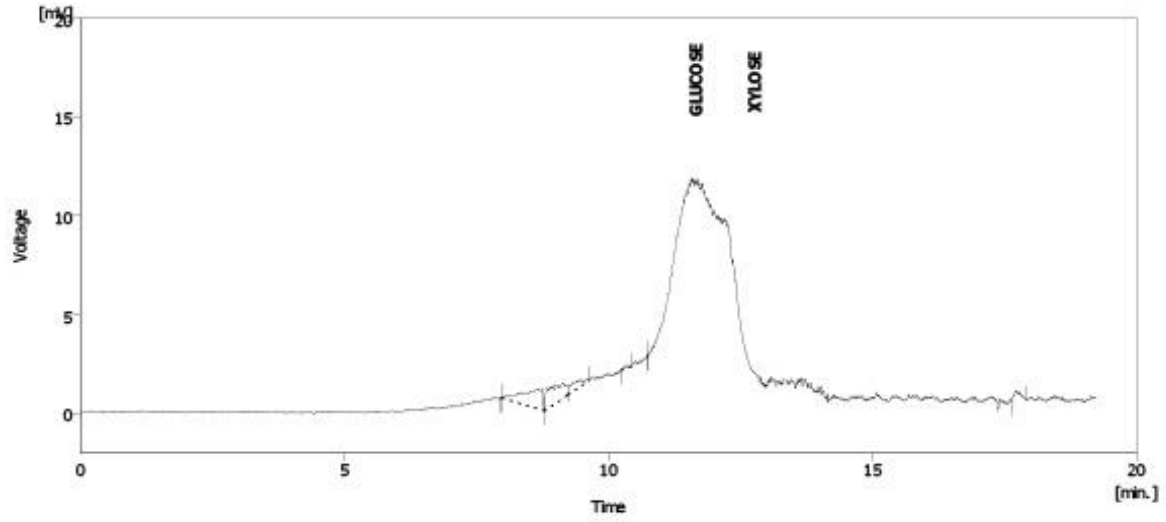

Figure C2-7. Chromatogram of [bmim][HSO_4]-90.

The HPLC chromatogram of [bmim][HSO_4]-100 is shown in Figure C2-8 below.

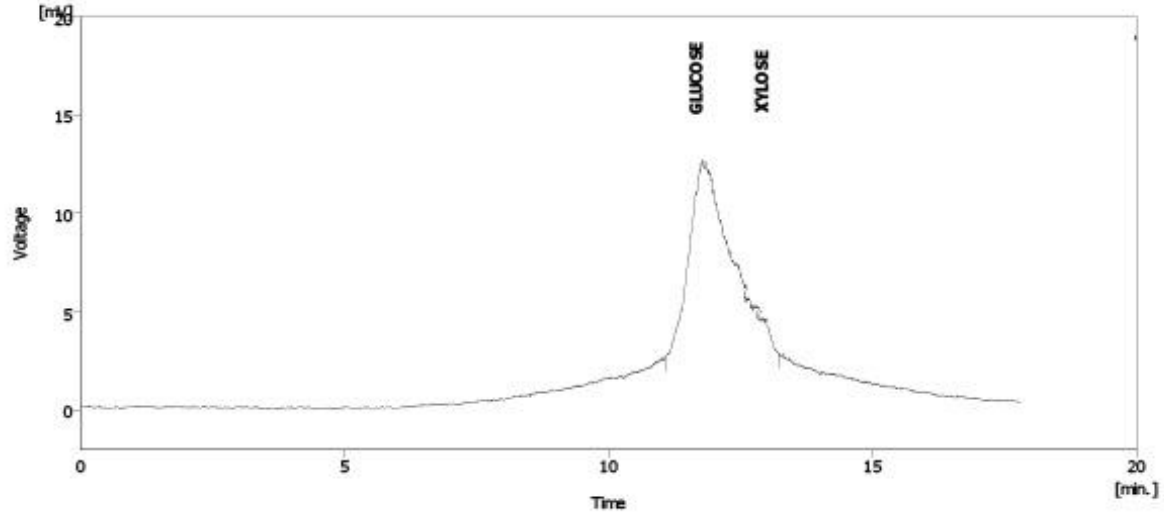

Figure C2-8. Chromatogram of [bmim][HSO_4]-100.